

Electronic Thesis and Dissertation Repository

4-30-2014 12:00 AM

Oriented Collagen and Applications of Waveguide Evanescent Field Scattering (WEFS) Microscopy

Qamrun Nahar
The University of Western Ontario

Supervisor
Dr. Silvia Mittler
The University of Western Ontario

Graduate Program in Electrical and Computer Engineering
A thesis submitted in partial fulfillment of the requirements for the degree in Master of Engineering Science
© Qamrun Nahar 2014

Follow this and additional works at: <https://ir.lib.uwo.ca/etd>



Part of the [Bioimaging and Biomedical Optics Commons](#), [Biomaterials Commons](#), [Biomedical Commons](#), [Biophysics Commons](#), [Nanoscience and Nanotechnology Commons](#), and the [Nanotechnology Fabrication Commons](#)

Recommended Citation

Nahar, Qamrun, "Oriented Collagen and Applications of Waveguide Evanescent Field Scattering (WEFS) Microscopy" (2014). *Electronic Thesis and Dissertation Repository*. 2089.
<https://ir.lib.uwo.ca/etd/2089>

This Dissertation/Thesis is brought to you for free and open access by Scholarship@Western. It has been accepted for inclusion in Electronic Thesis and Dissertation Repository by an authorized administrator of Scholarship@Western. For more information, please contact wlsadmin@uwo.ca.

ORIENTED COLLAGEN AND APPLICATIONS OF WAVEGUIDE EVANESCENT
FIELD SCATTERING (WEFS) MICROSCOPY

(Thesis format: Integrated Article)

by

Qamrun Nahar

Graduate Program in
Electrical and Computer Engineering

A thesis submitted in partial fulfillment
of the requirements for the degree of
Master of Engineering Science

The School of Graduate and Postdoctoral Studies
The University of Western Ontario
London, Ontario, Canada

© Qamrun Nahar, 2014

Abstract

In this thesis, Waveguide Evanescent Field Scattering (WEFS) microscopy is developed as a non-invasive, label-free live cell imaging technique. This new high-contrast imaging can be employed to study the first hundred nanometers from the surface as it utilizes the evanescent field of a waveguide as the illumination source. Previously, waveguide evanescent field fluorescence (WEFF) microscopy was developed as a fluorescence imaging technique comparable to the total internal reflection fluorescent (TIRF) microscopy. Both the WEFF and WEFS technique utilizes the same fundamental concepts except in WEFS microscopy imaging is accomplished without the application of any fluorescent labeling. In this work, bacterial biofilms and osteoblasts were cultured on waveguides and imaged with WEFS microscopy. It was possible to detect cell-substrate interactions as well as imaging of cell membrane and cytoplasmic granularity with this microscopy. This non-invasive microscopy can have wide applications for real time imaging of live/dead cells with enhanced sensitivity and contrast.

One of the major investigations in tissue engineering is the fabrication of biomaterials that can serve as cell responsive scaffolds. In the present work, collagen thin films were fabricated on hydrophobic glass substrates employing Langmuir-Blodgett (LB) technology. Different orientation distributions of collagen fibrils were found using various geometrical shaped hydrophobic glass substrates. It was observed that the substrate geometry plays a significant role for the collagen orientation distribution. The different orientations of the collagen on the thin films were found to be dependent on the direction of dipping, flow parameters on the LB trough and size and shape of the substrates. The collagen films were also found to be stable under different temperature and solvent conditions for up to three months. The oriented collagen films need to be tested in the future for their application as waveguide coatings for WEFF and WEFS microscopy.

Keywords

Waveguide, evanescent field, Label-free, scattering, microscopy, WEFS, biofilms, osteoblasts, collagen, Langmuir-Blodgett deposition.

Co-Authorship Statement

This thesis contains materials from previously published manuscripts co-authored by Qamrun Nahar, Jeremiah Shuster, David Minh Luan Quach, Behafarid Darvish, Frederik Fleishner, Michael Morawitz, Christopher Halfpap, Mihaela Stefan, Gordon Southam, Uwe Langbein, Harvey A. Goldberg, Bernd Grohe and Silvia Mittler. Qamrun Nahar conducted most of the experimental work and data analysis.

In chapter 3, Qamrun Nahar fabricated collagen thin films by Langmuir-Blodgett technology. Some of the collagen thin film deposition were performed by David Minh Luan Quach. All imaging was carried out by Qamrun Nahar. Bernd Grohe performed the stability test on collagen films.

In Chapter 4, Qamrun Nahar performed microscopy set-up, bacteria culture on waveguides, imaging and data analysis. Michael Morawitz fabricated the waveguides. Bacteria (*Nitrobacter* Sp. 263) culture preparation was done by Jeremiah Shuster. UV sterilization was carried out by Mihaela Stefan at Trojan Technologies. Frederik Fleissner did the quantitative analysis of bacteria after UV irradiation.

In Chapter 5, all microscopy, imaging and data analysis were conducted by Qamrun Nahar. Osteoblast culture was carried out by Elezabeth Pruski.

This thesis is dedicated to my son, Ayman, who makes this world a better place....

Acknowledgments

I would like to express my sincere gratitude to my thesis supervisor Dr. Silvia Mittler for her guidance, encouragement and mentorship during my research. It would have been very difficult to finish my studies without her support during my role as a new mother.

A lot of people has contributed to my research. I would like to thank Dr. Uwe Langbein for training me on ATSSOS, Hao Jiang for helping me with m-line spectroscopy, Behafarid Darvish for training on Langmuir-Blodgett deposition and Michael Morawitz and Christopher Halfpap for fabricating the waveguides. I am grateful to Jeremiah Shuster for culturing the bacteria and supplying them whenever required and Elezabeth Pruski for culturing osteoblasts. Special Thanks to Frederik Fleissner for taking care of the data analysis when I was on maternity leave. I am also thankful to my co-workers Dr. Erden Ertorer, Dr. Hao Jiang, Max Port, David Quach, Albrecht Staat, Maryam Gouran, Dr. Dmytro Grebennikov, Sivayini Kandeepan and Rony Sharon for a nice and supporting working environment.

Finally, I would like to thank my mother for her encouragements and my husband, Zayed, for his unconditional support and patience during my studies.

Table of Contents

Abstract.....	ii
Co-Authorship Statement.....	iii
Thesis Dedication.....	iv
Acknowledgments.....	v
Table of Contents.....	vi
List of Figures.....	xi
List of Abbreviation.....	xiv
Chapter 1.....	1
1 Introduction.....	1
1.1 Total Internal Reflection Fluorescence (TIRF) Microscopy.....	1
1.2 Waveguide based Microscopy.....	2
1.3 Waveguide Evanescence Field Fluorescence (WEFF) Microscopy.....	3
1.4 Waveguide Evanescence Field Scattering (WEFS) Microscopy.....	3
1.5 Development of Waveguide Evanescent Field Scattering Microscopy (WEFS) for Application in Biology.....	6
1.6 Collagen.....	6
1.7 Langmuir-Blodgett Technology.....	8
1.8 Aim of the Thesis.....	9
1.9 References.....	11
Chapter 2.....	15
2 Principle of WEFS Microscopy and Fundamentals.....	15
2.1 WEFS Working Principle.....	15
2.2 WEFS Microscopy Setup.....	16
2.3 Fundamental Theory of Waveguides.....	18

2.3.1	Total Internal Reflection	18
2.3.2	Evanescence Field.....	19
2.3.3	Optical Waveguides	21
2.3.4	Planar Waveguides.....	22
2.3.5	Modes in a Waveguide.....	23
2.3.6	Effective Refractive Index	24
2.3.7	Refractive Index profiles.....	24
2.3.8	Coupling Grating	25
2.4	Langmuir-Blodgett (LB) Trough	25
2.5	Langmuir-Blodgett (LB) Films.....	26
2.6	Surface Pressure-Area Isotherm	28
2.7	References:.....	29
Chapter 3		31
3	Orientation and Orientation Distribution of Collagen Deposited with Langmuir-Blodgett Technology onto Flat Surfaces with Different Geometrical Shapes.....	31
3.1	Introduction.....	31
3.2	Materials and Methods: Collagen on Glass	37
3.2.1	Preparation of Collagen Solution.....	37
3.2.2	Glass Substrate Cleaning	37
3.2.3	Creating -OH groups on Substrate Surface.....	38
3.2.4	Silanization for Hydrophobic Substrates	38
3.2.5	Langmuir-Blodgett Deposition	38
3.2.6	Optical Microscopy.....	39
3.3	Results.....	39
3.3.1	Surface Pressure vs. Trough Area Isotherm	39
3.3.2	Orientation of Collagen on LB Films	40

3.3.3	Analysis of Flow Characteristics of Collagen	44
3.3.4	Effect of Width to Height Displacement on Collagen Pattern.....	46
3.4	Materials and Methods: Effect of Environment on Collagen Samples.....	47
3.4.1	Effect of Environment and Time on the Collagen Samples	47
3.4.2	Optical Microscopy.....	48
3.5	Results.....	48
3.6	Summary	50
3.7	References.....	50
Chapter 4	53
4	WEFS Microscopy on Bacterial Biofilms.....	53
4.1	Introduction.....	53
4.2	Materials & Methods for Bacterial Colonization Experiment.....	57
4.2.1	Waveguides.....	57
4.2.2	Bacterial (Nitrobacter) Culture Preparation.....	57
4.2.3	Experiments on Bacterial Attachment and Colonization on Waveguides	58
4.3	Results.....	58
4.3.1	Colonization of Bacteria on Waveguide Surfaces	58
4.3.2	Quantitative Analysis of Scattering Intensity Distribution.....	60
4.3.3	Integrated Intensity Profiles for Single Cells and Microcolony	62
4.3.4	Counting the Number of Single Bacterium in Bright Field vs. WEFS.....	65
4.3.5	Comparison of Bright Field Image vs. WEFS Image	65
4.4	Materials and Methods: Attachment of Nitrobacter following UV Sterilization	68
4.4.1	Collimated Beam Apparatus.....	68
4.4.2	UV Sterilization Process.....	68
4.4.3	Experiment on Bacterial Attachment following UV Sterilization.....	69

4.5	Results.....	70
4.5.1	Attachment of Bacteria after UV Irradiance.....	70
4.5.2	Quantitative Analysis of Attachment of Bacteria after UV Doses.....	71
4.6	Summary.....	72
4.7	References.....	73
Chapter 5.....		76
5	Evanescent Field Scattering Microscopy of Osteoblasts.....	76
5.1	Introduction.....	76
5.2	Materials and Methods: Evanescent Imaging of Osteoblasts.....	80
5.2.1	WEFS and WEFF Microscopy.....	80
5.2.2	Cell Culture.....	81
5.2.3	Fluorescence Staining.....	81
5.3	Results.....	81
5.3.1	Imaging with Both WEFF and WEFS Microscopy.....	81
5.3.2	Imaging with WEFS Microscopy.....	83
5.4	Comparison with Fluorescence Microscopy.....	86
5.4.1	Fluorescence Staining and Microscopy.....	86
5.5	Results.....	87
5.6	Imaging Granularity in Cells.....	88
5.7	Results.....	88
5.8	Summary.....	90
5.9	References.....	91
Chapter 6.....		93
6	Conclusion and Outlook.....	93
6.1	Conclusion.....	93

6.2 Outlook	95
Appendix A.....	97
Appendix B.....	99
Curriculum Vitae	101

List of Figures

Figure 1-1: A schematic of WEFF microscopy	4
Figure 1-2: A schematic of comparison between WEFF and WEFS microscopy.....	5
Figure 1-3: Schematic diagram of Collagen Type I structure.....	8
Figure 2-1: Schematic diagram of WEFS microscopy	17
Figure 2-2: Total internal reflection.....	18
Figure 2-3: Generation of evanescent field by total internal reflection	19
Figure 2-4: Schematic of a slab waveguide	23
Figure 2-5: Schemes for refractive index profiles and waveguide geometry	24
Figure 2-6: Schematic of Langmuir-Blodgett Trough.....	26
Figure 2-7: (a) Schematic of the orientation of amphiphilic molecules at the air-water interface (b) Schematic of monolayer deposition on a substrate.	27
Figure 2-8: Typical area-pressure isotherm	28
Figure 3-1: An example of orientation of collagen	33
Figure 3-2: Silanization process for hydrophobic glass surface	34
Figure 3-3: Scheme of contact angle determination	35
Figure 3-4: Hairy rod macromolecules	36
Figure 3-5: Surface pressure-area isotherm	40
Figure 3-6: Sketches of orientation distribution of collagen microfibrils.....	41
Figure 3-7: Sketches of collagen fibril orientations on symmetric samples	43

Figure 3-8: Sketches of collagen fibril orientations on asymmetric samples	44
Figure 3-9: Comparison of width to height displacement in three equal width samples.....	46
Figure 3-10: (a) Collagen film stored in air at 37°C (b) Collagen film stored in buffer solution at 37°C and (c) collagen film at elevated temperatures.	48
Figure 3-11: Quantitative data on the measured distances between two collagen fibrils vs. storage time or vs. temperature respectively.....	49
Figure 4-1: Formation of Cytosine-Thymine Dimer in DNA	55
Figure 4-2: SEM image of Nitrobacter sp. 263 exposed to gold chloride	56
Figure 4-3: (a) Bright field image and (b) corresponding WEFS image	59
Figure 4-4: Close view of a microcolony.	60
Figure 4-5: WEFS images with increasing exposure times	61
Figure 4-6: (a) Bright field image and (b) corresponding WEFS image	63
Figure 4-7: (a) Bright field image of a starting colony and an individual cell with the highest magnification (b) Corresponding WEFS image with exposure time of 2s (c) The intensity profile for the WEFS image.....	67
Figure 4-8: (a-d) WEFS and (e-h) bright field images of UV treated bacteria.....	70
Figure 4-9: Percentage of area occupied by individual bacteria or colony.....	71
Figure 5-1: Schematic of Flow cytometry	79
Figure 5-2: Single fixed and stained osteoblast	82
Figure 5-3: WEFS microscopy image of osteoblasts captured with an exposure time of 2s..	84
Figure 5-4: WEFS microscopy of osteoblasts with increasing exposure times.....	85

Figure 5-5: Fluorescence microscopy and WEFS microscopy detecting focal adhesions	88
Figure 5-6: Inspection of granularities in live osteoblasts	89
Figure 5-7: WEFS image of a MC3T3 cell with increasing exposure times	90

List of Abbreviation

α -MEM: α -Minimum essential medium

CD: Circular dichroism

DI: Deionized

DPBS: Dulbecco's phosphate-buffered saline

DNA: Deoxyribonucleic acid

EPS: Extra-cellular polymeric substance

999993ECM: Extracellular matrix

FBS: Fetal bovine serum

HeCd: Helium-Cadmium

HeNe: Helium-Neon

LB: Langmuir-Blodgett

NOB: Nitrite oxidizing bacteria

OTS: n-octadecyltrichlorosilane

RIE: Reactive ion etching

RICM: Reflection interference contrast microscope

SEM: Scanning electron micrograph

TC: Tropocollagen

TE: Transverse electric

TM: Transverse magnetic

TIRF: Total internal reflection fluorescence

TIRM: Total internal reflection microscope

UV: Ultraviolet

WEFF: Waveguide evanescence field fluorescence

WEFS: Waveguide evanescence field scattering

Chapter 1

1 Introduction

Imaging in biology is currently undergoing a radical change [1]. All living beings, including humans, are made of cells [2]. Researchers have been captivated with the visualization of cellular structures since the beginning of the optical microscopes. The study of living cells and their interactions with each other and their surfaces contributes to the treatments of various diseases. In cellular biology and implant development, the interaction between a cell and its substratum is of enormous interest for many years. The spreading and proliferation of a cell depends on the interaction between the cell and the substrate [3]. Cell adhesion is an important process for the assembly of individual cells and the organization of tissues in animals. The linkage of the adjacent cells together and/or to the extracellular matrix (ECM) and the connection of the adhesions systems to the intracellular cytoskeleton takes place via cell adhesion mechanisms [4][5][6]. Scientists are utilizing different kinds of microscopes to visualize the cellular components, processes and interaction between cells and their substrates. Fluorescence microscopy has been developed as an important technology in life science and medical imaging. For the visualization and quantification of adhesion proteins and contacts between a cell and its substrate, total internal reflection fluorescence (TIRF) microscopy is extensively used [7][8].

1.1 Total Internal Reflection Fluorescence (TIRF) Microscopy

In recent years total internal reflection fluorescent (TIRF) microscopy has proven to be a widely favorite tool for studying cell-substrate interactions at surfaces. TIRF utilizes the phenomenon of total internal reflection generating an evanescent wave at large angles of incidences. The evanescent wave in the total internal reflection fluorescence microscopy illuminates fluorescent particles in a thin region on a substrate surface and provides excellent resolution in the vertical direction and high signal to noise ratio [8]. TIRF microscopy allows for highly sensitive detection and even single molecules are possible to detect with this technology. Recently it has become a popular method for single molecule detection experiments [9]. However fluorescent labelling can be aggressive and

increases the risk of photo toxicity and photo bleaching effect. At present, there are two major non-fluorescent techniques available to visualize cell substrate contact region. One is reflection interference contrast microscopy (RICM) and the other is total internal reflection microscopy (TIRM) [10][11]. RICM is less sensitive than TIRF within the critical first 100 nm of the surface. TIRM implements the basic technology of TIRF without any fluorescence dye present in the sample and visualization is possible by creating an optical contrast due to scattering.

1.2 Waveguide based Microscopy

Over the past few years, different versions of waveguide total internal reflection microscopy systems have been reported. Imaging a fixed fibroblast cell on a waveguide interface by utilizing the evanescent field of the waveguide was attempted for the first time by H. M. Grandin et al. [12]. Grandin coupled a laser source into a planar waveguide via an optical grating integrated on it. This system offers high sensitivity of detection and multi-wavelength image, however the image quality obtained using this method was limited. A lot of stripy artifacts were present which are probably due to uneven illumination resulting from imperfections in the coupling grating. Agnarsson et al., used a symmetric waveguide structure to develop waveguide excitation fluorescence microscopy [13]. Chronis et al., have fabricated a lab-on-chip system where a microcavity filled with an optical quality polymer with a side wall mirror was used to couple a laser beam to a glass-sample interface achieving evanescent wave excitation of fluorescent samples. This system is also capable of rapid sample analysis as it is integrated with microfluids [14]. Asanov et al., developed a system with a beam conditioner that injects light at one end of the coverslip through a prism so that light is coupled into a rectangular cover slip [15]. Ramachandran et. al., exhibited an inexpensive TIRF device that utilizes LEDs to illuminate high index waveguides to achieve total internal reflection [16]. Most of this systems requires complicated optical set-ups and use of fluorescent labels to perform analysis on cells.

Waveguide Evanescence Field Fluorescence Microscopy (WEFF) was first developed by Abdollah Hassanzadeh in 2008 as an economical alternative to the TIRF microscopy available for commercial use [17]. Hassanzadeh et al., created a waveguide by

exchanging low polarizability ions with high polarizability ions and coupled a laser source to one end of the waveguide through a sub-micron grating to achieve propagating waveguide modes and the evanescent field [18][19].

1.3 Waveguide Evanescence Field Fluorescence (WEFF) Microscopy

Waveguide Evanescence Field Fluorescence microscopy (WEFF) is an evanescent field based microscopy technology which employs a waveguide to create the evanescence field at the waveguide surface. If a cell is cultured on the waveguide, the cell-substratum connection is illuminated by the evanescent field. In the WEFF method, laser light is coupled to a waveguide through an optical grating to generate an exponentially decaying evanescence field, which acts as the source of illumination to excite fluorescent dyes on the surface of the waveguide [3]. The fluorescence photons thus emitted then can be collected and imaged with a microscope connected to a camera. The illumination depth of the evanescent field is restricted to approximately 70-100 nm depending on the design of the waveguide. WEFF microscopy has a simple experimental set-up which includes an inverted microscope, a camera and a waveguide that serves as a microscope slide [20]. Therefore, only planar waveguides can be used. The WEFF microscopy implementing a multimode waveguide is able to use multiple evanescent field distributions and can be used to investigate thin film thicknesses and to visualize and quantify distances in cell-substrate contact regions. With WEFF, photobleaching and phototoxicity are also largely reduced due to the narrow depth of illumination of the specimens compared to other microscopy techniques.

1.4 Waveguide Evanescence Field Scattering (WEFS) Microscopy

Waveguide scattering microscopy was introduced by Frank Thoma et. al. for microstructures located on ion-exchanged waveguide surfaces [21]. Later, waveguide evanescence field scattering microscopy was very briefly attempted by Daniel Imruck on human muscle cells on ultrathin polymer coated waveguides [22]. Although the resulting images showed the shape and distributions of the cells with respect to the substrate, the

image quality was poor possibly because of the waveguides or due to the polymer film. Total internal reflection microscopy (TIRM), which is actually TIRF microscopy without fluorescence, was reported recently for the imaging of the attachment of microorganism to surfaces [11]. In all these techniques, image contrast was generated by the scattering intensity of the samples within the evanescent field.

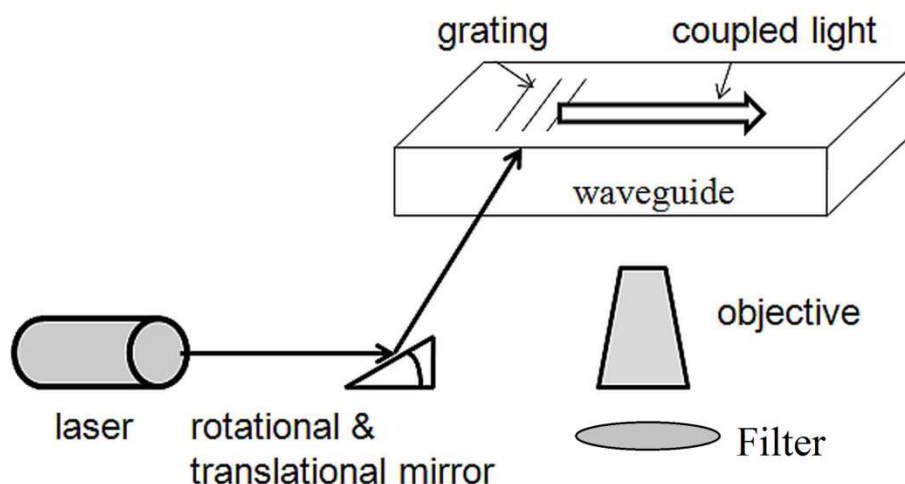


Figure 1-1: A schematic of WEFF microscopy where light from a laser is incident on a coupling grating by a rotating and translating mirror to achieve coupling angles. The light couples into the waveguide and propagates as a waveguide mode through it creating an evanescent field on the waveguide surface

Waveguide evanescent field scattering microscopy (WEFS) is introduced in this thesis by through experiments with osteoblasts and bacteria. It was shown to offer simplicity and high contrast imaging. WEFS technology also employs the evanescent field of a waveguide mode with an evanescent film thickness of 70-100 nm. The thickness of the evanescent film depends on the design of the waveguides. In this technique, the scattered photons from the biological cells illuminated by the evanescent field of a waveguide can be exclusively captured. Signals with high and low intensities are generated depending on the distance of the scattering sample from the surface of the waveguide and on the refractive index difference between the scatterer and its medium. WEFS technology permits imaging of adhesion points of a cell without the use of any kind of label thus absolutely no toxicity issues due to staining or other labelling forms are

present. This technology can be used for in-situ measurements of cell growth and proliferation without a disadvantageous effect of labeling on the cells.

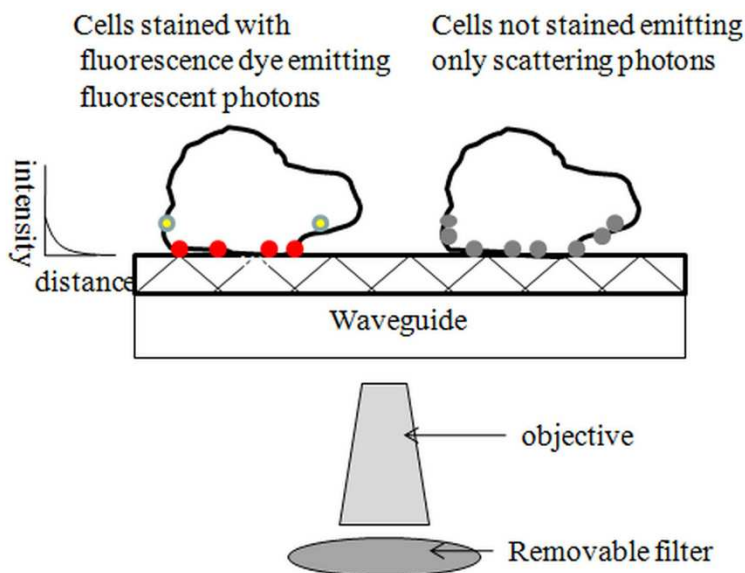


Figure 1-2: A schematic of comparison between WEFF and WEFS microscopy. In both cases, the same experimental set-up is used. In WEFF, the fluorescence photons from the specimen are captured with an objective implementing a filter to get rid of the excitation light whereas in WEFS, the specimen is not labelled and no filter is used.

Figure 1-2 shows the difference between WEFF and WEFS microscopy techniques. In WEFF microscopy, the cells are stained with a fluorescent dye and a filter is employed to remove the excitation wavelength of light thus capturing only the fluorescence photons for visualizing the cells. In WEFS microscopy technique, on the other hand, cells are not stained with any kind of labels. Thus cells are imaged by capturing the scattered photons by the source light only. No filters are necessary as in this case as only excitation wavelength of light is present. Otherwise there is no change in the experimental setup for the microscope.

1.5 Development of Waveguide Evanescent Field Scattering Microscopy (WEFS) for Application in Biology

In the present work, WEFS microscopy is employed to visualize biological cells and their interactions with the substrates. It is already mentioned that WEFM and WEFS has similar working principle and set-up. To alter from fluorescence mode to scattering mode, a few modifications were made. For scattering microscopy, it is important to keep the scattered and reflected light from outside to a minimum otherwise they will interfere with the imaging. For this reason, a sample holder was constructed with black plastic material. The purpose of using black plastic is that it absorbed all reflected light. The metal objectives and other metallic parts in the microscope were all covered with plastic tape or painted black for the same reason. A o-ring construct had to be made to use on the surface of the waveguides so that it can contain the growth medium while imaging live cells. The WEFM microscope was equipped with a green HeNe laser. To achieve more wavelengths of light with different powers, an multiline argon-ion laser (Melles-Griot, Model: 35 LAP 431-208) was included and aligned with the set-up in conjunction with the HeNe laser with the help of a few mirrors. The two lasers with different output wavelengths and powers also helped to switch between WEFM and WEFS mode. However, only the HeNe laser was used for the experiments done in this thesis. To achieve higher magnification and field of view, an 63x objective (ZEISS LD Plan-NEOFLUAR) was added and the height of the sample holder had to be adjusted to ensure sufficient distance is present between the sample holder and the 63x objective for proper focusing. A removable filter was used to block the fluorescent light when both fluorescent and scattering was present to capture only scattering image. The waveguides are the key component of WEFS microscopy. The high quality waveguides used in this work made it possible to capture the WEFS images free from non-uniform and inhomogeneous patterns.

1.6 Collagen

Collagen is the main structural component in the extracellular matrix (ECM) of all animals. In humans, collagen represents one third of the total protein, responsible for three quarters of the dry weight of skin, and is the most dominant component of the

extracellular matrix (ECM) [23]. The collagen molecule, the so called tropocollagen, is composed of three left-handed helical polypeptide chains forming a right-handed triple-helical structure with a length of 300 nm and a thickness of 1.5 nm as shown in Figure 1-3. The three chains are around 1000 amino acids in length. Between these chains, hydrogen bonds are formed which accounts for the strength in the structure. [24]. These chains can assemble to form different types and higher level structures. The collagen molecules align themselves along the helical axis and gather as a bundle to form collagen fibrils. Type I collagen is the major component which offers mechanical stability, strength and toughness to a range of tissues such as tendons, ligaments, skin, cornea, bone and dentin. The fibres formed by type I collagen gives tendons or ligaments their high tensile strength but other types of collagen usually form smaller or branched structures. For example type IV collagen does not form fibrils but a mesh like structure. This shows the versatility of collagen as a building material for tissues.

Most tissues in animal bodies display structural alignment of collagen fibrils. Depending on the functions of the tissues, the collagen fibres can be oriented in a particular direction or present layers of oriented fibres angled to each other or they can even be randomly distributed [25][26][27][28]. Imitating the natural fiber arrangements and orientations of collagen remains a major research in the field of medicine and tissue engineering as the oriented collagen fibrils can qualify for a suitable scaffold for cell-ECM interactions. [26] The advantage of this scaffold is that cells can be directly influenced by the alignment of collagen fibrils as they grow. The influence of collagen alignment on the growth and proliferation of both human fibroblast cells and stem cells has been studied before and it was found that the collagen coated substrates cause the cells to become aligned in one single direction and oriented parallel to the collagen orientation [29][30].

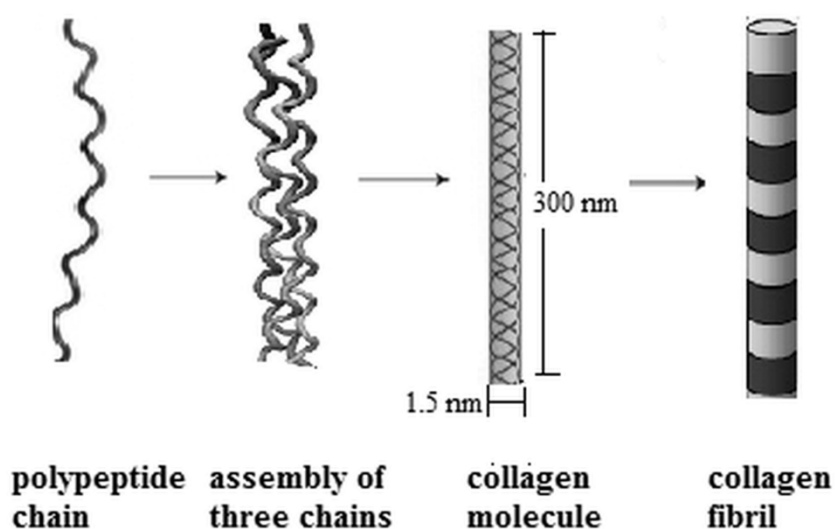


Figure 1-3: Schematic diagram of Collagen Type I structure. Three polypeptide chains form helical collagen molecule which is 300 nm in length and 1.5 nm in diameter. The collagen molecules associate to form collagen fibrils.

1.7 Langmuir-Blodgett Technology

Various approaches have been used previously to fabricate oriented collagen for artificial constructs for the replacement and regeneration of damaged tissues. Collagen from animals can be extracted, processed and used for different applications such as wound dressings, scaffolding, cornea augmentations etc. Sun et al. fabricated an ordered array of collagen microfibrils on a mica substrate from monomeric solutions of collagen [31]. This process was rapid and spontaneous and dependent on the crystallographic orientation of the mica substrates. However this method was unable to produce additional layers with different orientations. On gold coated substrates, thiol is immobilized first and collagen is chemisorbs to the thiol head groups [32]. It was not possible to achieve any order or orientation of collagen for the films fabricated by this process. Torbet et al. had been able to fabricate a 3D scaffold of orthogonal lamellae composed of aligned collagen fibrils by applying a horizontal magnetic field [33]

Langmuir-Blodgett (LB) technology can be used to successfully deposit collagen onto substrates [34][35][36]. According to Wagner et. al., it is possible to achieve an internal architecture within LB monolayer films of a synthetic polymer known as hairy rod

macromolecules. The hairy -rod molecules are comparable to the tropocollagen molecules when using the Langmuir-Blodgett (LB) technology for deposition [37]. Wegner et al. found that LB deposition of these hairy rods molecules onto surfaces resulted in the formation of monomolecular thin films with oriented molecules which preferentially align themselves along the dipping direction. Besides, Wegner et al. have shown that alignment of these molecules can be accomplished in both upstroke and downstroke film transfer directions,. Schwiegk et al. analyzed the influence of the flow, convergent or non-convergent, on the LB trough toward the substrate by varying the substrate width and thickness and found that alignment of the hairy rod polymers depend on the flow of the LB trough [38].

In a previous study by Tenboll et al., it was demonstrated that the LB fabrication process allows successful deposition of highly oriented collagen on hydrophobic substrates using either silanized glass or gold coated substrates carrying a self-assembled monolayer [26]. The LB process was also able to control the thickness of individual collagen layers, the orientation of successive layers, and the number of layers within the construct by controlled deposition of Type 1 collagen on both glass and gold-coated substrates.

1.8 Aim of the Thesis

The aim of the thesis is twofold:

- a)** In this thesis, the waveguide evanescent field scattering (WEFS) microscopy is presented showing its advantages and disadvantages. WEFS is introduced with its potential applicability as a label-free real-time imaging technology for living bacteria and animal cells, in particular the formation of contact regions between cells and their substratum. Waveguide evanescent field fluorescence (WEFF) microscopy was developed previously to image cell-substratum interactions onto a glass waveguide surface. Both WEFS and WEFF techniques employs the exponentially decaying evanescent field of waveguide modes of a waveguide. The big advantage of scattering over fluorescence microscopy is the label-free approach. This technique is able to contribute to long-term or time-lapse studies of cells because there is no photo-bleaching effect involved in imaging. In this

work, animal osteoblast cells and bacterial biofilms were imaged with WEFS microscopy. The WEFS microscopy proved to be a competent tool for creating high contrast images by analyzing the attachment of bacteria to surfaces and their development into microcolonies leading to biofilm formation. In case of the osteoblast cells, it was possible to locate the cell outline, the nucleus, the granular structures and/or adhesion points where the cell is attached to the substrate. The development of this new evanescent microscopy technology is a very valuable tool as it is able to deliver image information with high contrast and sensitivity. This study aims to demonstrate WEFS microscope system can be used for high contrast imaging of biofilms, cells, granularity in cells and cell/surface interface without any fluorescent labelling.

- b)** Collagen provides the structural support for most of the tissues in the body and is an essential element in the function of tissues. Collagen-based biomaterials in the field of tissue engineering applications are extensively used over the past decades. Collagen possesses a major advantage in being biodegradable and biocompatible. In case of tissue engineering, mimicking collagen natural fibre arrangement remains a major research goal. This thesis aims to study how LB technology can be used to fabricate particular collagen orientation distributions mimicking the collagen alignments in bone, tendon, cornea and other tissues and for widespread applications. In the present work, we applied the LB technology to form highly oriented collagen films on hydrophobic glass substrates of different geometrical sizes and shapes. The orientation distribution of the transferred LB films on glass substrates was studied using an optical microscope.

Due to time constraints, the combination of WEFS microscopy and collagen coated waveguides could not be performed. Waveguides can be coated with collagen films by LB technology in future and WEFS microscopy can be applied to study the suitability of collagen films as an appropriate collagen-based biomaterial.

1.9 References

1. Dobbie, I. M., King, E., Parton, R. M., Carlton, P. M., Sedat, J. W., Swedlow, J. R., & Davis, I. (2011). OMX: a new platform for multimodal, multichannel wide-field imaging. *Cold Spring Harb Protoc*, 2011, 899-909.
2. Vodyanoy, V. (2005). High resolution light microscopy of live cells. *Microscopy Today*, 13, 26-28.
3. Hassanzadeh, A. (2009). Waveguide evanescent field fluorescence microscopy & its application in cell biology, Ph.D. diss., The University of Western Ontario.
4. Fagotto, F., & Gumbiner, B. M. (1996). Cell contact-dependent signaling. *Developmental biology*, 180(2), 445-454.
5. Palovuori, R. (2003). Regulation of cell-cell adhesion and actin cytoskeleton in non-transformed and transformed epithelial cells. Ph.D. diss. University of Oulu.
6. Velinov, T., Asenovska, Y., Marinkova, D., Yotova, L., Stoitsova, S., Bivolarska, M., & Stavitskaya, L. (2011). Total internal reflection imaging of microorganism adhesion using an oil immersion objective. *Colloids and Surfaces B: Biointerfaces*, 88(1), 407-412.
7. Todd, I., Mellor, J. S., & Gingell, D. (1988). Mapping cell-glass contacts of *Dictyostelium amoebae* by total internal reflection aqueous fluorescence overcomes a basic ambiguity of interference reflection microscopy. *Journal of cell science*, 89(1), 107-114.
8. Toomre, D., & Manstein, D. J. (2001). Lighting up the cell surface with evanescent wave microscopy. *Trends in cell biology*, 11(7), 298-303.
9. George, N. (2004). TIRF microscopy: the evanescent wave of the future. *American laboratory*, 36(8), 26-28.
10. Curtis, A. S. G. (1964). The mechanism of adhesion of cells to glass A study by interference reflection microscopy. *The Journal of cell biology*, 20(2), 199-215.
11. Byrne, G. D., Pitter, M. C., Zhang, J., Falcone, F. H., Stolnik, S., & Somekh, M. G. (2008). Total internal reflection microscopy for live imaging of cellular uptake of sub-micron non-fluorescent particles. *Journal of Microscopy*, 231(1), 168-179.

12. Grandin, H. M., Städler, B., Textor, M., & Vörös, J. (2006). Waveguide excitation fluorescence microscopy: a new tool for sensing and imaging the biointerface. *Biosensors and Bioelectronics*, 21(8), 1476-1482.
13. Agnarsson, B., Ingthorsson, S., Gudjonsson, T., & Leosson, K. (2009). Evanescent-wave fluorescence microscopy using symmetric planar waveguides. *Optics express*, 17(7), 5075-5082.
14. Chronis, N., & Lee, L. P. (2004). Total internal reflection-based biochip utilizing a polymer-filled cavity with a micromirror sidewall. *Lab on a Chip*, 4(2), 125-130.
15. Asanov, A., Zepeda, A., & Vaca, L. (2010). A novel form of Total Internal Reflection Fluorescence Microscopy (LG-TIRFM) reveals different and independent lipid raft domains in living cells. *Biochimica et Biophysica Acta (BBA)-Molecular and Cell Biology of Lipids*, 1801(2), 147-155.
16. Ramachandran, S, Cohen, D. A., Quist, A. P., and Lal, R., (2013). High performance, LED powered, waveguide based total internal reflection microscopy. *Scientific Reports*. doi:10.1038/srep02133.
17. Hassanzadeh, A., & Mittler, S. (2011). Waveguide evanescent field fluorescence microscopy: high contrast imaging of a domain forming mixed lipid Langmuir-Blodgett monolayer mimicking lung surfactant. *Journal of Biomedical Optics*, 16(4), 046022-046022.
18. Hassanzadeh, A., Nitsche, M., Armstrong, S., Nabavi, N., Harrison, R., Dixon, S. J., Langbein, U. & Mittler, S. (2010). Optical waveguides formed by silver ion exchange in Schott SG11 glass for waveguide evanescent field fluorescence microscopy: evanescent images of HEK293 cells. *Journal of Biomedical Optics*, 15(3), 036018-036018.
19. Hassanzadeh, A., Armstrong, S., Dixon, S. J., & Mittler, S. (2009). Multimode waveguide evanescent field fluorescence microscopy: measurement of cell-substratum separation distance. *Applied Physics Letters*, 94(3), 033503-033503.
20. Halfpap, C. (2010). Optimization of Sputtered Waveguides for Evanescent Microscopy. Master Thesis, University of Applied Sciences, Russelheim.

21. Thoma, F., Armitage, J., Trembley, H., Menges, B., Langbein, U., & Mittler-Neher, S. (1998, September). Waveguide scattering microscopy in air and water. In Society of Photo-Optical Instrumentation Engineers (SPIE) Conference Series (Vol. 3414, pp. 242-249).
22. Imruck, D. (2009), Evanescent Field Waveguide Fluorescence Microscopy of Cells on Biopolymers, Master Thesis, University of Applied Sciences, Russelheim.
23. Shoulders, M. D., & Raines, R. T. (2009). Collagen structure and stability. Annual review of biochemistry, 78, 929.
24. JPK Instruments, "Observing the Levels of Alignment and Organisation in Collagen Structures Using Atomic Force Microscopy"
25. Hulmes, D. J. (2002). Building collagen molecules, fibrils, and suprafibrillar structures. Journal of structural biology, 137(1), 2-10.
26. Tenboll, A., Darvish, B., Hou, W., Duwez, A. S., Dixon, S. J., Goldberg, H. A., Grohe, B. & Mittler, S. (2010). Controlled deposition of highly oriented type I collagen mimicking in vivo collagen structures. Langmuir, 26(14), 12165-12172.
27. Currey, J. D. (2002). Bones: structure and mechanics. Princeton University Press.
28. An, Y. H., & Draughn, R. A. (Eds.). (2010). Mechanical testing of bone and the bone-implant interface. CRC press.
29. Stylianou, A., Politopoulos, K., Kyriazi, M., & Yova, D. (2011). Combined information from AFM imaging and SHG signal analysis of collagen thin films. Biomedical Signal Processing and Control, 6(3), 307-313.
30. Nahar, Q., Quach, D. M. L., Darvish, B., Goldberg, H. A., Grohe, B., & Mittler, S. (2013). Orientation distribution of highly oriented Type I Collagen deposited on flat samples with different geometries. Langmuir. 29(22), 6680-6686.
31. Sun, M., Stetco, A., & Merschrod S, E. F. (2008). Surface-templated formation of protein microfibril arrays. Langmuir, 24(10), 5418-5421.
32. Mrksich, M., & Whitesides, G. M. (1996). Using self-assembled monolayers to understand the interactions of man-made surfaces with proteins and cells. Annual review of biophysics and biomolecular structure, 25(1), 55-78.

33. Torbet, J., Malbouyres, M., Builles, N., Justin, V., Roulet, M., Damour, O., Oldberg, A., Ruggiero, F. & Hulmes, D. J. (2007). Orthogonal scaffold of magnetically aligned collagen lamellae for corneal stroma reconstruction. *Biomaterials*, 28(29), 4268-4276.
34. Chen, Q., Xu, S., Li, R., Liang, X., & Liu, H. (2007). Network structure of collagen layers absorbed on LB film. *Journal of colloid and interface science*, 316(1), 1-9.
35. Usha, R., Dhathathreyan, A., Mandal, A. B., & Ramasami, T. (2004). Behavior of collagen films in presence of structure modifiers at solid–liquid interface. *Journal of Polymer Science Part B: Polymer Physics*, 42(21), 3859-3865.
36. G. G. Fuller.(2007). Langmuir-Blodgett films of oriented collagen films as cell culture substrates, 81st ACS Colloid & Surface Science Symposium.
37. Wegner, G. (2003). Nanocomposites of Hairy-Rod Macromolecules: Concepts, Constructs, and Materials. *Macromolecular chemistry and physics*, 204(2), 347-357.
38. Schwiegk, S., Vahlenkamp, T., Xu, Y., & Wegner, G. (1992). Origin of orientation phenomena observed in layered Langmuir-Blodgett structures of hairy-rod polymers. *Macromolecules*, 25(9), 2513-2525.

Chapter 2

2 Principle of WEFS Microscopy and Fundamentals

This chapter presents the working principle and the set-up for WEFF/WEFS microscopy. The fundamental theory of waveguides like total internal reflection, evanescent field, planar waveguides and the modes present in a waveguide are discussed. The Langmuir-Blodgett film deposition techniques with the Langmuir-Blodgett trough and area-pressure isotherms are explained.

2.1 WEFS Working Principle

The WEFS microscopy utilizes the evanescent field of a waveguide to illuminate samples for example a biological specimen. The evanescent field represents the light source for WEFS microscopy with a decaying exponential field distribution from the waveguide surface into the cladding material which can be air ($n=1$) or a liquid medium for cell culture. The intensity distribution of the evanescent field stays constant over time. The intensity of light decreases vertically with increasing distance from the surface of the waveguide [1]. This exponentially decaying evanescent field is exploited in WEFS microscopy to visualize the samples or the cells on the surface of the waveguides. The propagating waveguide mode is usually seen as a light streak. Both WEFF and WEFS microscopy have a similar operating principle and set-up. For WEFF microscopy, the plasma membrane of the cells are stained with a fluorescent dye and the resulting fluorescence signals are captured with the help of a camera and a filter which blocks the excitation wavelength of the dye. But fluorescent staining has several disadvantages like toxicity which restricts their application in live cell imaging. They also show photobleaching which limits the time for examining and analyzing the cells. Moreover fluorescent dyes are expensive. On the other hand, for WEFS microscopy, only scattered photons from the specimen are required to acquire the images. As a result, there is no need for the fluorescent labelling. No filters are necessary either as there is only one wavelength of light. This enables the analyzing and imaging of biological samples for an infinite amount of time and use of live cells. WEFS microscopy offers easy sample

preparation without labelling and/or fixation. A schematic of WEFS microscopy is given in Figure 2-1.

2.2 WEFS Microscopy Setup

The main component in WEFS microscopy is the waveguide which is utilized as a microscope slide. This waveguide is the central element of the microscopy system where all the observations are taking place. The microscopy setup consists of a regular inverted microscope (Axiovert 25CFI, Karl-Zeiss, Germany) with several objective lenses (10x (Olympus-U plan FLN), 20x (Olympus LUC plan FLN), 40x (ZEISS LD Plan-NEOFLUAR) and 63x (ZEISS LD Plan-NEOFLUAR)) to achieve different field of views and magnifications of the specimen. The inverted microscope is favourable for the study of cells because the specimen is located on top of the waveguide. This allows easy and user-friendly manipulation of the live cells and the medium. The cells and their medium on the surface of the waveguide are held in place in a chamber formed with an o-ring construct. A green HeNe laser $\lambda = 543$ nm (0.5 mW, LHGP-0051 Research Electro-Optics) is used as the illumination source for coupling a propagating waveguide mode to create the evanescent field. The laser beam is incident on the coupling grating of the waveguide with the help of a mirror mounted on a rotating and translating stage. To achieve a specific waveguide mode the mirror has to be rotated and laterally shifted to a certain angle to couple the light to waveguide. The sample is illuminated with the coupled waveguide mode. A polarizer is used to obtain either TE mode or TM mode. A digital camera (Pursuit XS, Diagnostic Instruments) is employed to acquire the images from the samples and connected to the microscope with a specific coupler (HRD076-CMT, Diagnostic Instruments). The camera is connected to a computer with a imaging software (Image Pro Express 6, Media Cybernetics Inc.) for image capturing with a range of exposure times. As only scattered light from the samples were used for visualizing the images, no filters or any fluorescent dyes were necessary.

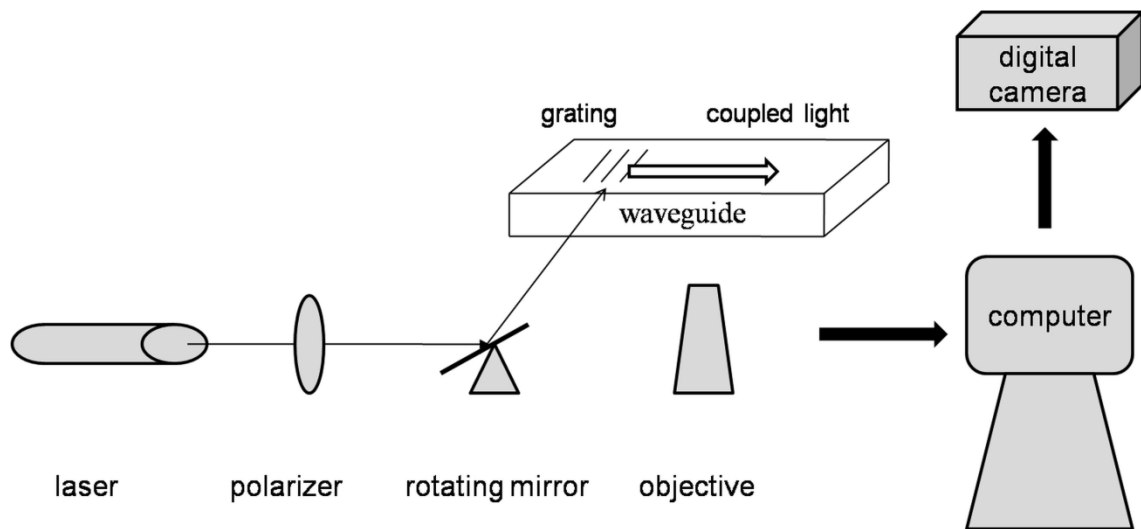


Figure 2-1: Schematic diagram of WEFS microscopy

2.3 Fundamental Theory of Waveguides

2.3.1 Total Internal Reflection

Total internal reflection occurs when light propagates from a dielectric medium with a higher refractive index n_1 through an interface to another dielectric medium with a lower refractive index n_2 where $n_1 > n_2$ [2][3]. Light rays that are incident on the boundary of an interface at angles higher than the critical angle of reflection undergo total internal reflection. As a result, no light is refracted. The critical angle of reflection φ_{crit} is the angle of incidence at which the light is refracted such that it travels along the interface at $\varphi_t = 90^\circ$.

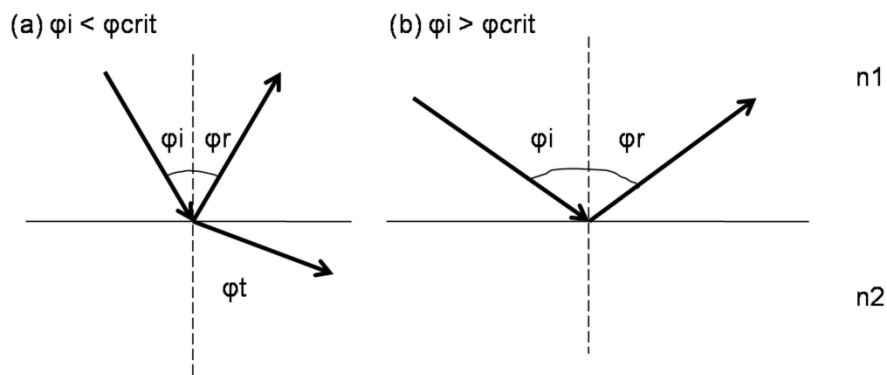


Figure 2-2: Total internal reflection at an interface between two media with refractive indices n_1 and n_2 ($n_1 > n_2$). (a) A light ray reflects and refracts when incident with an angle less than critical angle $\varphi_i < \varphi_{\text{crit}}$ and (b) Total internal reflection occurs when light rays are incident with angles larger than critical angle ($\varphi_i > \varphi_{\text{crit}}$).

For total internal reflection, the incident angle must be larger than the critical angle which is represented with the Snell's law:

$$n_1 \cdot \sin \varphi_i = n_2 \cdot \sin \varphi_t \quad (2.1)$$

where φ_i and φ_t are angles of incidence and refraction respectively.

2.3.2 Evanescence Field

Evanescence waves are produced when light waves are reflected off an interface at an angle which is larger than the critical angle ϕ_{crit} so that total internal reflection occurs. In ideal cases, no light should escape the medium with the higher refractive index. Nevertheless, a portion of light called the “evanescent field” penetrates into the medium with the lower index of refraction. The electric field of this film of light exponentially decays with the distance and displays its highest intensity at the interface [4][5][6]. As intensity is the square of the electric field, intensity always shows the evanescent behavior.

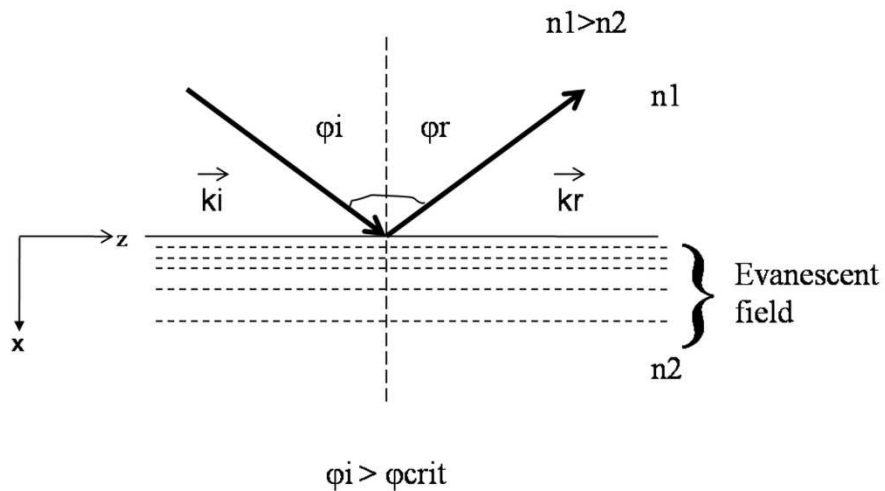


Figure 2-3: Generation of evanescent field by total internal reflection of the incident light beam. The dashed lines represent the evanescent field which has highest intensity at interface and decays exponentially with distance away from the interface. Here, i and r stands for incident and reflection respectively.

Light is an electromagnetic wave. Every plane wave of light can be described with the help of electromagnetic field equations. Light can be described by the following equation for electric field as:

$$\vec{E}(r, t) = \vec{E}e^{j(\vec{k}\vec{r}-\omega t)} \dots\dots\dots(2.2)$$

In this equation, \vec{E} is the amplitude, j the imaginary unit, \vec{r} the position vector, \vec{k} the wave vector, ω is angular frequency, and t the time.

Wave vector \vec{k} in this equation can be represented by using the Cartesian coordinate system as :

$$\vec{k} = |\vec{k}|\{\cos\varphi, 0, \sin\varphi\}.....(2.3)$$

and this can be normalized by,

$$|\vec{k}| = \frac{2\pi}{\lambda}.....(2.4)$$

Using the Pythagoras theorem, the trigonometric functions in equation (2.4) can be rewritten as,

$$\vec{k} = \left\{ \sqrt{\left(\frac{2\pi}{\lambda} n\right)^2 - k_z^2}, 0, k_z \right\}.....(2.5)$$

where $n = n_1$ for the incident and reflected wave and $n = n_2$ for transmitted wave. k_z in equation (2.5) can be described by:

$$k_z = \frac{2\pi}{\lambda} n_1 \sin \varphi_i = \frac{2\pi}{\lambda} n_2 \sin \varphi_t$$

In the case of total internal reflection, the incident angle φ_i is greater than the critical angle φ_{crit} and k_z becomes larger. As a result, $\sqrt{\left(\frac{2\pi}{\lambda} n\right)^2 - k_z^2}$ is negative and there is no real solution for the square root. With the imaginary unit $j=\sqrt{-1}$, this can be solved as,

$$\vec{k} = j \left\{ \sqrt{k_z^2 - \left(\frac{2\pi}{\lambda} n_2\right)^2}, 0, k_z \right\}.....(2.6)$$

From equation (2.2) and (2.6) we get,

$$\vec{E}(\vec{r}, t) = \vec{E} \cdot \left(\mathbf{e}^{-\sqrt{k_z^2 - \left(\frac{2\pi}{\lambda} n_2\right)^2} \cdot x} \right) \cdot e^{-jk_z \cdot z} \cdot e^{-j\omega t} \dots\dots\dots(2.7)$$

Hence, there is an exponentially decaying component in the x-direction and a pure propagating component in the z direction along the interface. With total internal reflection, this exponentially decaying electric field in the x-direction is called the evanescent field. The evanescent field is a thin film of light which can be used as a source of illumination for microscopy. The penetration depth of this film is defined by the depth where the film is decayed to e^{-1} :

$$d = \frac{\lambda}{2\pi\sqrt{n_2^2 \sin^2(\varphi_i) - n_1^2}} \dots \dots \dots (2.8)$$

2.3.3 Optical Waveguides

The optical waveguide is the most important element of the WEFS microscopy. The structure of a dielectric waveguide consists of a high refractive index optical medium, called the core which is surrounded by lower refractive index media, called the substrate and the cladding [7]. The refractive index of core needs to be higher than that of the substrate and the cladding. A guided optical wave propagates in the waveguide along the longitudinal direction. There are two basic types of waveguides which are planar waveguides and non-planar waveguides. In a non-planar waveguide which has two-dimensional transverse optical confinement, the cladding surrounds the core in all transverse directions, and the index of refraction $n(x, y)$ is a function of both x and y coordinates. An example of non-planar waveguides is the optical fiber. On the other hand, a planar waveguide has optical confinement in only one transverse direction, the core is sandwiched between a substrate and a cladding in only one direction, say the x direction, with an index profile $n(x)$ (Figure 2-5). For this thesis, we will only consider planar waveguides as for WEFS microscopy, planar waveguides have major advantages such as offering a wide illumination area, simple alignment, easy and inexpensive fabrication procedures.

The waveguides used in this thesis were fabricated by Mike Morawitz at RheinMain University of Applied Sciences, Department of Engineering Sciences, Rüsselsheim Geisenheim, Germany. The optical grating was fabricated using interferometric lithography, a laser interference lithography setup and reactive ion etching. After the grating was established within the substrate, the waveguide layer was deposited by a

radio frequency (RF) sputter process. The fused silica glass substrates used were purchased from Tedpella and Advaluetech (D-series) and from Hebo (E and G series) with dimensions 25x50 mm and a thickness of 1 ± 0.1 mm. The waveguiding layer for the series D, E and G were sputtered with the P-LASF 47 from Schott (Mainz) with a bulk refractive index of $n = 1.8111$. However, the refractive index of the sputtered waveguide layer was found to be increased to $n_1 = 1.8487 \pm 0.0133$ [8].

2.3.4 Planar Waveguides

A scheme of a planar waveguide is shown in Figure 2-4. The core region of the waveguide has a high refractive index n_1 and is deposited on a substrate which has a lower refractive index n_2 . A cladding is located on top of the waveguide with a refractive index of n_3 . n_3 can be equal to 1 if the region above the core is air or it can have some other value if the cladding is chosen as water or any other liquid medium. The refractive indices of these three layers should be: $n_1 > n_2$ and n_3 [9][10].

When the condition for total internal reflection at both interfaces are met, the wave inside the core is completely reflected at both interfaces and is trapped within the core. Every time light gets reflected, a phase shift occurs. This phase shift depends on the polarization and the angle of incidence ϕ with respect to the normal to the interface. There are two different types of polarization which are defined by their orientation of the electromagnetic field to the plane of incidence. Hence, the phase shift is also a function of the polarization. A mode in the waveguide is defined as a transverse field pattern whose amplitude and polarization profiles remain constant along the longitudinal z coordinate. Modes whose electric fields are oscillating in the y -direction and are vertically oriented are known as transverse electric (TE) modes, whereas modes in parallel orientation are known as transverse magnetic (TM). To achieve a guided mode profile, the waves in the film have to be coherent so that constructive interference between all reflected beams can occur. The two wave types that are propagating, the one reflected at the substrate and the one that is reflected at the cladding, carry positive and negative x -components in their respective wave vectors. The z -components of the wave vectors are equal. To achieve a constructive interference the sum of all phase shifts, the

optical retardation between the two beams and the two phase shifts at reflection, need to be an integer multiple of 2π .

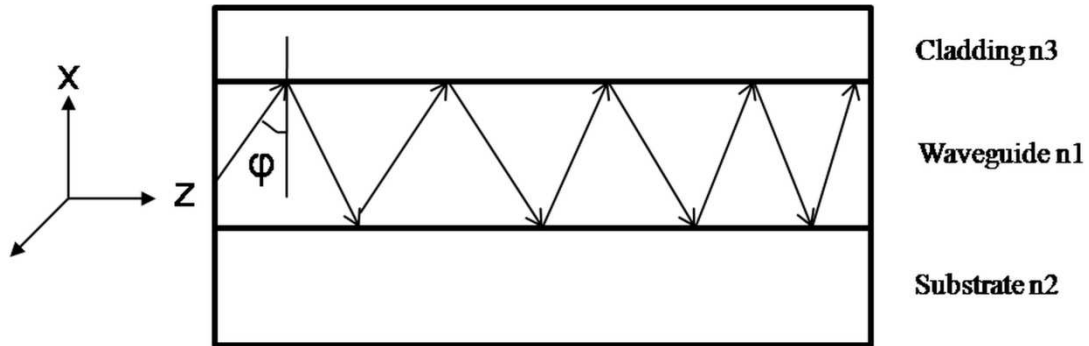


Figure 2-4: Schematic of a slab waveguide with core refractive index n_1 , substrate refractive index n_2 and cladding refractive index n_3 . The incoming ray makes an angle φ with the normal to the interface as shown.

2.3.5 Modes in a Waveguide

A waveguide mode is a transverse field pattern whose amplitude and polarization remain constant along the longitudinal z coordinate. A guided mode can exist only when a transverse resonance condition is satisfied that is when the repeatedly reflected wave undergoes constructive interference. Each mode has a typical field distribution and can be described by the propagation constant β as:

$$\beta_m = k_0 n_1 \sin \varphi_m \quad (2.9)$$

Since m can have only integral values, only certain discrete values of $\varphi = \varphi_m$ are able to satisfy the resonance condition. As a result, only discrete values of the propagation constant β_m can be obtained for guided modes specified by the mode number m . The guided mode with $m = 0$ is called the fundamental mode and those with $m = 1, 2, \dots$ are called higher-order modes. In this thesis, all the experiments were done with multimode planar waveguides.

2.3.6 Effective Refractive Index

The different modes in a waveguide have different propagation velocities in the x -direction [11]. Therefore an effective refractive index n_{eff} is defined for each mode as

$$n_{\text{eff}} = \beta_m / k_0 \quad (2.10)$$

The effective refractive index of a mode is smaller than the refractive index of the guiding layer because the evanescent field is influenced by the refractive indices of the cover and the substrate. For a planar waveguide as shown in figure 2.3 the refractive indices are:

$$n_3, n_2 < n_{\text{eff}} < n_1 \quad (2.11)$$

2.3.7 Refractive Index profiles

A waveguide in which the refractive index profile has sudden changes between the core and the cladding is called a step-index waveguide, while one in which the index profile varies gradually is called a graded-index waveguide. A simple step index waveguide represent three layers with three distinct refractive indices with no transition while a gradient index waveguide consists of an index profile along the depth which changes continuously [12].

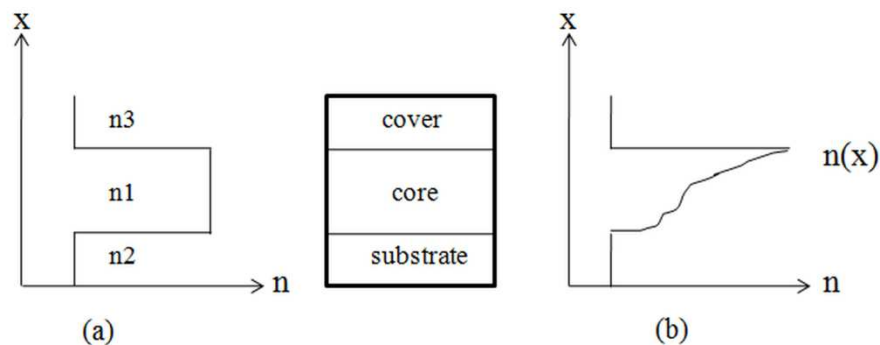


Figure 2-5: Schemes for refractive index profiles and waveguide geometry for (a) Step index and (b) graded index waveguides

2.3.8 Coupling Grating

Grating couplers are used to couple light into waveguides. With a grating coupler, light can be coupled into a waveguide and multimode coupling is possible to achieve [11]. The advantage of using a coupling grating is that it is easy to integrate into the WEF/WEFS microscope system. However, grating couplers has weak coupling efficiency and costly and time-consuming fabrication process. When the wave vector of a diffracted incident light beam at a given diffraction order matches to the wave vector of a distinct mode, the light is coupled resonantly into the waveguide. For each mode, there is a specific coupling angle. The grating has a certain periodicity Λ or a grating constant $g = 1/\Lambda$. The shape and amplitude of this constant depends on the manufacturing process. The normalized grating vector pointing perpendicular to the grating grooves is given by:

$$|\vec{G}| = \frac{2\pi}{\Lambda} \quad (2.12)$$

The effective refractive index can be measured by:

$$N_{\text{eff}} = n_1 \sin \phi_i + O \frac{\lambda}{\Lambda} \quad (2.13)$$

where n_1 the refractive index of cover, O the diffraction order, λ the wavelength of laser, ϕ_i the resonant coupling angle of the mode. The grating was fabricated with a positive photoresist AZ 1505 (Microchemicals) [8]. It was then interferometrically exposed by an helium-cadmium (HeCd) laser at 441.6 nm. A sinusoidal varying pattern in photoresist was obtained after development in AZ 726MIF (MicroChemicals). The structure transfer of the sinusoidal shaped grating from the photoresist into the substrate was achieved by reactive ion etching (RIE). Sulfur hexafluoride (SF_6) was used as the process gas. All of the mentioned work on grating coupler was carried out at the RheinMain University of Applied Sciences, Department of Engineering Sciences, Russelsheim, Germany.

2.4 Langmuir-Blodgett (LB) Trough

Langmuir-Blodgett technology is a promising technology for the fabrication of ultra-thin, highly ordered organic films. With this method monolayers are formed on the surface of a liquid with a high surface tension, by spreading non-volatile substances dissolved in a

volatile solvent onto the surface of the liquid. Spreading occurs when the molecules, typically amphiphilic, possessing a hydrophilic head and a hydrophobic tail are attracted to the air-water interface more than they attract each other. A one molecule thick film, termed Langmuir-Blodgett monolayer, is formed provided that the area of the surface is sufficient to accommodate all the molecules spread [13][14].

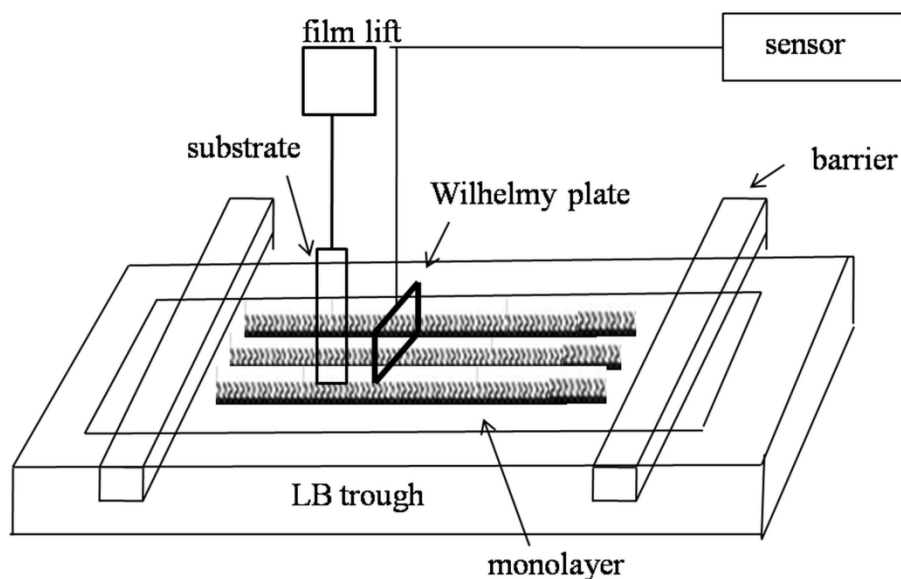


Figure 2-6: Schematic of Langmuir-Blodgett Trough

A Langmuir-Blodgett trough consists of an open Teflon container which holds a liquid called sub-phase on which a monolayer can be spread, a pair of barriers to allow film compression and a Wilhelmi balance plate for measuring surface pressure as well as a film lift for deposition purposes. The monolayer is spread on the air-water interface of the aqueous sub-phase with open barriers, then the solvent is allowed to evaporate before the film is compressed by means of the moveable barriers. The area per molecule is obtained from the total area given by the barrier position sensor. The film lift controls the immersion and withdrawal of a solid substrate for monolayer deposition.

2.5 Langmuir-Blodgett (LB) Films

As already mentioned, monolayer materials are applied to the substrate surface by dissolving them in an appropriate organic, volatile solvent [15]. The trough is filled with

water as sub-phase and the material is spread onto the air-water interface drop by drop between the barriers. The solvent evaporates within a short time and the molecules are then left spread out along the entire water surface. The monomolecular layer, which is known as the Langmuir-Blodgett monolayer, is compressed with the barriers and undergoes two phase transitions: gas-analog-to-liquid analog and liquid-analog-to-solid-analog. The amphiphilic nature of the molecules ensure that the individual molecules are aligned in the same direction with respect to the air-water interface: hydrophilic parts immersed in the water and hydrophobic parts sticking out in the air. Transferred Langmuir-Blodgett films are fabricated by immersing a substrate into the monolayer-covered subphase. Repeated dipping of the substrate through the monolayer at the air-water interface at a chosen, stabilized pressure (through feedback loop between Wilhelmy system and barrier control) will result in the deposition of a multilayer structures. A good deposition depends on monolayer molecules, pH of the subphase, temperature, dipping speed and on the particular molecules used [13].

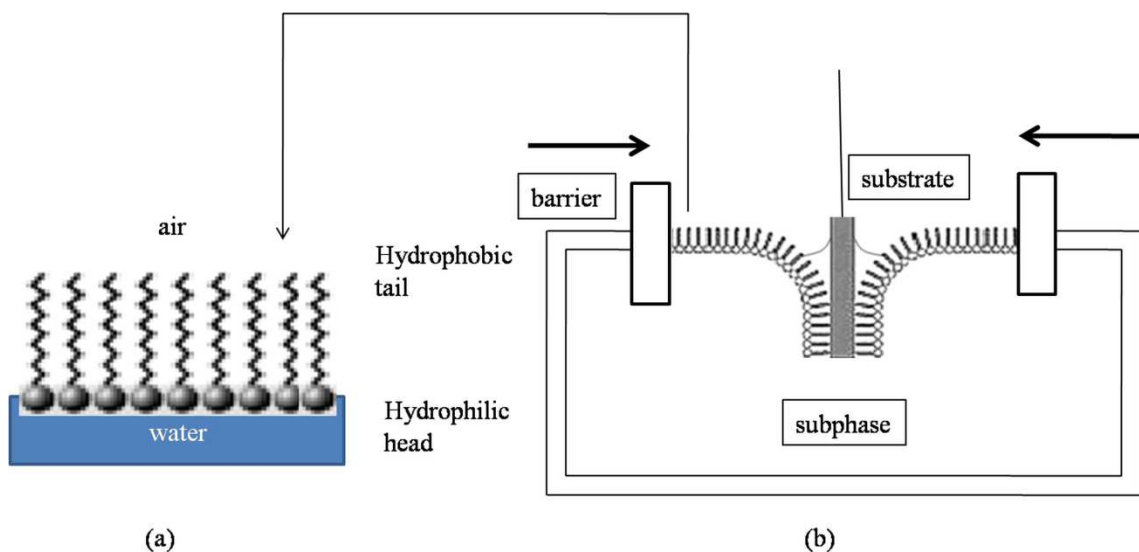


Figure 2-7: (a) Schematic of the orientation of amphiphilic molecules at the air-water interface (b) Schematic of monolayer deposition on a substrate.

2.6 Surface Pressure-Area Isotherm

An important indicator of the monolayer properties and its behavior is given by measuring the surface pressure as a function of the area available to the molecules [16] [17]. This procedure is carried out at constant temperature and is known as a surface pressure-area isotherm. While the layer is compressed and the surface pressure increases, it passes the equivalent states of vapour, liquid and solid seen in the area-pressure isotherms as kinks. This has to be studied as it provides information about the behaviour and the maximum pressure applicable to the used substance. When the state of a solid is reached and the layer is further compressed, a collapse of the monolayer occurs due to monolayer breakdown. Usually the deposition is carried out at $\sim 3/4$ of the maximum pressure to ensure that the monolayer is not collapsed [6]. To achieve a reproducible result, repeated compressions and expansions may be necessary depending on the material being studied,. A schematic of the surface pressure vs. area is shown in Figure 2-8.

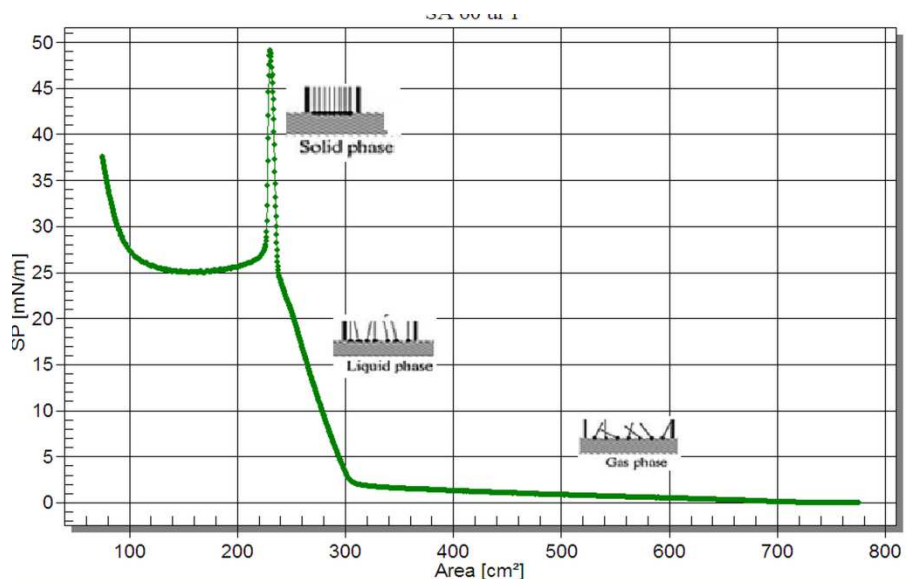


Figure 2-8: Typical area-pressure isotherm with schemes of molecular alignment in the three phases: gas analog, liquid analog and solid analog.

In this thesis, LB technology was used to fabricate thin film coatings of type I collagen. Collagen does not behave as a typical LB material as it is not amphiphilic. Collagen is

hydrophobic and therefore able to be spread onto the air-water interface without dissolving into the water subphase. As we recall from chapter 1, the behavior of collagen molecules during film processing is comparable to a particular class of synthetic polymers known as hairy rod polymers which were designed to be hydrophobic in nature. LB technology was used previously in our laboratory to deposit collagen on glass substrates [18]. It was found that the deposited individual collagen films had thicknesses up to 20 nm which was much thicker than the theoretical thickness of 1.5 nm of a collagen monolayer. There was no film collapse in the area-pressure isotherms which depend on the amount of material spread. The deposited films contained a matrix of thick fibrillar aggregates. With this technique, it was possible to control the thickness of individual layers, the orientation of collagen fibrils and the number of layers within the construct. LB technology was employed in this thesis to deposit collagen thin films on hydrophobic substrates of different geometrical shaped glass substrates of various sizes.

2.7 References:

1. Harlepp, S., Robert, J., Darnton, N. C., & Chatenay, D. (2004). Subnanometric measurements of evanescent wave penetration depth using total internal reflection microscopy combined with fluorescent correlation spectroscopy. *Applied physics letters*, 85(17), 3917-3919.
2. Snyder, A. W., & Love, J. (1983). *Optical waveguide theory* (Vol. 190). Springer.
3. Syms, R. R., & Cozens, J. R. (1992). *Optical guided waves and devices* (pp. 138-139). London: McGraw-Hill.
4. de Fornel, F. (2001). *Evanescent waves: from Newtonian optics to atomic optics* (Vol. 73). Springer.
5. Halfpap, C. (2010). *Optimization of Sputtered Waveguides for Evanescent Microscopy*. Master's Thesis, The University of Western Ontario.
6. Imruck, D. (2009). *Evanescent Field Waveguide Fluorescence Microscopy of Cells on Biopolymers*. Master's Thesis, The University of Western Ontario.
7. Liu, J. M. (2005). *Photonic devices* (Vol. 58). Cambridge: Cambridge University Press.

8. Morawitz, M. (2012). distance Determination via Waveguide Evanescent Field fluorescence Microscopy. Master's Thesis, The University of Western Ontario.
9. Okamoto, K. (2010). Fundamentals of optical waveguides. Second Edition (Optics and Photonics Series). Access Online via Elsevier.
10. Doerr, C. R., & Kogelnik, H. (2008). Dielectric waveguide theory. *Journal of Lightwave Technology*, 26(9), 1176-1187.
11. Saleh, B. E., Teich, M. C., & Saleh, B. E. (1991). Fundamentals of photonics (Vol. 22). New York: Wiley.
12. Tröger, F. (Ed.). (2007). Springer handbook of lasers and optics. Springer-Verlag New York.
13. Oliveira Jr, O. N. (1992). Langmuir-Blodgett films—properties and possible applications. *Brazilian Journal of Physics*, 22, 60-69.
14. Hussain, S. A. (2011). Langmuir-Blodgett Films. GRIN Verlag.
15. Petty, M. C. (1996). Langmuir-Blodgett films: an introduction. Cambridge University Press.
16. Somasundaran, P. (Ed.). (2006). Encyclopedia of surface and colloid science (Vol. 1). CRC Press.
17. Iwamoto, M., & Wu, C. X. (2001). The physical properties of organic monolayers. River Edge, NJ: World Scientific.
18. Tenboll, A., Darvish, B., Hou, W., Duwez, A. S., Dixon, S. J., Goldberg, H. A., Grohe, B. & Mittler, S. (2010). Controlled deposition of highly oriented type I collagen mimicking in vivo collagen structures. *Langmuir*, 26(14), 12165-12172.

Chapter 3

3 Orientation and Orientation Distribution of Collagen Deposited with Langmuir-Blodgett Technology onto Flat Surfaces with Different Geometrical Shapes

This chapter describes the deposition of collagen molecules with the Langmuir-Blodgett film deposition technique and how the orientation and its distribution on the samples was investigated and found. Collagen was deposited on different geometrically shaped glass substrates. For the deposition, it was necessary due to the hydrophobic nature of collagen, to modify the surface of the glass substrates to achieve hydrophobic glass substrates. Therefore, attractive hydrophobic interaction between the collagen and the substrate was achieved. Previous research, on rectangular substrates only, had shown that collagen aligns in an LB-process preferentially parallel to the dipping direction. It was found here that collagen molecule alignment distribution was highly dependent on the geometry of the substrates. The collagen thin films were also found to be stable under various storage and treatment conditions. This study can have a huge impact on tissue engineering with collagen.¹

3.1 Introduction

Collagen has become a major choice for biomedical applications because it is biodegradable, biocompatible, highly versatile and easily available. Collagen based medical devices are in widespread use in tissue engineering for example in wound healing, tissue regenerations, implants or scaffold designs. Engineered scaffolds in tissue engineering are designed to supplement or replace injured, missing, or compromised tissue or organs. The main challenge in this research area is to create scaffolds that mimic

¹ A version of this chapter has been published. Nahar, Q., Quach, D. M. L., Darvish, B., Goldberg, H. A., Grohe, B., & Mittler, S. (2013). Orientation distribution of highly oriented Type I Collagen deposited on flat samples with different geometries. *Langmuir*. 29(22), 6680-6686.

the structure and function of the extracellular matrix (ECM). The primary function of extracellular matrix in biology is to provide structural, physiological and biochemical support to the surrounding cells [1]. Cell-ECM interactions play an important role in cell attachment and migration and promote cellular differentiation and gene expression levels [2]. ECM consists of two major classes of macromolecules: proteoglycans (PGs) and fibrous proteins. The most abundant fibrous protein within the interstitial ECM is collagen. Collagen supports tissue development, regulates cell adhesion and provides tensile strength to the organs and tissues. The most widespread family of collagen is the fibril forming collagen of types I, II, III, V and VI. Type I collagen forms more than 90% of the mass of bone and can also be found in tendons, skin, ligaments, cornea and many connective tissues [3][4]. Collagen is a protein characterized by a unique triple-helix formation [5]. The subunit of a collagen molecule is known as the tropocollagen (TC) macromolecule [6]. It consists of three polypeptide chains having the conformation of a left-handed helix. These chains are twisted together to form a right-handed helix. Each chain is composed of about 1050 amino acid residues where every third acid is glycine and about 25% of the residues are proline and hydroxyproline. The right-handed helical structure is stabilized by many hydrogen bonds. It is approximately 300 nm long and 1.5 nm in diameter. The structure of collagen type I can be found in Figure 1.3 in chapter 1.

The microfibrils formed by tropocollagen aggregates are the major tensile strength bearing components of connective tissue [7][8]. The formation of collagen fibrils is basically a self-assembly process [9] For most soft and hard tissues and their functions, collagen fibres are highly ordered and have specific orientation directions [10]. For example, woven bone, which is typically mechanically weak, is composed of randomly oriented fibres [11]. But mechanically strong lamellar bone has a well-organized orientation of collagen fibres. An example of the orientation distribution of collagen in woven bone and lamellar bone is shown in Figure 3-1. In tendons, collagen fibrils are generally longitudinally oriented so that it can support tensile strength and mechanical properties. On dermis, collagen is randomly oriented as bundles. On the other hand, it was found that corneal stroma has two orientations orthogonal to each other in a layered fashion [12]. Imitating these fibril orientations and arrangements of different organs is a major effort in tissue engineering.

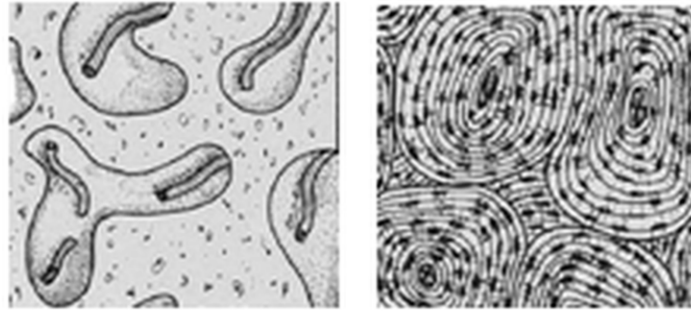


Figure 3-1: An example of orientation of collagen in (a) woven bone or immature bone where collagen fibers are randomly oriented and (b) lamellar or mature bone where collagen fibers are oriented in a circular pattern (Figure adapted from [13])

Cellular adhesion on an artificial material can be enhanced by coating the material with an extracellular matrix protein like collagen [14]. In recent years, collagen type I is being utilized to coat the surface of cell culture substrates to promote the growth and proliferations of cells [15]. The simplest method to prepare this coating involves adsorption of collagen from solution onto the substrate surface. The interaction between the collagen and surface can have a significant effect on the structure of the collagen layers. Interactions between the adjacent collagen molecules as well as electrostatic and hydrophobic interactions can alter the orientation, conformation and density of the collagen layer [14]. Previous studies done by several groups have confirmed that the amount of collagen adsorbed from solution and the structure of the collagen on the substrates depends on the hydrophobic nature of the substrates [16]. The term hydrophobic refers to the interaction of a boundary layer of a solid phase with water vapor or water. If a solid surface tends to not adsorb any water or to be wetted by water, it is called a hydrophobic surface while a surface which is easily wetted by water is called hydrophilic [17][18].

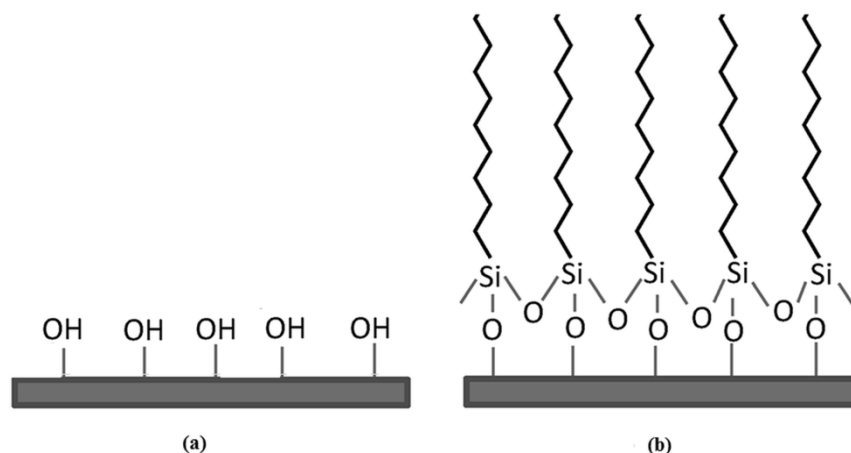


Figure 3-2: Silanization process for hydrophobic glass surface (a) Initially hydroxyl groups are introduced on a glass surface and (b) formation of highly ordered self-assembled monolayer by forming a covalent Si-O-Si bond

Silanization is a process to modify glass surfaces with a high degree of control. In silanization, the surface of glass is covered with functional alkoxy silane molecules through self-assembly [19]. The alkoxy groups can be either methoxy ($-\text{OCH}_3$) or ethoxy ($-\text{OCH}_2\text{CH}_3$) groups. Hydroxyl groups introduced on a glass surface can replace the alkoxy groups present in the silane and allow forming a covalent $-\text{Si}-\text{O}-\text{Si}-$ bond structure.

A quantitative method for measuring hydrophobicity or hydrophilicity of a surface is to determine the contact angle of a water droplet on that surface. Water will form a distinct droplet on a hydrophobic substrate and surfaces with contact angles larger than 90° are designated as hydrophobic. On the other hand, water will spread over a hydrophilic substrate and the contact angles are usually less than 30° [17]. This is shown in Figure 3-3.

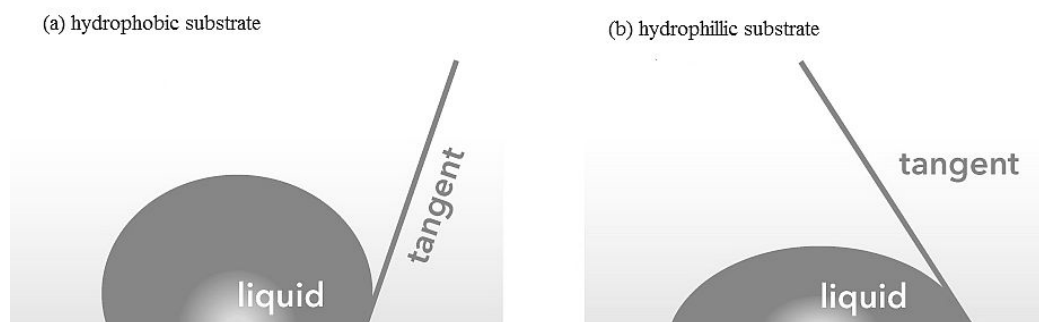


Figure 3-3: Scheme of contact angle determination (a) Hydrophobic substrate with a contact angle larger than 90° and (b) hydrophilic substrate with a contact angle less than 90°

Collagen has been reported to be deposited as a thin film by the Langmuir-Blodgett (LB) technology [20]. Highly oriented collagen type I thin films were successfully deposited on rectangular glass substrates using the LB technique [21]. It was found that collagen behaves similarly as a class of synthetic polymers known as "hairy rod polymers" during LB film processing. Synthetic hairy rod polymers consist of a rigid, typically conjugated backbone with a dense system of side chains [22][23][24]. The backbone is preferably of cylindrical symmetry attached with the short side chains to provide a solvent shell. In solid and solvent free environment, the side chains formed a continuous matrix where backbones are embedded as reinforcing elements. The size of the macromolecules depends on the architecture of the side chains and is typically around 0.5 to 2 nm. The flexible side chains need to be present as they can provide processability and conformational disorder. The side chains can be chosen as hydrophobic elements so that if they interact with water, a repulsive interaction can be achieved. These polymers tend to self-organize, forming nanoscale structures in bulk and in solution. One particular similarity between hairy rod macromolecules and collagen is the shape persistence. The shape persistence can be achieved by direct synthesis of a bonding pattern of this synthetic polymer's constitutive elements so that the randomization of the chain trajectories can be prevented [22].

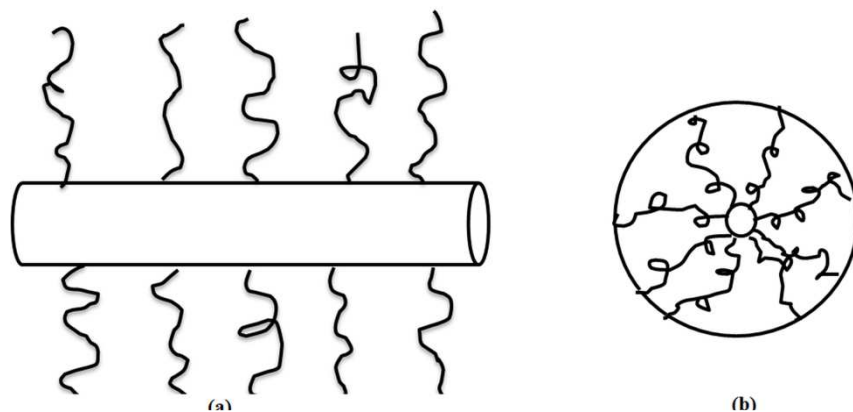


Figure 3-4: Hairy rod macromolecules (a) Typical cylindrical backbone with side chains and (b) side view showing the side chains forming a shell like structure around a rigid backbone (Figure adapted from [22])

Using the Langmuir Blodgett technique, the hydrophobic hairy rod macromolecules can be transferred easily to a planar substrate. Moreover, monomolecular thin films of highly oriented macromolecules can be achieved. The orientation or alignment of these molecules in the films preferentially follows the dipping direction in both upstroke and down-stroke. The flow of liquid subphase towards the substrate in a LB trough also has an influence in the alignment of these rods. For only convergent flows, the alignments of these rods would be parallel to the dipping direction while for non-convergent flow, the rods would be aligned perpendicularly to the dipping direction [25].

Previous work by Tenboll et al. has shown that controlled deposition of highly oriented collagen type I fibres on rectangular glass substrates are possible with the LB technique [21]. It was found that the collagen molecules do not behave like classic LB amphiphilic molecules. Rather they form thick multilayer collagen films when compressed and are visible to the naked eye. Collagen molecules form fibrillar aggregates during compression on the LB trough. This collagen fibres in the resultant LB films were observed to be oriented preferentially along the dipping direction of the substrates.

In this study, the Langmuir-Blodgett fabrication process was applied to deposit thin films of collagen on planar hydrophobic glass substrates with different geometrical shapes and dimensions. The purpose of this work was to study the influence of the geometry and to

achieve various orientation distributions of collagen molecules and aggregates with a systematic change in the shape and size of the substrates. The shapes of glass substrates used were rectangles, squares, circles, triangles, diamonds etc. with different dimensions such as from squares with 10 mm edges to rectangles with a dimension of 25 mm x 75 mm. The surface of the substrates were chemically modified to achieve hydrophobic surfaces. The thin films were also treated under different storage conditions to verify their stability. The thin films with different collagen orientations can have applications as a biomaterial in tissue engineering and medical devices, for example to control cellular growths, in wound dressings, implants or scaffolds .

3.2 Materials and Methods: Collagen on Glass

3.2.1 Preparation of Collagen Solution

Collagen type I was prepared from fresh rat tail tendons and dissolved in acetic acid. The procedures for purifying collagen from washed tendons can be found in reference [25]. For Langmuir-Blodgett deposition, 2 μ M collagen (type I with a molecular weight of 300 kDa) solutions is prepared by dissolving 0.6 mg of collagen in a mixture of 0.9 mL acetic acid and 0.1 mL n-propanol for 12 hours at 4°C in motion. n-propanol supports LB film formation without denaturing effects on collagen molecules [20][21]. It also provides the right vapour pressure and therefore allows fast evaporation during experiments on LB trough. The triple helical structure of tropocollagen in the 0.9 mL acetic acid and 0.1 mL n-propanol solution was also confirmed via circular dichroism (CD) spectroscopy, which is an extensively used spectroscopic technique to analyze the structure or conformation of macromolecules [21].

3.2.2 Glass Substrate Cleaning

For collagen deposition, microscopy glass slides (Fisher Scientific) were cut into different geometrical shapes and sizes with a diamond glass cutter or a glass saw. The geometrical shapes used were rectangles, triangles, discs and squares with small sizes (from 10 mm to 25 mm). The glass substrates were cleaned with a standard laboratory protocol. The substrates were first sonicated in 2% Hellmanex (Hellma, Germany) for 15 minutes, followed by sonication in deionized water ($\rho \geq 18 \text{ M}\Omega\text{-cm}$, Millipore) for 5

minutes, sonication in ethyl alcohol (97%, Sigma Aldrich, Canada) for 15 minutes and again sonication in deionized water for 5 minutes. After sonication with Hellmanex and ethyl alcohol, the slides were washed five times with deionized water. They were then blown dry with nitrogen.

3.2.3 Creating -OH groups on Substrate Surface

For silanization of the glass substrates, creating -OH groups on their surfaces was necessary. To create -OH groups on the substrate surface, the glass slides were immersed in a mixture of 4:1 solution of concentrated sulphuric acid (97%, Sigma Aldrich) and hydrogen peroxide (30%, Sigma Aldrich) for 24 hour in a fumehood. They were then washed with ample amounts of deionized water and dried under nitrogen. Contact angle measurements were carried out on the dried glass substrates using a goniometer (Model 100-00, Ramé-Hart Instrument Co.). The contact angles were found to be less than 10° which confirmed hydrophilicity of the substrates.

3.2.4 Silanization for Hydrophobic Substrates

To obtain hydrophobic substrates, a 10 mM solution of n-octadecyltrichlorosilane (OTS, Sigma Aldrich) in anhydrous toluene (Sigma Aldrich) was prepared. To prepare 50 mL of this solution, 200 µL of OTS was added with 49.8 mL of anhydrous toluene in a laboratory flask. Since atmospheric moistures can easily hydrolyze OTS, the solution was always prepared in a glovebox under nitrogen atmosphere. Slides were immersed in this solution for 24 hour to give enough time for OTS assembly onto the glass surface. After 24 hour, substrates were carefully rinsed with toluene and dried with nitrogen. Hydrophobicity of the substrates were confirmed with contact angle measurement delivering angles larger than 100°.

3.2.5 Langmuir-Blodgett Deposition

A LB trough (KSV Instruments Ltd., model: KSV3000-2LB) in the Western Nanofabrication Facility was used for the deposition of the collagen onto the substrates. The LB trough was first cleaned thoroughly with ethyl alcohol. After cleaning, the trough was filled with deionized water which acted as the subphase. Afterwards, 400 µL of

prepared collagen in acetic acid and n-propanol was added drop-wise with a microsyringe (Hamilton). Following a 20 minute solvent evaporation time, the barriers were allowed to compress at a speed of 5 mm/min to measure the area-pressure isotherm. For LB film deposition, the substrates were immersed almost completely inside the subphase. The barriers were allowed to compress the collagen at a speed of 5 mm/min up to three-fourth of the highest surface pressure (obtained from isotherm) to avoid monolayer breakdown. For collagen film transfer, the substrate was moved out of the water subphase with the lowest speed of 5 mm/min. The film was allowed to dry in air for 30 minutes before storing. For each sample, the trough was thoroughly cleaned and the procedure repeated from the first step to avoid any pre-orientations.

3.2.6 Optical Microscopy

To study and analyse the collagen orientation and its distribution on the samples, an optical inverted microscope (Axiovert 25CFI, ZEISS) was employed.

3.3 Results

3.3.1 Surface Pressure vs. Trough Area Isotherm

Classic amphiphilic materials and also the hairy rod polymers usually show a breakdown or collapsing when they are compressed in the area-pressure isotherms. In usual LB isotherms, there is a gas analogue phase, a liquid analogue phase and a solid analogue phase followed by the collapse after the highest possible surface pressure is reached. It was found that collagen does not behave like the classic amphiphilic molecules or hairy rod polymers. There was no breakdown or collapsing of the films in the area-pressure isotherms regardless of surface pressures. They seemed to be stable close to barrier contact. The surface pressure increased with the compression up to the safety stop of the barriers close to touching. Tenboll et. al. have proven that this behaviour is independent of the collagen spreading volume [21]. It had been assumed that due to the non-amphiphilic and hydrophobic nature of collagen, no classical monolayer formation has occurred at the air-water interface. Instead, a multilayer collagen film had been obtained. A comparison between the isotherms of classical LB material (stearic acid) vs. collagen is shown in Figure 3-5. The stearic acid isotherm is clearly showing the breakdown region

after the highest surface pressure was reached as well as the gas analogue, liquid analogue and solid analogue phases. In the collagen isotherm, gas analogue phase and liquid analogue phases are similar to that of stearic acid but the solid analogue is not as clearly defined as in stearic acid. In this case, surface pressure continued to increase until the minimal area is reached with barriers compressed as close as possible. The surface pressure was also rather high in the stearic acid isotherm than that of collagen although the volume of spread stearic acid was only 60 μL compared to collagen spread volume of 400 μL .

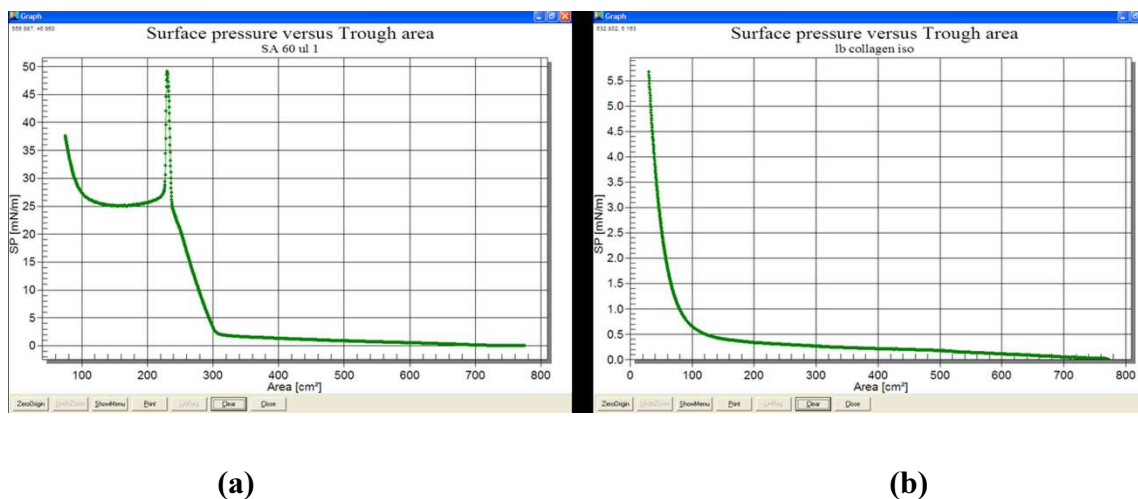


Figure 3-5: Surface pressure-area isotherm for (a) stearic acid with a spread volume of 60 μL and (b) collagen with a spread volume of 400 μL

Previous studies on our laboratory showed that collagen produces large fibrillar aggregates during LB film compression where the length of the fibrils can be up to 100 μm [21]. This was also confirmed in the present study.

3.3.2 Orientation of Collagen on LB Films

The LB films were fabricated on substrates with different shapes. To achieve different orientation pattern, these substrates were mounted in the LB trough with different directions and angles with respect to the dipping direction. The sizes of the samples were kept small enough (width ≤ 25 mm) to satisfy overall convergent flow condition on the LB trough.

It was found that substrate geometry plays an important role in the orientation distribution of the collagen in the LB films. For example, when a rectangular substrate (70 mm x 25 mm) was dipped with its long axis parallel to the direction of dipping, collagen fibrils were aligned parallel to the dipping direction on more than two-third of the collagen coated area. On the remaining one-third area closer to the "previous" air-water interface, collagen was oriented perpendicular to the dipping direction but parallel to the air-water interface. Collagen fibrils produced an "orientation arch" in the upper transition region of the film where the fibrils changed their orientation from perpendicular to parallel orientation. The orientation of collagen on rectangular substrates as reported by Tenball et. al. were confirmed here [21]. The collagen orientations on a rectangular substrate are shown in Figure 3-6(a).

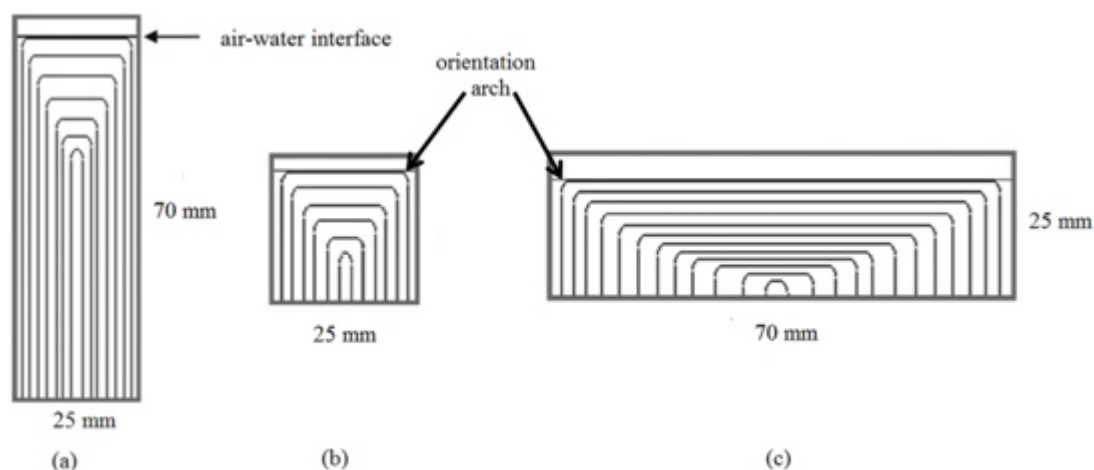


Figure 3-6: Sketches of orientation distribution of collagen microfibrils according to bright field microscopy images of a collagen coated rectangular substrate (70 mm x 25 mm) and a square (25 mm x 25 mm): (a) dipping direction parallel to the long axis (70 mm) (b) square sample (c) dipping direction parallel to the short axis. The samples were almost completely immersed in the subphase. Arrow in (a) indicates position of air-water interface before film lift operation. In case (c), the arch covers the entire sample surface. (Copyright obtained from American Chemical Society)

When collagen was coated on a square with a width of 25 mm, it showed slightly different orientation distribution pattern within the film (Figure 3-6(b)). In this case, the

orientation arch was covering more than half of the surface area of the sample. The fibers were also aligned parallel to the dipping direction but these were found only on the bottom part of the sample. Comparing the rectangular sample with the square one, it became clear that the length of the sample is an important parameter in the orientation distribution of collagen. To be certain, another rectangular sample with same dimensions (70 mm x 25 mm) was coated with collagen with its long axis parallel to the air-water interface (perpendicular to dipping direction). This time the orientation arch was present over almost the entire sample surface. There was also parallel orientation of collagen fibers with respect to the dipping direction in the bottom part of the sample only. This is shown in Figure 3-6(c). It was also noted that for all of the samples, the fibers were always aligned parallel to the edges at the air-water interface.

To further study the effect of substrate shape and size on collagen orientation distribution, triangular, circular and rhombic substrates with different dimensions were coated with collagen where substrates were dipped at various angles. Also rectangles and squares with smaller dimensions were coated. For convenience, the shapes were divided into two groups: symmetric samples and asymmetric samples. The sketches of symmetric samples with different orientation patterns are shown in Figure 3-7.

For all symmetric samples, some observations were made as follows:

1. An orientation arch was formed for all samples regardless of the sample top which were either straight (Figure 3-7 a-e), round (Figure 3-7f) or pointed (Figure 3-7 g-m).
2. A symmetry line in the middle of the sample parallel to the dipping direction could be seen in all samples.
3. As the samples had different geometical shapes, increasing or decreasing the sample width during film lift resulted in formation of orientation arches dominating the entire sample.
4. At the start of the film lift for LB transfer, collagen fibrils were aligned parallel to the air-water interface regardless of mounting angles for almost all cases.
5. The substrates which had a pointed tip downward during film lift (Figure 3-7 (i, k and m)), showed a preferential collagen alignment parallel to the dipping

direction. Due to this collagen formed an angle between dipping directions and sample edges.

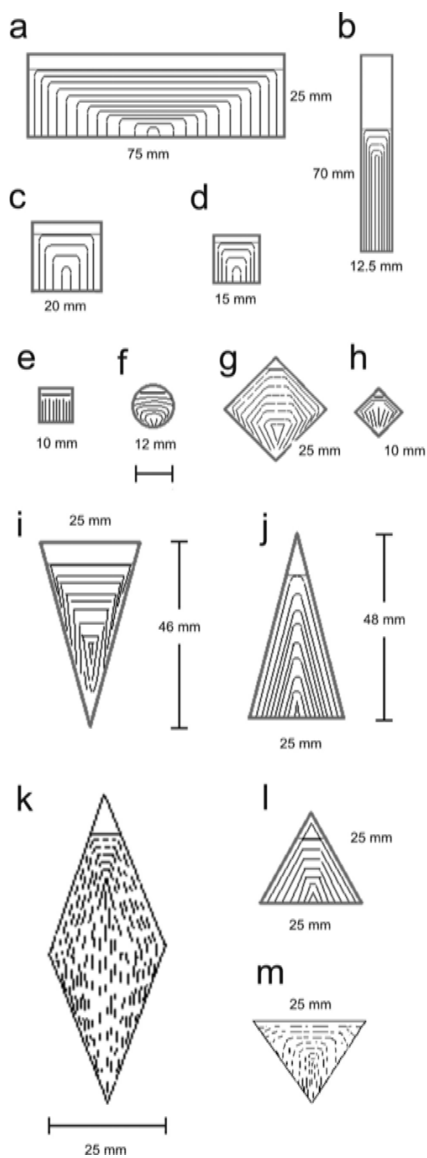


Figure 3-7: Sketches of collagen fibril orientations on symmetric samples with different geometrical shapes and dimensions. The dipping direction is always downward vertical. Not to scale.[copyright obtained from American Chemical Society]

6. The small round sample (Figure 3-7f) showed an alignment of collagen which was non-parallel to either dipping direction or sample edges.
7. Squares with a pointed tip during film lift (Figure 3-7g) showed collagen alignments non-parallel to the dipping direction. In this case, collagen was aligned parallel to the sample edges on the top region and then the alignment became non-parallel to the edges at the bottom.
8. Small squares (Figure 3-7 e and h) are an exception to the other samples. In these cases, an orientation arch was not formed. The collagen orientation was mostly parallel to the dipping direction for the small square with straight bottom (Figure 3-7e). The absence of the arch allowed a smooth transition from parallel to edges to the pointed region at the bottom of sample (Figure 3-7g).

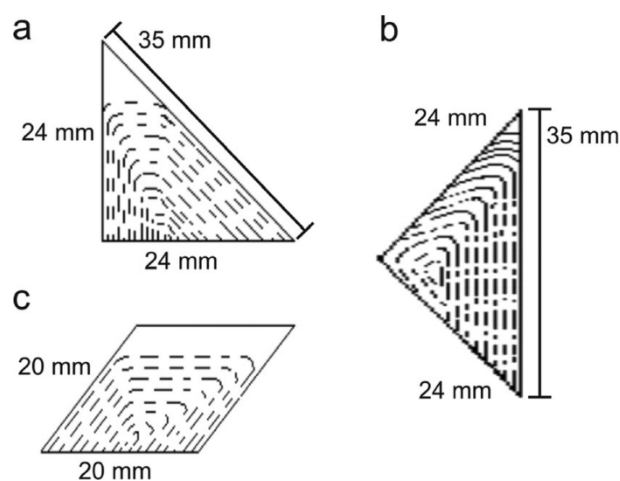


Figure 3-8: Sketches of collagen fibril orientations on asymmetric samples with different geometrical shapes and dimensions. The dipping direction is downward vertical. Not to scale. [copyright obtained from American Chemical Society]

3.3.3 Analysis of Flow Characteristics of Collagen

During the collagen film transfer, some symmetric samples (Figure 3-7(j and l) and top of 3-7(g, h and k)) and asymmetric samples, had collagen oriented parallel to the edges but not necessarily following the dipping direction. An explanation of this behaviour can be found in part from the work of Schwiegl et. al. who did a thorough theoretical and

experimental analysis of the flow dynamics of LB films [25]. According to them, moving the substrate during film transfer causes the molecules to flow along the air-water interface and arrange themselves in a way that point toward the substrate i. e. the long axis of the molecules are perpendicular to substrate. For rectangular substrates, when the substrate is pulled out of the subphase, the molecules will arrange themselves parallel to the edges and also parallel to the dipping direction (Figure 3-6 and 3-7 (a-d) [21][25]).

For substrates with different geometrical shapes where the sample width changes during film transfer, the collagen alignment pattern is mostly influenced by the changing sample width and therefore the available deposition area on substrate. By taking these observations in account, it is possible to achieve four different flow changes by changing the width of the substrate while pulling it out of subphase during film transfer. These are as follows:

- I. Both the width of the sample and LB transfer position are fixed relative to the subphase (Figure 3-7 a-c)
- II. The width of the sample is fixed but LB transfer position is changing during subphase (Figure 3-8 c)
- III. The width of the sample is increasing at a fixed LB transfer position ((Figure 3-7 j and l) and top of Figure 3-7 (g and k))
- IV. The width of the sample is decreasing at a fixed LB transfer position ((Figure 3-7 i and m), bottom of Figure 3-7 (f, g, h and k) and Figure 3-8 b).

It is to be noted that only the samples which had a decreasing width during film transfer did not show any collagen oriented parallel to the edges. In this case, collagen fibrils were aligned parallel or near-parallel to the dipping direction.

It was concluded from the experimental results that the flow of the LB film on the trough have a significant effect on the collagen patterns and orientation distributions on the substrates. For samples with a constant width during film transfer, the molecular flow is convergent. Samples with a constant width such as rectangles, squares or parallelograms, the orientation pattern was usually parallel to the edges while the orientation arch covers only a small region on top. For samples with an increasing width during film lift, the

convergence of molecular flow decreased. This gave rise to a pronounced orientation arch and collagen orientations parallel to the edges of the samples. On the other hand, samples with a decreasing width during film transfer had collagen orientation parallel to the dipping direction and not parallel to the edges due to an increase in the convergence of molecular flow on the trough.

3.3.4 Effect of Width to Height Displacement on Collagen Pattern

A comparison was made for collagen distribution between the samples with similar widths but different heights. The diamond shaped sample in Figure 3-9 (a) and triangle shown in Figure 3-9 (b) both have a maximum width of 25 mm but their heights are different.

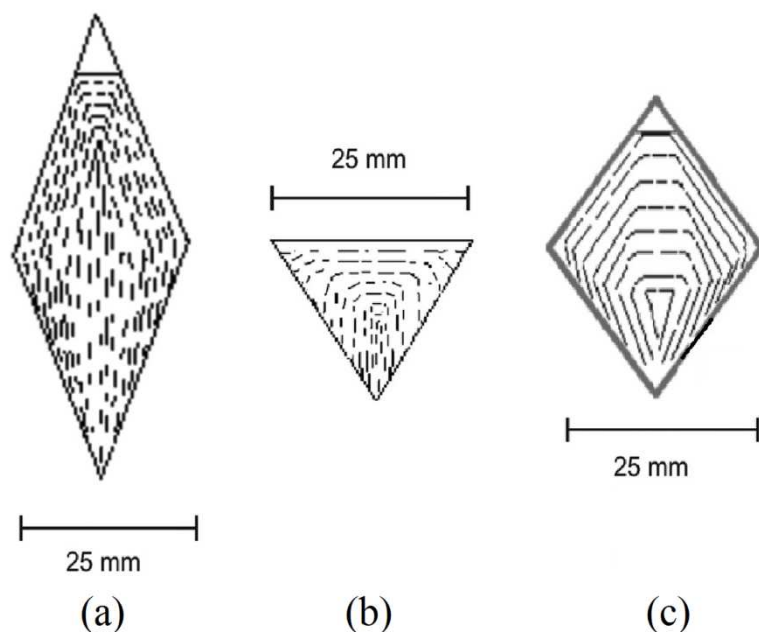


Figure 3-9: Comparison of width to height displacement in three equal width samples. (a) a diamond shaped sample with 25 mm width but longer length (b) a triangle with 25 mm width (c) a square with 25 mm width mounted at its tip.[copyright obtained from American Chemical Society]

The lower half of the diamond shaped sample in Figure 3-9(a) and the triangle shown in Figure 3-9(b) were similar in shape but their collagen orientation pattern was not same. This suggests that there was an effect of the change in width (Δw) with respect to the change in height (Δh) displacement during collagen film transfer. The long diamond shaped sample had a lower tip angle, which was the angle between two adjacent sides on the bottom part, than the tip angle of triangle for which tip angle was 45° as it has three equal sides. For this reason, pulling the diamond shaped sample out of the subphase by a displacement in height Δh resulted in less change in width Δw than that of the triangle. Therefore, the orientation of collagen parallel to the dipping direction was more distinct in the diamond shaped sample which also had a larger deposition area. The same effect was also observed with the square in Figure 3-9 (lower half c) mounted with its tip so that the lower half of it was a triangle.

3.4 Materials and Methods: Effect of Environment on Collagen Samples

3.4.1 Effect of Environment and Time on the Collagen Samples

For application of the collagen thin films in biological scaffolds, the stability of the prepared collagen samples on glass substrates were studied against different environmental conditions. The collagen samples were tested by storing them in three different conditions as below:

1. in air at 37°C for three months
2. in buffer (Ringer) solution at 37°C for three months and
3. in air with an increasing temperature range from 37°C to 60°C

For 1 and 2, the films were kept at a fixed temperature of 37°C and film stability was examined every week. Two large fibrils were randomly chosen at the beginning of these experiment and the distance between them was measured for all of the three experiments for the duration of the study.

3.4.2 Optical Microscopy

To study the effect of environment and storage time on collagen films, an optical microscope (Nikon Eclipse TE 300 Japan) was used. The stability of the films were analyzed every week at the same location and under the same conditions. Bright field microscopy images were taken right after the collagen films were prepared and then at regular intervals for films stored for three months.

3.5 Results

Figure 3-10 shows the bright field microscopy image of a collagen film stored in air at 37°C, in buffer solution at 37°C and at an increasing temperature of up to 60°C. Figure 3-10(a) shows the image of a collagen film stored in air at the first day of the study which means day 0 and after 77 days. The two images were taken at the same location of the collagen films under similar conditions. Distances were measured between two randomly chosen fibrils on the first day as a further assessment of stability. It was observed that the two images taken 77 days apart were almost identical and the distance between the same two fibriller aggregates were also similar.

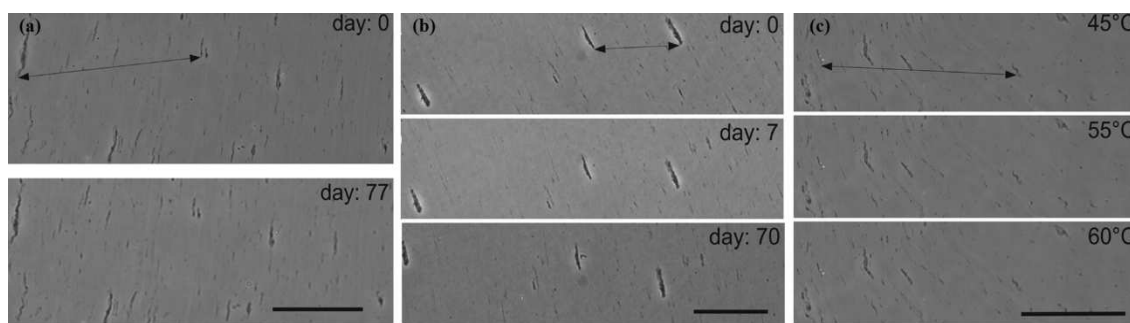


Figure 3-10: (a) Collagen film stored in air at 37°C (b) Collagen film stored in buffer solution at 37°C and (c) collagen film at elevated temperatures. The arrows indicate the distance between two fibrils. Scale bars represent 100 μm . [copyright obtained from American Chemical Society]

In figure 3-10(b), three images are shown for the same collagen film stored in a buffer solution at 37°C at the first day of storage i.e. day 0, at day 7 and day 70. The images appeared identical and distances between fibrils were unchanged. Figure 3-10(c) shows

three images of the same collagen film at the same location but treated at different temperature of 45°C, 55°C and 60°C. In all cases, collagen fibrils appeared to be unaffected by the temperature changes. The distances between the fibrils were uninfluenced by the higher temperatures.

The measured distance data between collagen fibrillar aggregates for all three testing conditions for the entire testing period are represented in Figure 3-11. These data proves that for all collagen samples, there was no significant changes on the measured distances. From this, it was concluded that these collagen films prepared on glass substrates via LB technique are stable under the applied conditions and time. However, the orientation or order of the films during the tests under different storage time and temperature were not evaluated. Although the orientations of the fibrils were found to be similar on day 0 and after a significant number of days, the collagen matrix could still undergo an orientation change during testing. However, Cha et al. found that annealing hairy rod macromolecule films prepared by LB technique up to 130°C has enhanced the orientation of the molecules and also improved the order parameters of the films [26]. It is therefore possible that the order of the collagen films were actually improved during the stability tests.

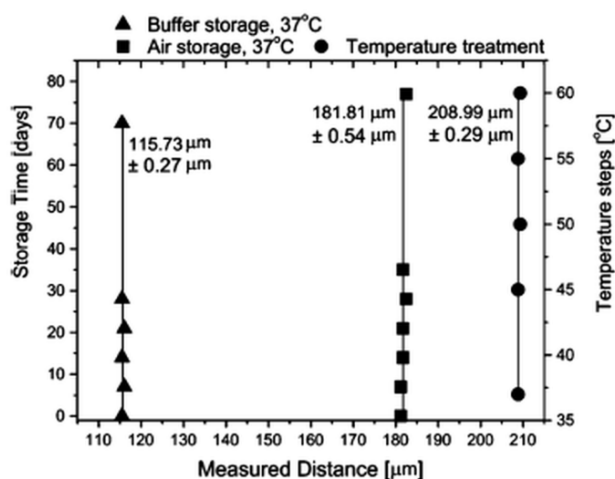


Figure 3-11: Quantitative data on the measured distances between two collagen fibrils vs. storage time or vs. temperature respectively. The lines represent average distances.

[copyright obtained from American Chemical Society]

3.6 Summary

In this study, collagen films with a high degree of orientation were prepared using Langmuir-Blodgett technique. It was shown that it is possible to achieve a specific collagen orientation distribution by selecting a specific substrate shape. It was found that this orientation distribution of collagen depended primarily on substrate geometry and dimensions as well as the convergent or divergent flow of the LB film on the trough. The stability of the collagen films in different environments and temperatures was evaluated to verify its stability in long time applications and storage. It was determined from these results that the collagen films are stable for at least three months in air and buffer solution and also up to a temperature of 60°C. The orientation distribution and order of the collagen films were also determined to be stable from optical microscopy results. This study of collagen films prepared with LB technique can have immense impact in tissue engineering and biomedical applications.

3.7 References

1. Frantz, C., Stewart, K. M., & Weaver, V. M. (2010). The extracellular matrix at a glance. *Journal of Cell Science*, 123(24), 4195-4200.
2. Gelse, K., Pöschl, E., & Aigner, T. (2003). Collagens—structure, function, and biosynthesis. *Advanced drug delivery reviews*, 55(12), 1531-1546.
3. Bunyaratavej, P., & Wang, H. L. (2001). Collagen membranes: a review. *Journal of Periodontology*, 72(2), 215-229.
4. Ricard-Blum, S., & Ruggiero, F. (2005). The collagen superfamily: from the extracellular matrix to the cell membrane. *Pathologie Biologie*, 53(7), 430-442.
5. Pachence, J. M. (1996). Collagen-based devices for soft tissue repair. *Journal of biomedical materials research*, 33(1), 35-40.
6. Petruska, J. A., & Hodge, A. J. (1964). A subunit model for the tropocollagen macromolecule. *Proceedings of the National Academy of Sciences of the United States of America*, 51(5), 871.
7. Hulmes, D. J., Wess, T. J., Prockop, D. J., & Fratzl, P. (1995). Radial packing, order, and disorder in collagen fibrils. *Biophysical Journal*, 68(5), 1661-1670.
8. Currey, J. D. (2002). *Bones: structure and mechanics*. Princeton University Press.

9. Kadler, K., Holmes, D., Trotter, J., & Chapman, J. (1996). Collagen fibril formation. *Biochem. J*, 316, 1-11.
10. Cen, L., Liu, W., Cui, L., Zhang, W., & Cao, Y. (2008). Collagen tissue engineering: development of novel biomaterials and applications. *Pediatric research*, 63(5), 492-496.
11. Ramalingam, M., Vallittu, P., Ripamonti, U., & Li, W. J. (Eds.). (2013). *Tissue Engineering and Regenerative Medicine: A Nano Approach*. CRC Press.
12. Daxer, A., & Fratzl, P. (1997). Collagen fibril orientation in the human corneal stroma and its implication in keratoconus. *Investigative ophthalmology & visual science*, 38(1), 121-129.
13. Khurana, J. S. (2009). *Bone Pathology*. 2nd ed. Springer.
14. Elliott, J. T., Woodward, J. T., Umarji, A., Mei, Y., & Tona, A. (2007). The effect of surface chemistry on the formation of thin films of native fibrillar collagen. *Biomaterials*, 28(4), 576-585.
15. Dufrêne, Y. F., Marchal, T. G., & Rouxhet, P. G. (1999). Influence of substratum surface properties on the organization of adsorbed collagen films: in situ characterization by atomic force microscopy. *Langmuir*, 15(8), 2871-2878.
16. Arkles, B., & Pan, Y. (2011). Hydrophobicity, hydrophilicity and silane surface modification. Gelest Inc, Morrisville.
17. Gao, L., & McCarthy, T. J. (2006). A perfectly hydrophobic surface ($\theta_A/\theta_R=180/180$). *Journal of the American Chemical Society*, 128(28), 9052-9053.
18. Arslan, G., Özmen, M., Gündüz, B., Zhang, X., & Ersöz, M. (2009). Surface modification of glass beads with an aminosilane monolayer. *Turkish Journal of Chemistry*, 30(2), 203-210.
19. Li, Y., Zhang, S., Guo, L., Dong, M., Liu, B., & Mamdouh, W. (2012). Collagen coated tantalum substrate for cell proliferation. *Colloids and Surfaces B: Biointerfaces*, 95, 10-15.
20. Usha, R., Dhathathreyan, A., Mandal, A. B., & Ramasami, T. (2004). Behavior of collagen films in presence of structure modifiers at solid-liquid interface. *Journal of Polymer Science Part B: Polymer Physics*, 42(21), 3859-3865.

21. Tenboll, A., Darvish, B., Hou, W., Duwez, A. S., Dixon, S. J., Goldberg, H. A., Grohe, B. & Mittler, S. (2010). Controlled deposition of highly oriented type I collagen mimicking in vivo collagen structures. *Langmuir*, 26(14), 12165-12172.
22. Wegner, G. (2003). Nanocomposites of Hairy-Rod Macromolecules: Concepts, Constructs, and Materials. *Macromolecular chemistry and physics*, 204(2), 347-357.
23. Stepanyan, R., Subbotin, A., Knaapila, M., Ikkala, O., & Ten Brinke, G. (2003). Self-organization of hairy-rod polymers. *Macromolecules*, 36(10), 3758-3763.
24. Cheung, D. L., & Troisi, A. (2009). Molecular structure and phase behaviour of hairy-rod polymers. *Physical Chemistry Chemical Physics*, 11(12), 2105-2112.
25. Schwiegk, S., Vahlenkamp, T., Xu, Y., & Wegner, G. (1992). Origin of orientation phenomena observed in layered Langmuir-Blodgett structures of hairy-rod polymers. *Macromolecules*, 25(9), 2513-2525.
26. Cha, M., Neher, D., Embs, F. W., Mittler-Neher, S. & Stegeman, G. (1993). Determination of the First two non-trivial orientational order parameters in LB films of rod like molecules by third order sum frequency mixing. *Chemical physics letters*, 202 (1), 44-50.

Chapter 4

4 WEFS Microscopy on Bacterial Biofilms

In this chapter WEFS microscopy was employed for the imaging of bacterial biofilms. Bright field and WEFS images of bacterial biofilms are compared and proved that WEFS microscopy is capable of distinguishing between bacterial attachment versus suspended cells or cells located very close to the surface. Furthermore, the response of bacteria to UV irradiation has been investigated and analyzed quantitatively. This sterilization experiment was performed as a first step for WEFS microscopy to application: monitoring bacterial sterilization processes for example, in water treatment facilities.²

4.1 Introduction

Adhesion of bacteria to surfaces is one important research area both in the fields of engineering of technical surfaces and biomedical applications [1][2]. Adhesion of bacterial cells to surfaces is important as it defines the distinction between single-cell and multi-cellular organisms. Bacterial contamination of surfaces typically begins with the initial adherence of only a few individual microorganisms to the surface and then subsequent development into a biofilm by continuous growth and division [3][4]. This process takes less than 24 hours when provided with suitable nutrient conditions. However, it is difficult to precisely measure bacterial adhesion to surfaces and is also time consuming because bacterial cell sizes are typically on the micrometer scale. Their adhesion forces are also generally low typically 0.1–100 nN [5]. In recent years, imaging systems have been used extensively for studying bacteria at surfaces. Total Internal Reflection Fluorescent (TIRF) microscopy has been demonstrated to be an effective method for investigating proliferation and growth of bacteria at the cell-surface interface

²A version of this chapter has been published. Nahar, Q., Fleissner, F., Shuster, J., Morawitz, M., Halfpap, C., Stefan, M., Lanbein, U. & Mittler, S. (2013). Waveguide evanescent field scattering microscopy: bacterial biofilms and their sterilization response via UV irradiation. *Journal of biophotonics*. DOI: 10.1002/jbio.201300135.

[6][7]. Total Internal Reflection Microscopy (TIRM) utilizes the basic technology of TIRF without any fluorescence dyes present in the sample by creating an optical contrast due to scattering [8]. TIRM has been reported for the imaging of microbial adhesion using oil immersion objectives [9].

In this chapter, Waveguide Evanescent Field Scattering (WEFS) microscopy is used as a simple, label free imaging technique suitable for studying the attachment of bacteria to a surface and subsequent imaging of bacterial growth forming microcolonies. As we recall from chapters 1 and 2, the WEFS technique utilizes the exponentially decaying evanescent field of a propagating waveguide mode as the sole illumination source with a probing evanescent field thickness between 70-100 nm. WEFS microscopy allowed for imaging the attachment of bacterial biofilms to a glass substrate (waveguide) without the use of toxic labels or additional treatment, enabling us to examine the interaction between viable bacteria and the waveguide surface. Bacterial microcolonies and single bacteria were discriminated both by their bright field images and by their evanescent scattering images and also quantitatively by their scattering intensity. The attached bacteria generated strong signals whereas unattached bacteria but located very close to the surface generated weak signals due to the exponentially decaying nature of the evanescent field.

"Every year around 3.4 million people die from water-related diseases, mainly amoebiasis and diarrhoea caused by bacteria" [10]. Ultra-violet (UV) light disinfection is employed to reduce the number of pathogens to such a low level in drinking water that the risk of infection can be avoided. UV disinfection, unlike chlorine does not present any negative effect on taste, health and environment. Ultraviolet light is commonly divided into three regions: UVA which has a wavelength range from 315 nm to 400 nm, UVB which has a wavelength range from 280 nm to 315 nm and UVC which has a wavelength range from 200 nm to 280 nm. Although many microorganism can be killed or inactivated with UV wavelengths ranging from 100 to 400 nm, the UVC wavelength of 254 nm is the most effective [11][12]. UVC radiation is capable of denaturing the DNA of microorganism by forming pyrimidine dimers between two adjacent bases [13]. In the pyrimidine dimers, two bases: adjacent cytosine (C) and/or thymine (T) are linked into an abnormal structure. As a result, the shape of the DNA double helix is distorted. These

dimers also block the ability of microorganism to replicate their DNA. Thus UV light has the ability to prevent bacterial growth and colony formation but not viability. These dimers are formed less efficiently with UVA and UVB, however UVC at 254 nm has proved to be the most efficient [14].

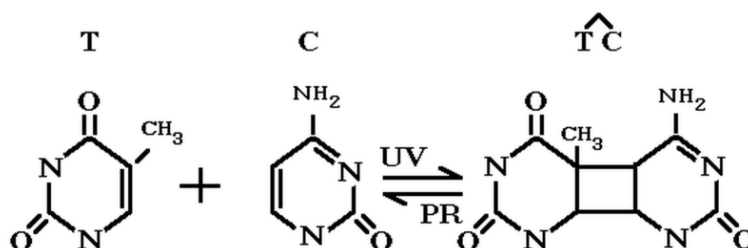


Figure 4-1: Formation of Cytosine-Thymine Dimer in DNA [15]

Thus UV irradiation of bacteria limits their biofilm forming capability. In the present study, an experiment was carried out involving sterilization of bacteria with UV irradiation before culturing them onto the waveguide substrates. This method of UV photo sterilization was chosen for its common use in industrial applications in water purification. The UV treated bacteria were later cultured on waveguides and analyzed with WEFS microscopy.

In this study *Nitrobacter* sp. 263 was used for biofilm formation. *Nitrobacter* sp. 263 was chosen because it is a common, gram-negative bacterium which has been found in several environments, including soil, natural water and sewage sludge, where it typically grows as a biofilm [16] [17] [18]. *Nitrobacter*, as a genus, are nitrite-oxidizing bacteria (NOB) which oxidize nitrite to nitrate to fulfill its energy needs and fix carbon dioxide for their carbon requirements [18][19]. The organism uses nitrite as an electron donor, thereby reducing the compound to ammonia [20][21]. *Nitrobacter* can either be pleomorphic which means they can have more than one shape during their life, or they can be pear-shaped or rod-shaped. A low resolution scanning electron micrograph (SEM) of *Nitrobacter* sp. 263 used in the experiments of this study showed they were rod-shaped

[22]. The rod-length of the cells were measured to be about 1-2 μm , the diameters varies from 0.3-0.5 μm .

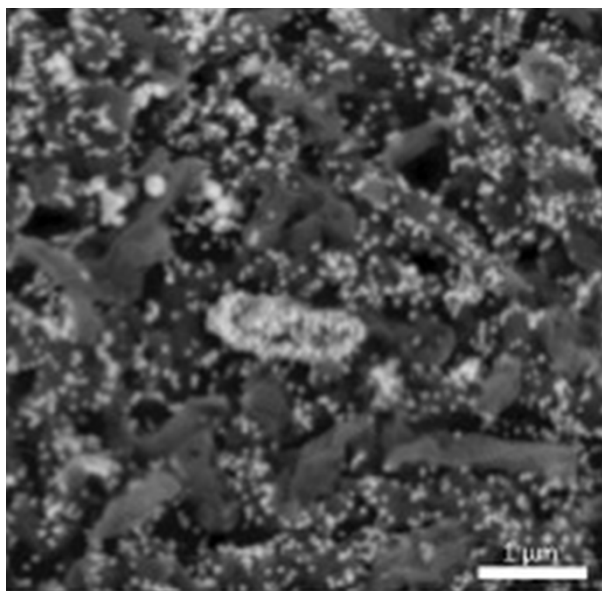


Figure 4-2: SEM image of *Nitrobacter sp. 263* exposed to gold chloride [22]

Nitrobacter usually reproduces by budding which is a form of asexual reproduction. In this process, a new bacterium grows on another and remains attached to the parent until mature. The new bacterium is therefore genetically identical to the parent cell [23]. In aqueous solutions, this bacteria reproduces via a process called binary fission. The binary fission is an asexual reproduction form in which the parent cell divides into two genetically identical equal sized daughter cells [23]. In this process, the cell increases in size and doubles in length. The genome replicates itself and the cell divides its resources into half. When cell is about to double in size, membrane pinches inward and new cell wall forms separating two cells. Overall, the *Nitrobacter* are widely distributed in nature and might significantly contribute to global nitrite oxidation. Bacteria, such as *Nitrobacter sp. 263*, require solid substrates and nutrients in order to grow and form microcolonies on surfaces.

4.2 Materials & Methods for Bacterial Colonization Experiment

4.2.1 Waveguides

The waveguides are the key element for the WEFS microscopy. The waveguides used in this study are step-index waveguides with permanent holographic coupling gratings. The substrate used was fused silica (FQVIS2, Hebo, Germany) or BF33 (Schott, Mainz, Germany) with refractive indices 1.46 and 1.47, respectively at a wavelength of 543.8 nm. The waveguides had a dimension of 25 x 50 mm and a thickness of 1 ± 0.1 mm. The coupling gratings formed by laser interference lithography and subsequent reactive ion etching using sulfur hexafluoride as reactive gas had a periodicities in the order of 600-650 nm. The waveguiding layer was produced by depositing a high refractive index glass film (P-LASF 47, Schott, Germany) onto the substrates by an HF-sputtering technique. The refractive index of the waveguide layer was 1.845 and layer thicknesses varied from 500 - 750 nm. All the waveguides used in the study were manufactured at the RheinMain University of Applied Sciences, Department of Engineering Sciences, Russelsheim, Germany. The waveguide fabrication process can be found in detail in reference [25].

An important aspect of these waveguide substrates is their reusability. However, the waveguides have to be cleaned very carefully after each experiment to remove all residual cells from previous experiments. Before each culturing of bacteria, the waveguides were cleaned with a standard cleaning procedure. They were first sonicated in an ultrasonic bath (Branson 2510, Branson, USA) with 2% Hellmanex (Hellma, Germany) in deionized water for 5 minutes and washed with copious amount of deionized water. Then they were submersed in 70% ethanol (Sigma Aldrich, Canada) in the ultrasonic bath for 20 min. They were then blown dry with nitrogen gas.

4.2.2 Bacterial (Nitrobacter) Culture Preparation

Nitrobacter sp. 263 was cultured on a commercially available culture medium R2A agar (DifcoTM), in sterile plastic petri dishes at room temperature (approximately 23°C) for two weeks. For gaining 1 mL bacterial solution, bacteria from one R2A plate were removed and suspended in 1 mL of filter-sterilized (0.45 mm pore size) distilled deionized water to produce an aqueous bacterial suspension. This solution was used for

each set of the imaging experiment with a concentration of 10^6 bacteria/mL. The bacteria were mixed by a digital vortex mixer (Fisher Scientific) for 3 minutes at 1200 rpm prior to culturing on waveguides as the bacteria have a tendency to adhere to the tube they are stored in. A separate stock solution of R2B was made by dissolving R2A in sterile, distilled, deionized water and filtering this solution to remove the agar constituent. This solution with its dissolved nutrients was used as a culture medium for bacterial growth.

4.2.3 Experiments on Bacterial Attachment and Colonization on Waveguides

These experiments were performed for visualizing the formation of bacterial biofilms on waveguides via WEFS microscopy. A 50 μ l aliquot of the prepared bacterial suspension was placed on the surface of a clean waveguide for 1 hour at 37°C. After 1 hour, the waveguide was examined under an inverted optical microscope (Axiovert, 25CFI, Zeiss) to see if single bacteria were attached. The waveguide was then rinsed with sterile distilled water and placed in a sterile petri dish containing 20 mL of R2B. The petri dish along with the waveguide was incubated for 24 hours at 37°C in the laboratory to allow bacterial growth and biofilm formation. After 24 hours, the waveguide was again inspected with the inverted optical microscope. In all cases, microcolony formation was observed. These microcolony containing samples with living cells were inspected with WEFS microscopy. A simple o-ring construct was employed to contain the R2B medium on the waveguide surface allowing the entire experiment to be carried out with living bacteria for a significant amount of time.

4.3 Results

4.3.1 Colonization of Bacteria on Waveguide Surfaces

Figure 4-3(a) and 4-3(b) show the bright field and WEFS microscopy images of *Nitrobacter* sp. 263 cultured on a waveguide. Both microscopy technologies are able to display single bacteria and the microcolonies. Figure 4-3(a), the bright field image, clearly shows microcolonies and many individual bacteria. This image shows single bacteria as dark dots and lines (rod-shaped) and many microcolonies with different shapes as dark grey structures in a light gray background. In the WEFS image shown in

Figure 4-3(b), the bacteria are represented as white structures in a completely black background. This strong contrast is due to the reason that in WEFS microscopy, the exponentially decaying evanescence field is used as the source of light for imaging. As a result, only the structures that are close to the substrate are illuminated by this evanescence field and contribute with scattered light to the image formation, while everything remains dark.

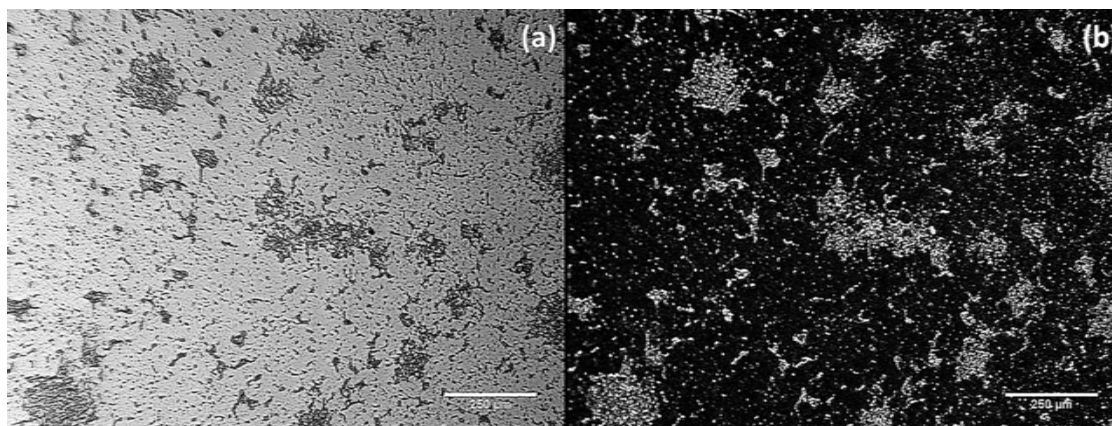


Figure 4-3: (a) Bright field image (objective: 10x, Olympus-U plan FLN) and (b) corresponding WEFS image (objective: 10x, Olympus-U plan FLN) of Nitrobacter sp. 263. Exposure time of 300 ms and TM_2 mode is used to capture this image. WEFS provided excellent images of the bacteria present in the evanescence field.

In the bright field image of Figure 4-3(a), more bacteria are visible as single individual cells than in the WEFS image shown in Figure 4-3(b). As the microcolonies have more bacteria per unit area, they scatter more light. In a biofilm, initially parent cells adhere to the surface and colonization is a result of continuous cell division. These adherent cells are embedded within a matrix of extra-cellular polymeric substance (EPS) produced by the bacteria. The high numbers of bacteria within a colony and the presence of EPS contributes to the scattering intensity. As a result, microcolonies should have an overall higher intensity than individual bacteria that are spread over a region. This was quantitatively determined and shown in Figure 4-5. Although the bright field images showed many rod-shaped and round bacteria, the WEFS images did not depict any rod-shape structures but only round features at identical magnification. This implies that

bacterial attachment mostly was initiated at the cell poles producing a round scattering fingerprint.

A closer view of a microcolony is shown in Figure 4-4. This microcolony clearly shows bacteria as bright white spots on a dark background. As mentioned, bacteria adhered to the waveguide could be visualized only as round dots. Also, when closely inspected, some spots seemed to be brighter than the rest. As the source of illumination here is the exponentially decaying evanescent field, the brightest spots must be the bacteria which are closest to the surface.

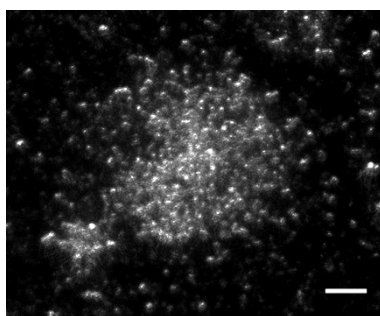


Figure 4-4: Close view of a microcolony (Objective 20x-Olympus LUC plan FLN) of Nitrobacter sp. 263. This image was taken with exposure time 500 ms and TM_2 mode. Scale bar represents 25 μm). The closer the bacteria is to the surface, the higher is its intensity. Brightness and contrast enhanced for better visualization.

4.3.2 Quantitative Analysis of Scattering Intensity Distribution

To determine a quantitative scattering intensity difference between microcolony and individual cells, WEFS imaging and scattering intensity analysis was performed with different exposure times. Figure 4-5(a-d) shows four images with increasing exposure times of 150 ms, 200 ms, 250 ms and 300 ms, respectively. With the increased exposure time, more and more bacteria appeared as individual cells. However, the shape of the microcolony remained constant. For the analysis, some areas are chosen from microcolony and from single cell region. The squares in the figure represent the chosen areas. The integrated and area normalized intensities of these region were calculated using Matlab. The results in Figure 4-5(e) showed systematically and reproducibly less intensities in regions with only individual cells in comparison to colony regions. Both the

intensity of individual bacteria and the colony increased linearly with increasing exposure time. The overall intensity distribution within microcolonies did not change with increased exposure times.

We recall from Chapter 1 and 2 that, the evanescence field only extends 70-100 nm above the waveguide surface and therefore only illuminates bacteria that are closest to the surface. Hence bacteria that were visible already with the lowest exposure time, are bacteria which adhered closest to the substrate. Bacteria that appeared only with increased exposure times are bacteria located further away from the surface but still within the evanescence field depth of the waveguide.

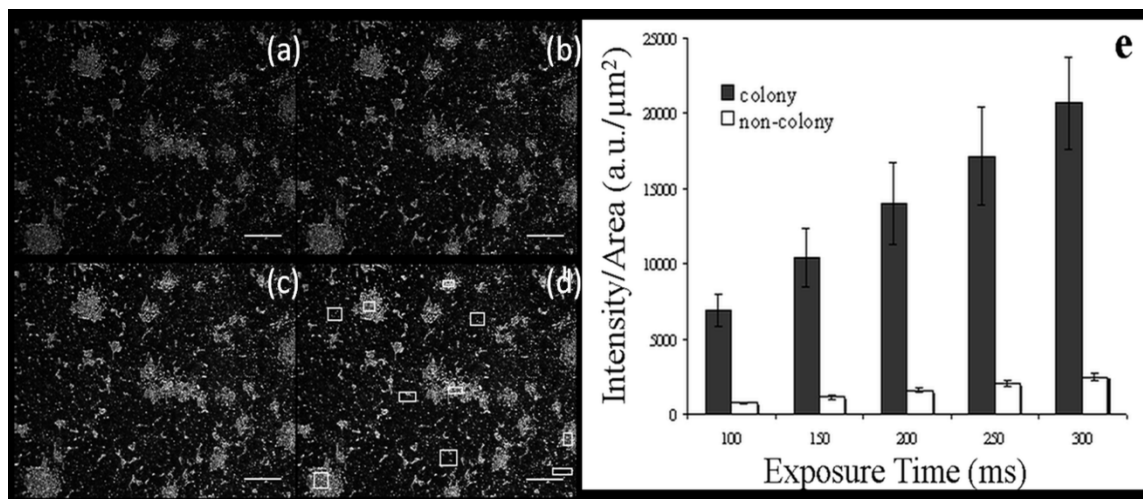


Figure 4-5: WEFS images (objective: 10x, Olympus-U plan FLN) with increasing exposure times (a) 150 ms (b) 200 ms (c) 250 ms and (d) 300 ms. Figure (e) Plot of Intensity/Area for microcolonies (black) and individual cells (white) as a function of exposure times. The squares shown in (d) depicts where the intensity has been measured. Intensity values were measured at the same location for all the exposure time. The error bars represent standard deviations of the mean and the number of measurement is $N=5$. Scale bars represent $200 \mu\text{m}$

In evanescent fluorescence microscopy systems, epi-fluorescence is a major concern due to randomly scattered photons. These randomly scattered photons can be a result of inhomogeneties in the waveguide or due to the excited fluorescent labels outside the evanescence field. Although for WEFS microscopy no labelling was used, scattered

photons can contribute to the signal from cells that are not within the evanescence field of the waveguides. The images from Figure 4-5(a-d) show almost no changes in the position of bacteria, especially in the microcolony region. As live bacteria were used for the experiments, some individual cells may have changed position during the imaging but the number of such bacteria is negligible. The displacement of such cells did not affect the intensity/area calculation within the squares chosen for integration of intensity. It was not possible to distinguish between reversibly attached bacteria or bacteria that attached weakly to a surface and motile bacteria within the depth of evanescence field from the stationary images. However the positions of the cells in the microcolonies were quite consistent with the increasing exposure time. This means that these bacteria must be adhered to the substrate. In a fluidic environment, particles are not static for more than a fraction of second due to Brownian motion. But if the cells are adhered to a surface, they will remain motionless. The images in Figure 4-5 with different integration time and taken one after another over a sufficient span of time are a proof that bacteria are stably attached to the waveguide surface within the evanescence depth.

The plot in Figure 4-5(e) shows the integrated intensities within the chosen squares for individual bacterial cells and for microcolonies. Both of them showed a linear increase in the intensity values for all exposure times. As expected, there was a remarkable difference in the intensity values between the microcolonies and the single cells. The linear increase in the intensity values also confirms that scattered photons due to non-uniformities in the waveguide or any other particle are negligible otherwise the intensity plots would be non-linear.

4.3.3 Integrated Intensity Profiles for Single Cells and Microcolony

Figure 4-6(a) and 4-6(b) show a bright field microscopy image and the corresponding WEFS image with an objective of magnification 63x. Two regions were selected (frames in the bright field and the WEFS images) to evaluate the integrated intensity profile for single cells (right frame) and a colony (left frame) in Figure 4-6(a and b). The integrated intensity was calculated along the y-axis (height) and plotted as a function of distance (width). The intensity profiles for the colony and the single bacteria are depicted in Figure 4-6 (c) and (d), respectively.

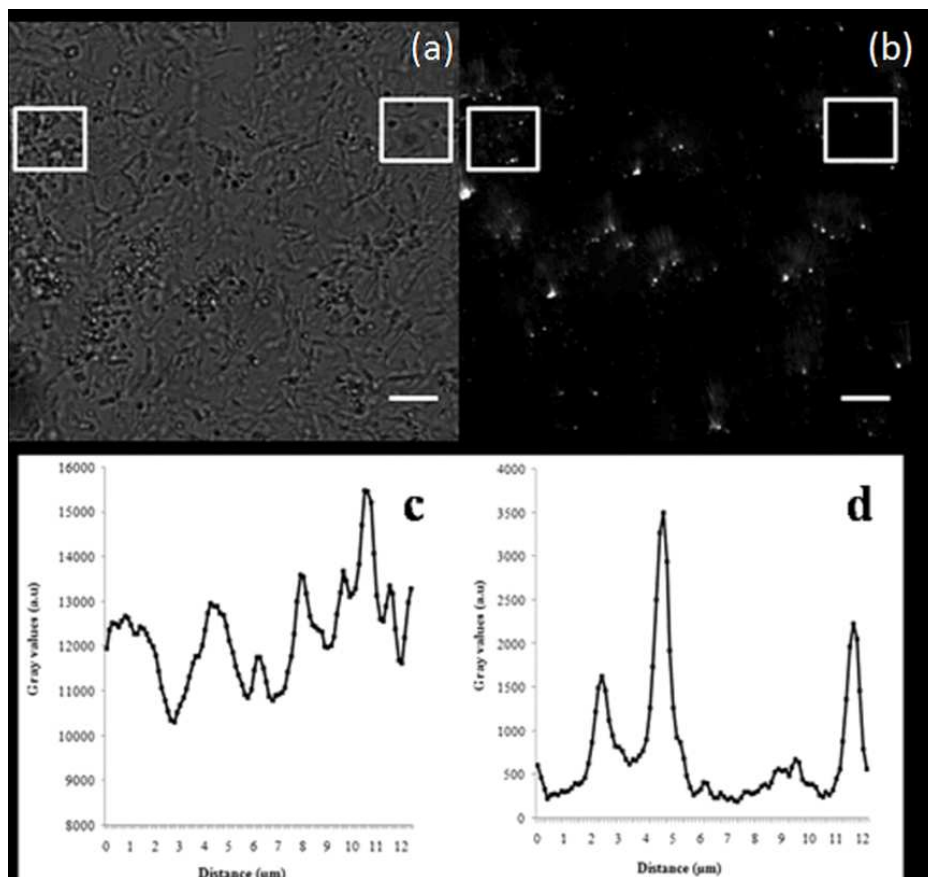


Figure 4-6: (a) Bright field image (Objective: 63x, ZEISS LD Plan-NEOFLUAR) and (b) corresponding WEFS image with same magnification. The small white frames indicate two regions: colonized area (left) and only individual cells (right). The intensity profiles are from the WEFS image in 4.6 (b) where y-axis depicts integrated intensity as a function of distance (x-axis) for (c) colony and (d) individual cells. Scale bars represent 10 μm .

As before, the scattering intensity of the colony region is significantly higher than that of the individual cell region. For the colony region, the intensity was very high and varied between 10,000 a.u and 15,500 a.u. along the entire distance axis (x-axis in Figure 4-6 (c)). This is due to the fact that the colony has a large number of bacteria acting as scattering centers within a small region. Moreover, EPS present between bacteria also contributed to the overall scattering intensity [39]. This plot also demonstrates a continuous intensity fluctuation for the bacteria in a colony present in the evanescence field. Inside the colonies, bacteria are obviously situated at slightly different distances

within the evanescence field. As a result, cells located at different depths of the evanescent field displayed different intensity values. Moreover, as the density of the bacteria is not homogeneous inside the colonies, the intensity distribution was also heterogeneous. All the colonies behaved in a similar manner.

Figure 4-6(d) shows the intensity profile of the individual bacteria within the region on the right side of the image. There were three distinct peaks ranging from 1500 a.u to 3500 a.u. and some fluctuations in intensity which was less than 700 a.u. Fluctuations below 500 a.u was considered as background noise which might arise because of the presence of some EPS or some randomly scattered photons. There were some values in the distance axis where almost no scattering intensity was present. The three peaks located approximately at 2.5, 5 and 12 mm distances in Figure 3(d) confirmed the attachment of three bacterial cells to waveguide surface. The presence of three bacterial cells can be visualized clearly from the left frame in Figure 4-6(a). It was not possible to interpret why the micrometer-sized bacterial cells which are one order of magnitude larger than the penetration depth of the evanescence field, produced scattering intensities on a comparable scattering-spot size. There can be many possible causes for the different peak heights, for example different bacteria heights, presence of more EPS, orientation of the cells on the surface etc. All three peaks were produced by individual bacterial cells. Hence, one of the reasons for the highest scattering peak may be because this rod-shaped bacterium was attached to the surface with its longer axis parallel to the waveguide surface occupying a larger scattering volume. On the other hand, the other two bacteria were attached perpendicularly with one of their poles occupying less scattering volume on the waveguide surface. It was unclear if the bacteria had secreted EPS as it can also be a source of scattering intensity. In order to find a solid interpretation for the intensity difference and attachment quality, a thorough theoretical investigation including size, shape, orientation, distance from surface, presence of EPS as well as the precise location of the cells is necessary.

4.3.4 Counting the Number of Single Bacterium in Bright Field vs. WEFS

An attempt was made to count the number of individual bacteria in Figure 4-3 and 4-6. The number of cells was different in the bright field images in comparison to their corresponding WEFS images. The number of cells represented as lines and dots in the bright field images were higher than the number of bright dots in the WEFS images. Approximately 150 ± 50 individual cells were counted in a defined unit area in a bright field image captured with 100 ms exposure time and 10x objective. (Figure not shown) However, the same unit area in the corresponding WEFS image showed only 12 ± 1 individual dots. For an exposure time of 500 ms, the number of dots was increased to 19 ± 5 . Many single cells clearly visible in the bright field image did not appear in the corresponding WEFS image even under a long exposure. This can only imply that these bacteria were not attached to the surface but they were planktonic in nature and remained suspended in the liquid growth medium. All colonies, on the other hand, were clearly visible in both the bright field and WEFS images. Therefore, the colonies were firmly attached to the surface. This study demonstrated the importance of bacterial colonization starting from an individual cell that proceeds to grow and divide and eventually form a colony which is the first step to produce biofilms.

4.3.5 Comparison of Bright Field Image vs. WEFS Image

Figure 4-7 shows the comparison between a bright field image and a WEFS image with highest possible magnification. In image 4-7(a), a very small colony with only three cells on the right side and a single individual cell on the left side were depicted. Various aspects between the bright field and WEFS images were compared.

1. In the corresponding WEFS image in 4-7(b), the colony was detected as one brightly scattering dot (bacterial cell) associated with two less brightly scattered dots nearby.
2. The bright field image and the WEFS image does not exhibit the same focal plane. The bright field image shows the uppermost three cells of the beginning

colony whereas the WEFS image demonstrates the lowest and closest plane to the surface.

3. A single dot with low scattering intensity appeared just left to the colony in WEFS image where no bacteria could be observed in the bright field image. This bacterium was probably weakly adhered to the waveguide surface.
4. The individual bacterium located on the left side of the bright field image is not depicted in 4-7(b) and no intensity could be found in the intensity profile in 4-7(c). This implies that this bacterium was not adhered to the surface.
5. During imaging, images were always taken with lowest possible plane for bright field microscopy. But as the inverted microscope (Zeiss Axiovert 25CFI) used in the setup has fairly coarse focussing mechanics, it was not possible to locate the exact focal plane of the waveguide surface. The single bacteria in 4-7(a) is in better focus than the colony. Therefore, it was interpreted to be located at a further distance than the colony. This interpretation is in excellent agreement with the WEFS image in 4-7(b) that shows no intensity at the same location.
6. The difference in focal plane can also be observed from the location of colony in the bright field image and the corresponding WEFS image. The positions of the three cells in bright field image are different compared to the positions in the WEFS image. The bacterium on top of the colony of the lowest plane of the bright field image is differently arranged than the three dots located on the waveguide surface in WEFS image.
7. The intensity profile in 4-7(c) shows that the beginning colony has a high intensity peak of more than 6000 a.u. with a shoulder at its left side. The high peak is assigned to the scattering of two clearly visible bacteria where one has a higher intensity than the other while the peak at the shoulder is attributed to the third bacterium with a lower intensity. Bacteria colonize by a single, parent cell that first attached to the surface by irreversible adhesion and then grows by binary division. The brightest cell with its high intensity must be this parent cell from which the colony started to grow. The other two cells in the small colony have less scattering intensity and therefore imply that they are located in the evanescent field and connected to the parent cell via EPS but not necessarily attached to the

surface directly and as closely as the parent cell. It was concluded that the development of the colony is a 3D process where the parent bacterium produced via binary division two daughter cells that were not directly attached to the surface.

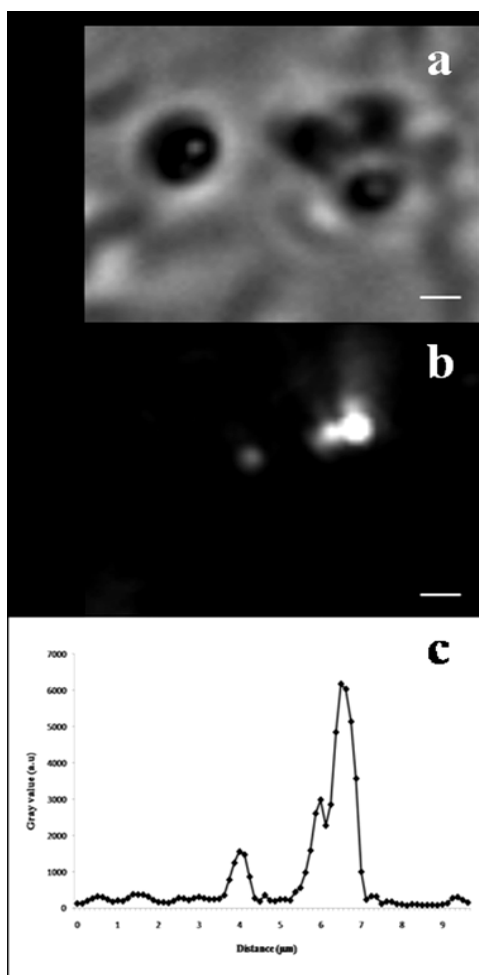


Figure 4-7: (a) *Bright field image of a starting colony and an individual cell taken with the highest magnification possible (Objective: 63x, ZEISS and the TM₂ mode)* (b) *Corresponding WEFS image with exposure time of 2s.* (c) *The intensity profile for the WEFS image depicts the integrated intensity (y-axis) as a function of distances (x-axis). Scale bars represent 1 μm.*

8. The intensity peak for the single dot located on the left side of colony in the WEFS image at 4 mm distance has a scattering intensity of less than 2000 a.u. This cell was not attached to the surface but it was close enough to produce a detectable signal. This cell was not located in the focal plane that depicted the top of the starting colony since this cell could not be observed in the bright field image. This cell was probably suspended close to the surface and could represent the beginning of the adherence of a bacterium to a surface.
9. In Figure 4-7(c), the intensity fluctuations of less than 500 a.u. in the first 3 mm distances is attributed to background noise due to scattering produced by irregularities in the inhomogeneous waveguide structure. However, to avoid detecting random scattering, a threshold intensity value needs to be defined above which only the scattering intensity from the cells will be detected.

4.4 Materials and Methods: Attachment of Nitrobacter following UV Sterilization

4.4.1 Collimated Beam Apparatus

For UV treatment of *Nitrobacter* sp. 263, a collimated beam apparatus (Trojan Technologies) was used. The main part of this apparatus is a low pressure mercury arc lamp which is monochromatic at 253.7 nm. The light from this lamp travels through a collimating tube which provides uniform distribution of light over the sample holder containing bacteria. A shutter is incorporated to regulate the time of exposure for calculating the UV dose. A thermally and physically stable platform is used to support the system and the petri dish/sample holder containing bacteria.

4.4.2 UV Sterilization Process

This experiment was carried out at the TROJAN Technologies, 320 Gore Road, London, ON, Canada. For the UV sterilization of *Nitrobacter* sp. 263, six 10 ml aliquot of prepared bacterial suspensions with 10^6 bacteria/mL each, was placed in separate sterile glass dishes. These were then UV-irradiated with six different UV doses of 2, 4, 8, 14, 20 and 30 mJ/cm². The applied doses were achieved by varying the irradiation time with the help

of a shutter in the beam apparatus. A calibrated radiometer (International Light Technologies Inc., USA) was used to measure the irradiance of the UV light from the collimated beam. The bacterial suspensions were constantly stirred with a magnetic stir bar during irradiation to assure equal irradiation for all bacteria in suspension. The UV doses were calculated using the equation:

$$\text{UV dose (mJ/cm}^2\text{)} = \text{Irradiance (mW/cm}^2\text{)} \times \text{Irradiation time (s)}$$

Several corrections were necessary for irradiance measurement as the radiometer only provides the irradiance at the center of the beam. For this reason, the average irradiance was calculated taking several factors in consideration namely petri factor (PF), reflection factor (RF), divergence factor (DF) and water factor (WF) [26]. The reflection factor represents the change in refractive index between two mediums such as air and water. The petri factor takes into account the varying irradiance over the surface area of the liquid sample. The water factor calculates the decrease in irradiance due to absorption as it passes through water. Divergence of the beam occurs when the beam is not perfectly collimated for finite distances from UV light to cell suspensions. All these factors were previously determined by Trojan facilities. The average irradiance is calculated as:

$$\text{Average irradiance} = \text{Measured irradiance} \times \text{PF} \times \text{DF} \times \text{RF} \times \text{WF}$$

4.4.3 Experiment on Bacterial Attachment following UV Sterilization

This experiment was performed for analyzing the behavior of bacteria for microcolony formation after a UV sterilization process. The WEFS microscopy can have application for quick and easy investigations of bacteria sterilization treatment in drinking water. UV treatment with moderate doses does not kill bacteria but alters their DNA in such a way that they become incapable of division and growing a biofilm. It was hypothesized that the sterilized and non-potent cells after UV treatment do not attach to the substrate and cannot form a colony.

After the UV treatment the bacteria in suspension were stained using Live/Dead BacLight viability staining kit (Invitrogen, USA) and examined using a fluorescence microscope

(Zeiss). It was found that UV treatment did not cause any bacterial death. One sample was not treated with any UV illumination and served as a control. Bacteria from each of the UV treated samples and from control were then cultured on waveguides for 24 hours at 37°C with the same protocol as before. Then they were examined using WEFS microscopy.

4.5 Results

4.5.1 Attachment of Bacteria after UV Irradiance

Figure 4-8 shows a series of WEFS images (a-d) and bright field images (e-h) of UV treated bacteria. When no UV dose was applied, the images depicted typical colony formation with many individual bacteria in both bright field and WEFS images 4-8(a and e). However, with increasing UV dose, there was less colony formation 4-8(b, c, f, g) and finally no colonies at all 4-8(d and h).

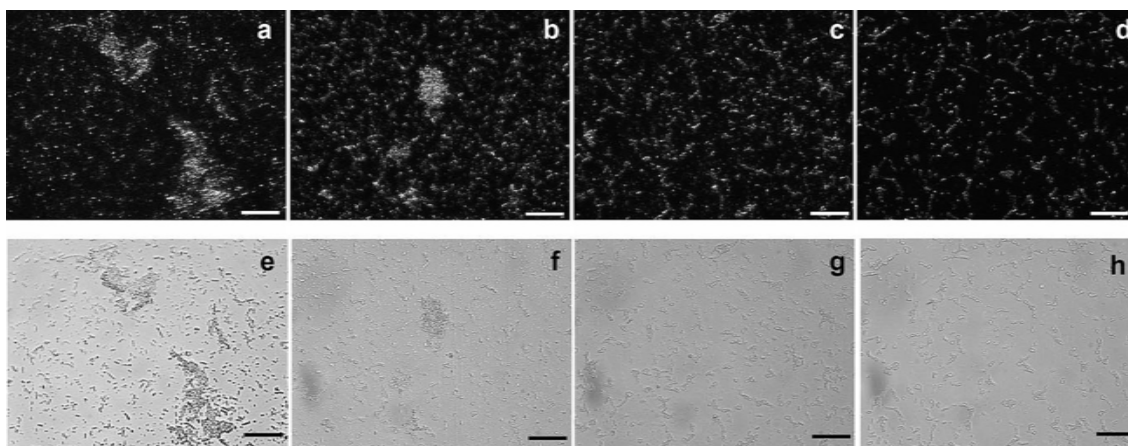


Figure 4-8: (a-d) WEFS and (e-h) bright field images of UV treated bacteria after 24 h of culturing taken with objectives: 40x ZEISS LD Plan-NEOFLUAR. The UV doses applied were (a) and (e) control: 0 mJ/cm² (b) and (f) 8 mJ/cm² (c) and (g) 20 mJ/cm² and (d) and (h) 30 mJ/cm². The scale bars represent 50 μm.

The attachment of bacteria could not be completely prevented even with the highest illumination dose of 30 mJ/cm². The scattering signal from colony and single cells also decreased with increased UV illumination. Both the microscopy techniques depicted that

microcolony formation could be reduced by illumination although attachment of bacteria to surface still took place. To completely prevent bacterial attachment to surfaces, possibly higher doses of UV radiation is needed.

4.5.2 Quantitative Analysis of Attachment of Bacteria after UV Doses

For these data to be analyzed quantitatively, a Matlab program was employed to investigate the intensity distribution of each of the WEFS images and to calculate the percentage of area occupied by bacteria in colonies and as single cells. Percentage of area means pixels with signals above a threshold signal defined as background noise. In the images some colonies appeared to be connected and occupied a particular number of pixels. The percentage of these was also calculated. This indicated that a large number of colonies with very small sizes were present. With increasing UV dose, the number of such colonies also decreased as expected.

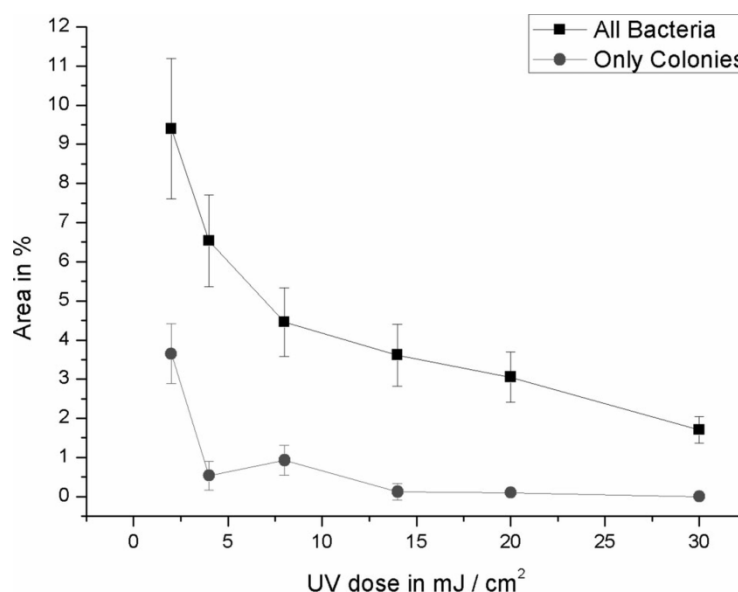


Figure 4-9: Percentage of area occupied by individual bacteria or colony with a minimum size of 400 pixels vs. UV dose. 100% means all pixels in the entire image.

Figure 4-9 shows the percentage of area occupied by bacteria as a function of applied UV dose. For comparison, a minimal area of 400 pixels was chosen as a threshold value for being counted as a colony. After the calculation of area, it was found that the area

occupied by these colonies were almost half the area inhabited by all bacteria. With enhanced UV doses, the percentage of colonies also decreased exponentially as the other bacteria. After a dose of 14 mJ/cm^2 , these distinct colonies disappeared.

With increasing UV doses, the percentage of occupied area decreased exponentially but it did not reach zero. Bacteria were still able to attach to the waveguide surface after a UV treatment of 30 mJ/cm^2 . It was approximated by extrapolating the curve (all bacteria in Figure 4-9) that to prevent bacterial attachment completely to the surface, approximately 100 mJ/cm^2 UV dose will be required. However, a dose of 200 mJ/cm^2 would be applied to completely sterilize these bacteria if it was a water purification treatment for double safety. Area vs. UV dose curves like this can be utilized for developing sterilizing protocols and controls by water purification facilities for harmful bacteria like *E. coli* or salmonella.

4.6 Summary

Results from this study signify that WEFS microscopy is a straight forward method for the detection of bacterial attachment to surfaces. This method has the ability to distinguish between attached bacteria and bacteria that are unattached or close to a surface. High contrast images were achieved by exclusively capturing the scattering light from the samples without the application of any labels.

The UV sterilization study confirmed the hypothesis that with increasing UV illumination doses, less bacterial attachment will occur. As a result less colonization was visualized in the images. This method has its potential application in many industries like water treatment facilities, anti-bacterial coatings and quick investigations of bacterial colonization in restaurants or hospital environments. The waveguides used in the experiments are reusable and capable of withstanding simple chemical cleansing procedures. In conclusion, WEFS microscopy is a novel method capable of detecting the viability and potency of bacteria and provides information about early stages of bacterial attachment and colonization on surfaces.

4.7 References

1. Hetrick, E. M., & Schoenfisch, M. H. (2006). Reducing implant-related infections: active release strategies. *Chemical Society Reviews*, 35(9), 780-789.
2. An, Y. H., & Friedman, R. J. (Eds.). (2000). *Handbook of bacterial adhesion: principles, methods, and applications* (pp. 1-27). Totowa, NJ: Humana Press.
3. Pires, L., Sachsenheimer, K., Kleintschek, T., Waldbaur, A., Schwartz, T., & Rapp, B. E. (2013). Online Monitoring of Biofilm Growth and Activity Using a Combined Multi-channel Impedimetric and Amperometric Sensor. *Biosensors and Bioelectronics*.
4. Madkour, A. E., Dabkowski, J. M., Nüsslein, K., & Tew, G. N. (2008). Fast disinfecting antimicrobial surfaces. *Langmuir*, 25(2), 1060-1067.
5. Kendall, K. (2004). The Future of Molecular Adhesion. *Molecular Adhesion and Its Applications: The Sticky Universe*, 409-421.
6. Smith, L. V., Tamm, L. K., & Ford, R. M. (2002). Explaining non-zero separation distances between attached bacteria and surfaces measured by total internal reflection aqueous fluorescence microscopy. *Langmuir*, 18(13), 5247-5255.
7. Vigeant, M. A. S., Ford, R. M., Wagner, M., & Tamm, L. K. (2002). Reversible and irreversible adhesion of motile *Escherichia coli* cells analyzed by total internal reflection aqueous fluorescence microscopy. *Applied and environmental microbiology*, 68(6), 2794-2801.
8. Byrne, G. D., Pitter, M. C., Zhang, J., Falcone, F. H., Stolnik, S., & Somekh, M. G. (2008). Total internal reflection microscopy for live imaging of cellular uptake of sub-micron non-fluorescent particles. *Journal of Microscopy*, 231(1), 168-179.
9. Velinov, T., Asenovska, Y., Marinkova, D., Yotova, L., Stoitsova, S., Bivolarska, M., & Stavitskaya, L. (2011). Total internal reflection imaging of microorganism adhesion using an oil immersion objective. *Colloids and Surfaces B: Biointerfaces*, 88(1), 407-412.
10. Maya, C., Beltran, N., Jimenez, B., & Bonilla, P. (2003). Evaluation of the UV disinfection process in bacteria and amphizoic amoebae inactivation. *Water Recycling in the Mediterranean Region*, 3(4), 285-291.

11. Sinha, R. P., & Häder, D. P. (2002). UV-induced DNA damage and repair: a review. *Photochemical & Photobiological Sciences*, 1(4), 225-236.
12. Durbeej, B., & Eriksson, L. A. (2002). Reaction mechanism of thymine dimer formation in DNA induced by UV light. *Journal of Photochemistry and Photobiology A: Chemistry*, 152(1), 95-101.
13. Summerfelt, S. T. (2003). Ozonation and UV irradiation: an introduction and examples of current applications. *Aquacultural engineering*, 28(1), 21-36.
14. Walker, R. W., Markillie, L. M., Colotelo, A. H., Gay, M. E., Woodley, C. M., & Brown, R. S. (2013). The Efficacy of Ultraviolet Radiation for Sterilizing Tools Used for Surgically Implanting Transmitters into Fish (No. PNNL-21126). Pacific Northwest National Laboratory (PNNL), Richland, WA (US).
15. <http://www.phys.ksu.edu/gene/chap3b.gif>
16. Cebon, A., & Garnier, J. (2005). Nitrobacter and Nitrospira genera as representatives of nitrite-oxidizing bacteria: Detection, quantification and growth along the lower Seine River (France). *Water research*, 39(20), 4979-4992.
17. Starkenburg, S. R., Larimer, F. W., Stein, L. Y., Klotz, M. G., Chain, P. S., Sayavedra-Soto, L. A., Poret-Peterson, A. T., Gentry, M. E., Arp, D. J., Ward, B. & Bottomley, P. J. (2008). Complete genome sequence of *Nitrobacter hamburgensis* X14 and comparative genomic analysis of species within the genus *Nitrobacter*. *Applied and environmental microbiology*, 74(9), 2852-2863.
18. Meiklejohn, J. (1953). The nitrifying bacteria: a review. *Journal of Soil Science*, 4(1), 59-68.
19. Delwiche, C. C., & Finstein, M. S. (1965). Carbon and energy sources for the nitrifying autotroph *Nitrobacter*. *Journal of bacteriology*, 90(1), 102-107.
20. Jeon, B. Y., Jung, I. L., & Park, D. H. (2012). Enrichment and Isolation of CO₂-Fixing Bacteria with Electrochemical Reducing Power as a Sole Energy Source. *Journal of Environmental Protection*, 3(1), 55-60.
21. Painter, H. A. (1970). A review of literature on inorganic nitrogen metabolism in microorganisms. *Water Research*, 4(6), 393-450.

22. Shuster, J. P. (2013). The biogeochemical cycling of gold under surface and near-surface environmental conditions. Ph.D thesis disst., University of Western Ontario.
23. Holt, J. G., Krieg, N. R., Sneath, P. H., Staley, J. T., & Williams, S. T. (1994). Bergey's manual of determinative bacteriology. Williams and Wilkins, Baltimore, 787.
24. Gerardi, M. H. (2003). Nitrification and denitrification in the activated sludge process. John Wiley & Sons.
25. HF-sputtered glass waveguide slides for waveguide evanescent field microscopy, C. Halfpap, M. Morawitz, A. Peter, N. Detrez, S. Mittler, and U. Langbein, DGaO Proceedings 2012, 0287-2012.
26. Bolton, J. R., & Linden, K. G. (2003). Standardization of methods for fluence (UV dose) determination in bench-scale UV experiments. Journal of Environmental Engineering, 129(3), 209-215.

Chapter 5

5 Evanescent Field Scattering Microscopy of Osteoblasts

This chapter describes imaging of osteoblast MC3T3 cell lines from mice with WEFS microscopy. Osteoblasts were cultured on waveguide surfaces and imaged with WEFS microscopy. Cells were also stained and imaged with WEFM microscopy for comparison between the two evanescent microscopy techniques. Conventional fluorescent microscopy was carried out on osteoblasts to obtain information about the typical position of the focal contacts. It could be shown that WEFS microscopy delivers information on cell form, focal adhesions and granularity. However, with the drawback that granularity and adhesions cannot be discriminated. In principle, WEFS microscopy is a new method to investigate cell granularity for immobilized cells not accessible for flow cytometry studies.

5.1 Introduction

Cellular imaging is emerging as a crucial tool for visualizing cell growth, proliferation, spreading and attachment. Over the past decades, the advances in cell imaging techniques have immensely changed biological research. To understand the function of a living organism, it is important to have an understanding of the cellular processes that occur within a cell. Current research is focused on direct imaging of single molecules and individual cells as well as interaction between individual cells and the substrates [1]. Live cell imaging has become a major analytical tool to provide critical insight and analysis for cellular function mechanisms. The plasma membranes, cytoplasm and extracellular matrix regions are the most investigated regions of a cell [2]. Biomedical applications ranging from tissue engineering to medical diagnostic requires a better realization of the interactions between biological cells and their surfaces. Attachment, adhesion and spreading describe the first phase of cellular growth and are the determining factors for the proliferation of cells on implants. To comprehend various diseases, it is pivotal to understand intracellular signaling and cell adhesion mechanisms. There are generally two types of adhesion: cell-cell adhesion and cell-matrix adhesion. In cell-cell adhesion, adjacent cells are physically bonded while in cell-matrix adhesion, cells are bonded with

the adhesive proteins present in the extracellular matrix [3]. The interactions between cells and extra cellular matrix (ECM) are known as adhesions. Adhesions are defined by structures which link the actin cytoskeleton to the ECM through integrins and other proteins [4]. Adhesions to ECM can be broadly classified into two types, namely focal contacts and fibrillar/focal adhesions [5]. Focal contacts are located at the periphery of cells and often subdivided into dot-like contacts having dimensions of about 1 square micron. Focal adhesions, on the other hand, are usually elongated structures up to a few μm s in length [5]. These adhesions play a major role in different processes such as cell differentiation, cellular trafficking and tissue architectures.

Imaging the cellular processes with conventional optical microscopes remains a challenge. Total internal reflection fluorescence (TIRF) microscope has been employed extensively by scientists to visualize cellular processes occurring at or near the membrane and the extracellular matrix. Cell-surface contact regions are also investigated and imaged using TIRF microscopy [6]. TIRF microscopy, which is also an evanescent field microscopy, utilizes the evanescent field to selectively excite fluorophores near the cell surface. TIRF microscopy is well-suited for the analysis of molecules and processes near the plasma membrane which lies within the evanescent field. Due to the low penetration depths of the evanescent field, background fluorescence is minimized and only regions near the surface can be visualized, thus giving rise to low signal to noise ratio.

Waveguide evanescent field fluorescence microscope (WEFF) described by Hassanzadeh et al. allows the imaging of close contact regions between cells and their substrates by employing ion-exchanged waveguides [7]. In this method, cells are stained with fluorescent dyes as the evanescent field is capable of selectively excite fluorophores within the range of the field [8]. This method is also capable of determining the cell-substrate separation distances by exciting fluorescent markers utilizing multimode waveguides. The plasma membrane of osteoblast cells, which are bone matrix forming cells, were successfully imaged and cell-substrate distances found with this method. The cells were found to be adhered to the waveguide at various attachment points. The rest of the plasma membrane was bend away from the evanescent intensity profile and invisible for imaging with WEFF microscopy.

The aim of this chapter is to demonstrate the application of waveguide evanescent field scattering microscopy as a high contrast imaging technique for individual cells and cell-substrate interactions. WEFS microscopy has been employed to image osteoblast cells in this work without the use of any kind of fluorescent dyes. Osteoblasts are the major cellular component of bone [9]. These cells are accountable for the synthesis, deposition and mineralization of bone during initial bone formation. They usually have only one nucleus [10]. Osteoblasts also produce new bone named osteoid, unmineralized, made of collagen and other proteins. In this study, osteoblast cells were cultured on the surface of waveguides and imaged with both WEFF and WEFS microscopy. For imaging with WEFF microscopy, the cells were fixed and stained with a widely used carbocyanine fluorescent dye DiIC₁₈. This amphiphilic dye is used to label cell membranes and is usually less toxic and highly stable. The excitation and emission wavelength peaks for DiIC₁₈ occur at 549 and 565 nm, respectively. Images of osteoblasts obtained from both techniques were compared. Images were also acquired using a standard fluorescence microscopy and these were also compared to the WEFS microscopy images.

Flow cytometry is a widely used laser-based powerful technique for rapid analysis of large numbers of cells as they flow quickly in a fluid stream through a beam of light [11]. Flow cytometry provides the opportunity for specific and detailed analysis of cell population, depending on the parameter read by the cytometer from the cells. This parameters can be scattered light intensity and direction, or a fluorescence signal, both intensity and/or spectral information. A wide range of cellular parameters can be measured with this technique which includes particle size, internal complexity such as granularity, intracellular pH, levels of cellular components such as DNA, protein, calcium and surface receptors as well as simultaneous multiparameter analysis of single cells [12][13]. Thousands of cells per second can be analyzed with this technology using light scattering, fluorescence and absorbance measurements. It is most frequently used for evaluating fluorescence intensities created by fluorescent-labeled antibodies to detect proteins binding to specific molecules. Recent advances offer the commercially available versatile and robust flow cytometry equipped with modern data acquisition and interpretation software. The development of many different staining assays was behind the tremendous success as well.

A flow cytometry device consists of five main units; namely a flow cell, a light source which can be a laser, an LED or a mercury lamp, optical filters to select specific wavelengths, photomultipliers for sensitive detection of signals and a data processing unit. A schematic diagram of a flow cytometer is shown in Figure 5.1(a). Cells in suspensions are injected into a flow cell where the cells pass across a laser beam, one cell at a time. When cells pass through the beam, they scatter light which is known as forward and side scattering. The forward scattered light supplies information about the size of the cells whereas side scattered light gives information about several parameters including cell granularity and morphology. When cells are stained with fluorescent dyes for selective assaying, fluorescent signals are also detected. Both the fluorescent and scattering signals are often combined to achieve all subpopulation data [12].

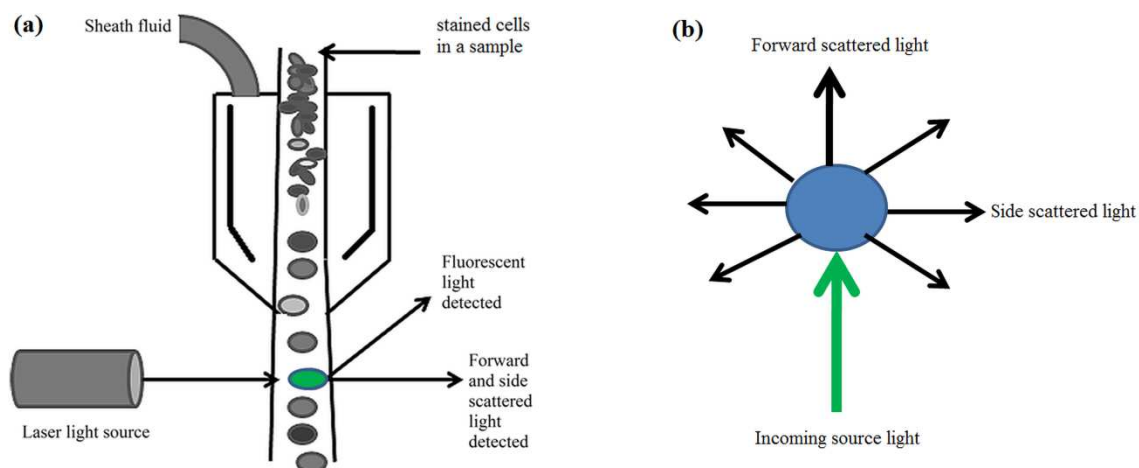


Figure 5-1: Schematic of Flow cytometry (a) flow cytometry device showing cells in a flow cell scattering light while passing across a laser beam and (b) a cell scattering light in two directions known as forward scattered light and side scattered light.

The most obvious difference between flow cytometry and microscopy is that flow cytometry sacrifices imaging and therefore location information entirely, however achieves high acquisition rates and high sensitivity. Thus many researchers combine fluorescence imaging and flow cytometry for both quantitative assessment and visual examination of cellular processes [14]. Recently, commercially available imaging flow cytometers have been developed to address this issue. The imaging cytometers can rapidly acquire multiple images of each cell by fluorescence intensities comparable to

conventional flow cytometry. Although imaging flow cytometry is a superior choice for cell analysis, it is highly expensive. The cost of regular conventional flow cytometers start from more than three hundred thousand US dollars not including the cost for the analysis software [15]. Imaging flow cytometer are even more expensive. In this chapter, we investigate the possibility to use WEFS microscopy for obtaining information about cellular granularity and adhesion in immobilized cells not accessible for flow cytometry. WEFS microscopy allows to image cells without the use of any fluorescent dyes. As a result, no additional staining is necessary for the samples. It is also fairly less expensive as WEFS microscopy only consists of a regular laboratory inverted microscope with a camera and waveguides to be used as microscope slides.

Flow cytometry is able to discriminate and quantify viable, apoptotic and necrotic cells through measurement of forward and side light scatter which are proportional to cell diameter and internal granularity, respectively. Granularity is a measure of the presence of granular structures in cells. Granularity in cells is an important parameter for clinical research as an increase in cytoplasmic granularity is considered to be a sign of cell injury [16]. Increases in intracellular granularity was found to be related to cell death and terminal growth arrest which are vital parameters as they provide useful markers to screen for cancer therapeutic agents [17]. Flow cytometry is an established method in this area capable to detect increases in side scatter light which is associated with intracellular granularity in cancer cell lines. In this study, WEFS microscopy was employed to detect the location of granules in osteoblast cells.

5.2 Materials and Methods: Evanescent Imaging of Osteoblasts

5.2.1 WEFS and WEFM Microscopy

WEFM and WEFS microscopy have similar experimental set-ups. A detailed description of the microscope was discussed in Chapter 2. For WEFM microscopy, a 560 nm long pass filter (omega optics) was used to block the excitation wavelength of the He-Ne laser at $\lambda=542.8$ nm collecting only the fluorescent wavelengths. For cells which were stained and then imaged using WEFS microscopy, a short pass filter with a cut-off wavelength of

550 nm (Thorlabs) was used to block the fluorescent emission wavelength of the dye DiIC₁₈ for detecting scattered light only.

5.2.2 Cell Culture

MC3T3-E1 osteoblast cell lines from mice were cultured with α -minimum essential medium (α -MEM, Gibco, catalog#12571) supplemented with 10% fetal bovine serum (FBS, Gibco, catalog#12483) and 1% antibiotic-antimycotic 100x (Gibco, catalog#15240). Cell release was confirmed by adding 0.05% Trypsin-EDTA (Gibco, catalog#25300) to culture flask and incubating for 5 minutes. To count the number of cells, 100 μ l of cell suspension was added to an Eppendorf tube containing 100 μ l of trypan blue. A hemacytometer, which is a glass slide with a gridded chamber in the middle, was used to count the number of cells. Cells were cultured on the surface of the waveguide with a density of 30,000 cells per waveguide and incubated for 24 hours at 37°C and 5% CO₂ atmosphere. After 24 hours, cells were washed with Dulbecco's phosphate-buffered saline 1x (DPBS, Gibco, catalog#14040) and WEFS microscopy was carried out immediately.

5.2.3 Fluorescence Staining

For evanescent fluorescence imaging, cells were fixed with 4% paraformaldehyde (Sigma Aldrich) in DPBS for 10 minutes at room temperature and rinsed three times with DPBS afterwards. The fixed cells were incubated with DiIC₁₈ (10 μ l of 1 mM DiI in 1 ml culture medium) for 20 minutes at 37°C, followed by three washes with DPBS, each for five minutes. The cells were always maintained in DPBS during microscopy.

5.3 Results

5.3.1 Imaging with Both WEFF and WEFS Microscopy

For imaging with both fluorescent and scattering microscopy, the osteoblast MC3T3-E1 cell lines were fixed and stained with fluorescent dye DiIC₁₈. Cells were imaged with WEFF microscopy first and then WEFS microscopy to ensure that WEFS microscopy is capable of acquiring images as well as WEFF microscopy. Figure 5.2(a-d) shows a series of images of a fixed and labelled osteoblast cell with high exposure times of the camera.

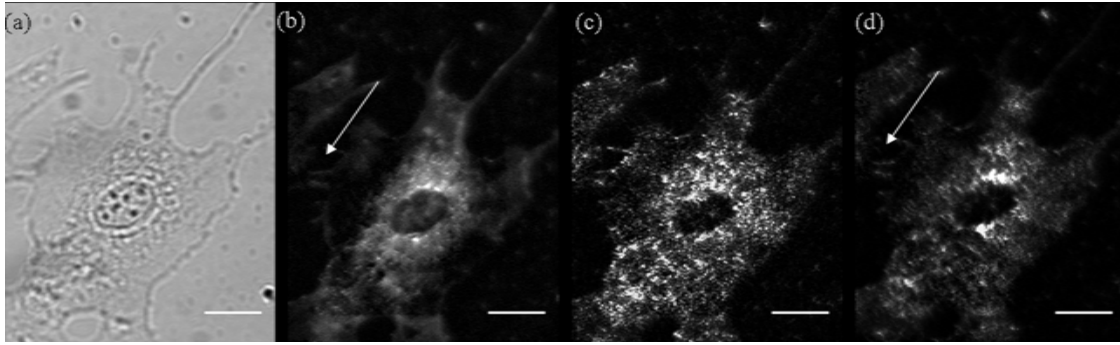


Figure 5-2: Single fixed and stained osteoblast (a) bright field image, (b) WEFF image (560 nm long pass filter to block excitation light of 543 nm), (c) image captured with no filters; hence both excitation and emission wavelengths of DiI are forming the image and (d) WEFS image (550 nm short pass filter blocking the fluorescent emission wavelengths) WEFF and WEFS images are captured with a TM mode and exposure time of 6s. The objective used was 40x (ZEISS LD Plan-NEOFLUAR). Arrows indicate where the cell is joined with an adjacent cell. Scale bars represent 20 μm .

Figure 5.2 (a) shows a bright field microscopy image of a single osteoblast. The nucleus and the outline of the cell were clearly visible in this image. To confirm the visualization of the entire cell with both fluorescence and scattering methods, the exposure time of the camera was set to a high exposure time of 6s. The WEFF microscopy image of the same cell with a 560 nm long pass filter is shown in Figure 5.2 (b). Both the cell outline and cell body were distinctly visible in the image. Furthermore, it was possible to identify the nucleus as a large black spot. The cell body was distinguishable from the other parts of the cell because of the presence of many densely packed bright spots around the nucleus. The outline of the cell which is actually the spread region of the cell was less bright than the rest of the cell but still unmistakable as it was identical to the bright field image of Figure 5.2 (a). The white arrow in these images refers to the region where the cell is connected with an adjacent cell. As it has already been discussed that the evanescent field is present only in the first 100 nm above the surface of the waveguide, only the close contact regions of the cell should be visible in the WEFF image. However, due to the high exposure time of 6s, the entire cell became visible as an epi-fluorescence like image. Parts of the cells located far away from the surface could also be seen. This is a typical

behaviour of evanescent microscopy technologies as with high exposure times multiple scattering occurs delivering photons into the entire cell. This has been shown in TIRF images and was also observed in WEFF images with human smooth muscle cells [18][19]. Unfortunately close contact regions and focal adhesions alone are not possible to visualize with this type of high exposure imaging.

Figure 5.2 (c) shows the same cell but captured with no filters. As a result, both the excitation and emission wavelengths of the fluorescent dye are forming the image. This image depicts both the scattering and fluorescence microscopy image. Although the cell outline was visible and the nucleus distinguishable, the image was too noisy with both scattering and fluorescence intensities present which made it impossible to distinguish between the spread region of the cell and the cell body. Figure 5.2 (d), however depicts the same cell captured with WEFS microscopy with an inserted 550 nm short pass filter blocking out the fluorescence. In this case only the excitation light from the laser was present and imaging was done exclusively by capturing the scattered photons from the cell. This image was similar to the image in Figure 5.2 (b) with the nucleus and cell outline visible, nevertheless the spread regions of the cell showed less scattered light and the cell body was identified with bright white spots around the nucleus. The connecting links joining the cell with an adjacent cell, indicated by an arrow, were less prominent when compared to the WEFF microscopy image. It was observed that the bright spots in the spread region of the cell were not evenly distributed. It might represent that the brighter regions were more closely located to the surface than the less bright regions as it was discussed for the bacterial experiment in Chapter 3. However, this hypothesis could not be confirmed from these image series due to the presence of large amounts of light from the high exposure time.

5.3.2 Imaging with WEFS Microscopy

For imaging with evanescence scattering microscopy only, cells were not fixed or stained and no filters were used as fluorescent wavelength exclusion was not necessary. Figure 5.3 shows a WEFS microscopy image of osteoblasts cultured on a waveguide surface. An exposure time of 2s was used to capture this image which depicted only the scattering photons from the cells.

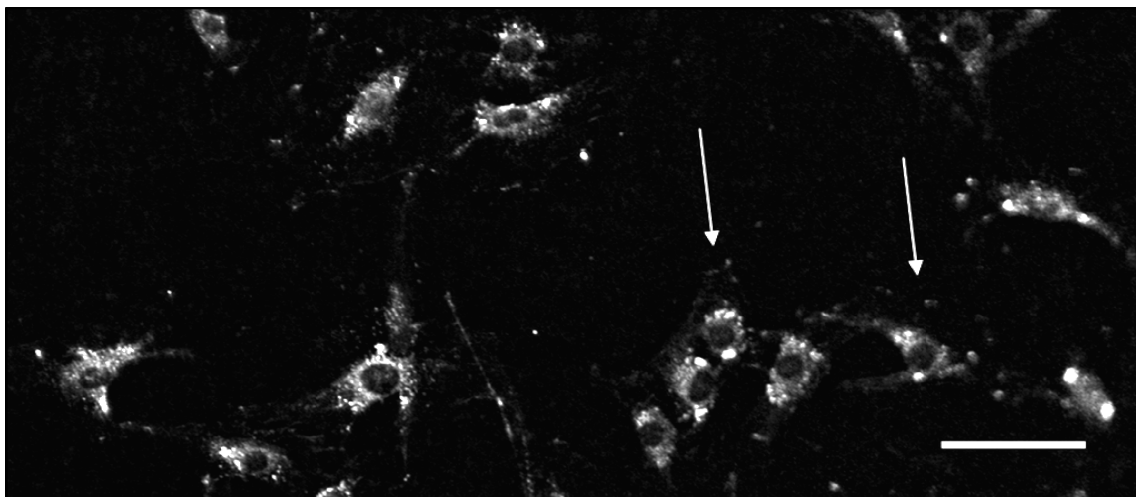


Figure 5-3: WEFS microscopy image of osteoblasts captured with an exposure time of 2s and TM mode with a magnification of 20x (Olympus LUC plan FLN). Arrows indicate bright spots along the edge of the spread regions. Scale bar represent 100 μm . Brightness and contrast enhanced for better visualization.

It was found that imaging with only WEFS microscopy without applying any fluorescent staining, produced better images than images acquired with both WEF and WEFS simultaneously employing fixed and stained cells. The reason might be the presence of left over dye particles and particle left from paraformaldehyde solution which scattered light when imaging with WEFS microscopy, hence the very large amount of scattering points in Figure 5.2 (d). There was as many as fifteen cells present in the image with distinguishable cell outlines and also the presence of large dark nuclei. The nuclei and cell bodies, located outside the evanescent field region, could still be clearly visible in the image acquired with 2s exposure time. For some of the cells, the spread regions of the cells were visible showing brighter regions along the edges, possibly due to close contact regions of the cells to the substrate. The white arrows in the image are pointing to some of those bright regions. It was not possible to determine whether these were focal adhesions from this image. The background of the image was not as dark as the background of images acquired with WEF microscopy. The reason behind the more noisy background is possibly the presence of scattered light resulting from inhomogeneities in the waveguide. The inhomogeneity of the waveguide was confirmed

from the presence of really clearly visible cells and comparatively less visible cells in the same image such as the one shown at the lowest rightmost corner of the image.

Previous work with WEFF microscopy had demonstrated that adhesion points of cells are visible with short exposure times and with increasing exposure times, other parts of the cell begin to appear [8][18]. Figure 5.4(a-d) depicts a series of images acquired with different exposure times of 0.5s, 1s, 1.2s and 1.5s, respectively. In Figure 5.4 (a), at low exposure time of 0.5s, only a few bright spots were visible. With increasing exposure time, more and more features started to be visible. The cells became fully visible at an exposure time of 1.5s. Surprisingly, the nucleus and the cell body was visible with the low exposure time of 1s, although they were not detectable with 0.5s. This is opposite to the previous results obtained with WEFF microscopy where the nucleus and cell body were not visible with short exposure but at high exposure times, the cell was visible with cell body and nucleus [8][18].

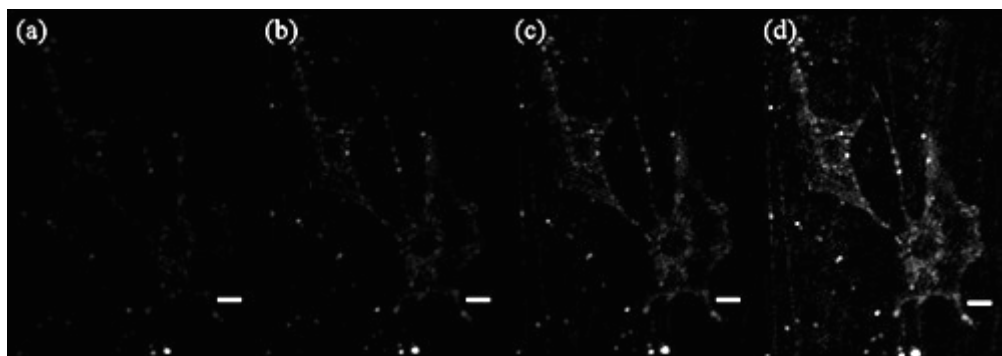


Figure 5-4: WEFFS microscopy of osteoblasts with increasing exposure times (a) 0.5s (b) 1s (c) 1.2s and (d) 1.5s. The images are acquired with a TM mode and magnification of 20x (Olympus LUC plan FLN). Scale bars represent 20 μ m. Brightness and contrast enhanced for better visualization.

The reason behind the visibility of both nucleus and cell body even at low exposure times might be that, nucleus and cell body scatter strongly even with very low illumination because these structures depict a relatively large refractive index contrast with respect to the cytoplasm. Hence even though they are not located in the evanescent field, scattered light from the waveguide is able to illuminate these features and they become visible. It

was observed that there were also some bright spots on the images which were located away from the two cells. Some of these spots could be adhesion points for some other cells which were surrounding these two cells and/or they could be scattered from precipitation in the phosphate buffered saline (DPBS) in which the cells were kept. As these cells were not stained, these scattering signals could not be a result from leftover dye particles. Although DPBS was filtered before using, there could still be some particles in the solution that also scattered light. Nevertheless, these problems should be addressed in future as it can produce errors when quantitative data are desired, such as calculating the number of adhesion points per cell.

5.4 Comparison with Fluorescence Microscopy

Although it was determined that WEFS microscopy is a competent method for capturing images showing granular structure in the cell and at its margins, visualizations of focal adhesions could not be ascertained, as it is done in WEFF microscopy. To further analyse the location and distribution of focal adhesions in osteoblasts, fluorescence microscopy was carried out. Fluorescence microscopy was performed on osteoblasts with vinculin staining. Vinculin is a cytoskeletal protein which is associated with the regulation of focal adhesion formation. Vinculin plays the key role in the attachment of cells by focal adhesion formation. The images acquired with fluorescence microscopy were later compared to WEFS microscopy images confirming the presence of focal adhesions in the WEFS images.

5.4.1 Fluorescence Staining and Microscopy

Cells were fixed with 4% paraformaldehyde (Sigma Aldrich) in DPBS for 10 minutes at room temperature and then they were washed with DPBS three times. They were then permeabilized with 0.1% triton-X 100 in PBS for five minutes. Cells were incubated with primary antibodies to vinculin (Millipore) in DPBS. After 1 hour, they were washed three times with DPBS and incubated with the secondary antibody goat anti-mouse IgG (Invitrogen) conjugated with Alexa fluor 488. The absorption and emission peak of Alexa fluor 488 is at 495 and 519 nm respectively. Later they were washed three times and kept in DPBS for examination. Cells were investigated with an Axioscope fluorescence

microscope (Carl-Zeiss). Imaging was performed using an Axiocam camera and a software called AxioImage.

5.5 Results

Images acquired with both fluorescence microscopy and WEFS microscopy are shown side by side in Figure 5.5. It is to be noted that the cells in these two images are not same in size. The two images were captured with different objectives. Figure 5.5 (a) shows the fluorescent image of an osteoblast cell which clearly showed the focal adhesion protein vinculin. Staining of vinculin is seen as small elongated structures due to the presence of vinculin in the fiber like protein assembly of adhesion within the cell. They were found in this image mostly along the outline of the cell. A few were also located on the body and spread regions of the cell. On the other hand, the cell in Figure 5.5(b) shows a WEFS microscopy image where small bright round spots could be seen on the body of the cell as well as along the spread region and outline of the cell. The very bright spots around the nucleus represents the cell body showing cytoplasm with granular structures. There were also many bright spots along and near the outline of the cell mostly in the upper part of the image. These bright spots depicts the adhesion points where the cell was attached to the substrate. Previously, focal adhesions were detected by staining cells with DiIC₁₈ employing WEFF microscopy [19]. By staining the plasma membrane with DiIC₁₈, the entire focal adhesions became visible in the fluorescence spectrum. Hence elongated focal adhesions could be seen in the WEFF images. However, with WEFS microscopy, neither the plasma membranes nor the focal adhesions were stained. Nevertheless, cell-substrate interactions could still be visualized as small scattering spots. These spots might represent the focal contacts which are very small ($\sim 1 \mu\text{m}^2$) adhesion points [5]. These small spots were also brighter than the surrounding (except the region around nucleus). This confirms that these spots are closest to the substrate due to the fact that evanescent field has its highest intensity at the interface. The comparison between these two images supports the fact that WEFS microscopy can also be employed to visualize cell-substrate interactions.

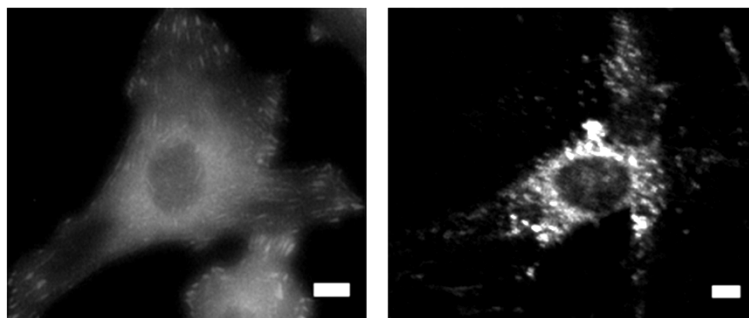


Figure 5-5: Fluorescence microscopy and WEFS microscopy detecting focal adhesions (a) fluorescence microscopy image of MC3T3 cells stained to detect cytoskeletal protein vinculin, scale: 10 μm (b) WEFS microscopy image with no staining showing bright spots along the edges and on cell body. Scale bar: 20 μm . Brightness and contrast enhanced for better visualization.

5.6 Imaging Granularity in Cells

Cellular granularity is an important parameter in detection of diseases. As WEFS microscopy images showed the cell body with increased scattered intensity, this microscopy method was employed to visualize the granular structures inside cells.

5.7 Results

Figure 5.6(a-d) shows a series of WEFS microscopy images of live osteoblasts. The cells in these images were neither stained nor fixed. They were captured with very high exposure times and the nucleus and the cell body could be identified. Imaging with WEFS microscopy revealed the presence of a lot of granules in the cell body. The granules were located mostly around the nucleus. These granules appeared with moderate illumination and more and more granules appeared with higher exposures. Comparing with WEFF microscopy images, for example as the one shown in Figure 5.6 (e), it was found that the images captured with WEFS microscopy on unstained cells were able to detect and localize these granules, whereas WEFF images do not yield this information. The WEFF image acquired with high illumination shown in Figure 5.6 (e) also depicted the nucleus and cell body clearly but the granular area around the cell body was conceived as a dense object rather than individual granules.

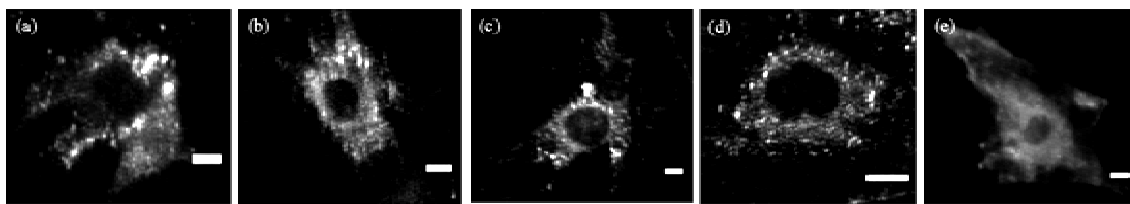


Figure 5-6: Inspection of granularities in live osteoblasts: (a-d) WEFS microscopy images acquired with exposure times of more than 3s showing granules around the nucleus and (e) WEF microscopy image depicting the cell clearly but without granularity information. Scale bars are 10 μm . All images are brightness increased for better visibility.

Images acquired with WEFS microscopy with small exposure times, usually below 1s, only showed a few granules around the nucleus, however with high exposure times, there was a significant increase in the visible amount of granules present in the cell body around the nucleus. Figure 5.7 (a-d) shows a series of WEFS image of the same cell with increasing exposure times up to 5s. Figure 5.7 (a) shows a bright field image of a cell with some dark spots mostly in the upper and right side of cell body. These dark spots also appeared in the WEFS microscopy images with all three exposures. With an exposure time of 2s, the cell is visible with its nucleus as a dark round object as well as the cell body with many granules around the nucleus region and also the spread region was visible on the lower part of the cell. When the exposure time was increased to 3s, the granules looked brighter than in the previous image. Finally with an exposure time of 5s, the granules became significantly brighter and more granules appeared even on the spread region of the cell. The entire osteoblast became completely visible in the WEFS microscopy image and granules could be distinctly seen.

The granularity in cells can be thus examined with WEFS microscopy. It delivers similar information as flow cytometry. In WEFS microscopy, the cells are immobilized on substrates and in flow cytometry experiments, cells are floating contactless. The big advantage over other evanescent field microscopy is that with WEFS microscopy, there is no need for staining the granules for visualizing them. This can be immensely advantageous to detect diseases associated with increased granularity in cells. Even it

might be possible to detect individual granules and granular movement (if any) with time-lapse microscopy and higher magnification objectives [20].

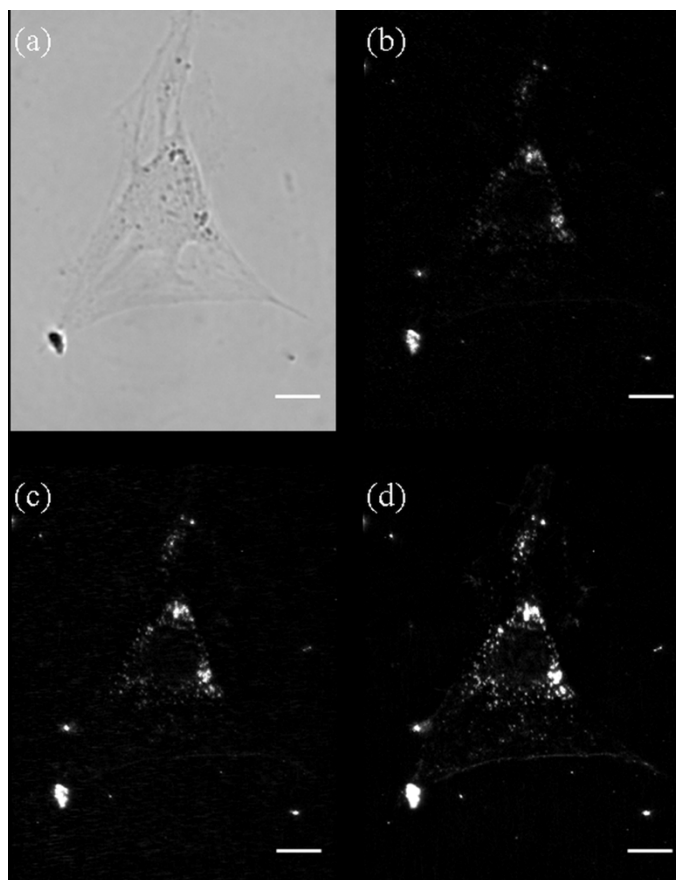


Figure 5-7: WEFS image of a MC3T3 cell with increasing exposure times: (a) bright field image (b) 2s (c) 3s (d) 5s. Scale bars represent 20 μm .

5.8 Summary

WEFS microscopy was successfully employed for imaging of both live and fixed osteoblast MC3T3 cells from mice. This new microscopy technique was able to detect the adhesions of cells to substrate and cell granularity. It was possible to visualize the nucleus and cell body even with comparatively low illumination times. There was a background illumination present due to impurities and/or inhomogeneities from the waveguides producing scattered light outside the evanescent field. In addition, particles in the medium, in which cells were kept might have scattered photons as well. These issues need to be addressed in future for better noise control and successful employment

of WEFS microscopy at the cell-substrate interface only to focus on adhesions. The granules present in the cells also scattered light. As a result, granularity in the cells was possible to detect with the application of high exposure times. The granularity data of these immobilized cells are similar to granularity data from flow cytometry of unattached cells.

5.9 References

1. Lang, P., Yeow, K., Nichols, A., & Scheer, A. (2006). Cellular imaging in drug discovery. *Nature Reviews Drug Discovery*, 5(4), 343-356.
2. Ramachandran, S., Cohen, D. A., Quist, A. P., & Lal, R. (2013). High performance, LED powered, waveguide based total internal reflection microscopy. *Scientific reports*, 3.
3. Ruoslahti, E., & Öbrink, B. (1996). Common principles in cell adhesion. *Experimental cell research*, 227(1), 1-11.
4. Ivaska, J. (2012). Unanchoring integrins in focal adhesions. *Nature cell biology*, 14(10), 981-983.
5. Aroush, D. R. B., Zaidel-Bar, R., Bershadsky, A. D., & Wagner, H. D. (2008). Temporal evolution of cell focal adhesions: experimental observations and shear stress profiles. *Soft Matter*, 4(12), 2410-2417.
6. Mattheyses, A. L., Simon, S. M., & Rappoport, J. Z. (2010). Imaging with total internal reflection fluorescence microscopy for the cell biologist. *Journal of cell science*, 123(21), 3621-3628.
7. Hassanzadeh, A., Nitsche, M., Mittler, S., Armstrong, S., Dixon, J., & Langbein, U. (2008). Waveguide evanescent field fluorescence microscopy: Thin film fluorescence intensities and its application in cell biology. *Applied Physics Letters*, 92(23), 233503.
8. Hassanzadeh, A. (2009). Waveguide evanescent field fluorescence microscopy & its application in cell biology, Ph.D. diss., The University of Western Ontario.
9. Hadjidakis, D. J., & Androulakis, I. I. (2006). Bone remodeling. *Annals of the New York Academy of Sciences*, 1092(1), 385-396.
10. Aubin, J. E. (1998). Bone stem cells. *J. Cell. Biochem.*, 72: 73–82.

11. Shapiro, H. M. (2005). Practical flow cytometry. John Wiley & Sons.
12. Rieseberg, M., Kasper, C., Reardon, K. F., & Scheper, T. (2001). Flow cytometry in biotechnology. *Applied microbiology and biotechnology*, 56(3-4), 350-360.
13. Biosciences, B. D. (2000). Introduction to Flow Cytometry: A learning guide. Manual Part, (11-11032), 01.
14. Basiji, D. A., Ortyn, W. E., Liang, L., Venkatachalam, V., & Morrissey, P. (2007). Cellular image analysis and imaging by flow cytometry. *Clinics in laboratory medicine*, 27(3), 653-670.
15. Rowley, T. (2013). Flow Cytometry-A Survey and the Basics. *Materials and Methods*.
16. Biesele, J. J., & Goldhaber, P. (1955). A study of cytoplasmic lipid granularity in tissue culture cells. *Cancer research*, 15(11), 767-773.
17. Haynes, M. K., Strouse, J. J., Waller, A., Leitao, A., Curpan, R. F., Bologna, C., Oprea, T. I., prossnitz, E. R., Edwards, B. S., SKlar, S. A. & Thompson, T. A. (2009). Detection of intracellular granularity induction in prostate cancer cell lines by small molecules using the HyperCyt® high-throughput flow cytometry system. *Journal of biomolecular screening*, 14(6), 596-609.
18. Imruck, D. (2009), Evanescent Field Waveguide Fluorescence Microscopy of Cells on Biopolymers, Master Thesis, University of Applied Sciences, Rüsselsheim.
19. Hassanzadeh, A., Nitsche, M., Armstrong, S., Nabavi, N., Harrison, R., Dixon, S. J., Langbein, U., & Mittler, S. (2010). Optical waveguides formed by silver ion exchange in Schott SG11 glass for waveguide evanescent field fluorescence microscopy: evanescent images of HEK293 cells. *Journal of biomedical optics*, 15(3), 036018-036018.
20. Steyer, J. A., & Almers, W. (1999). Tracking single secretory granules in live chromaffin cells by evanescent-field fluorescence microscopy. *Biophysical journal*, 76(4), 2262-2271.

Chapter 6

6 Conclusion and Outlook

6.1 Conclusion

This thesis demonstrates the applicability of waveguide evanescent field scattering microscopy for the imaging of biological cells. The two types of cells successfully imaged with this microscopy technique are bacteria and osteoblast MC3T3 cells. The WEFS microscopy system was able to display high contrast cellular images. There are still some issues that need to be addressed for the larger cells such as presence of background illuminations due to waveguide inhomogeneities, scattering from particles present in the medium in which cells are kept and therefore appearance of parts of the cells outside the range of evanescent field. It may be possible to change the medium in which fixed cells are kept in deionized water after culturing them for 24 hours if imaging can be done immediately. This may help eliminate all the scattering from the bulk phosphate buffer solutions. Besides, filters with very small pore sizes (less than 0.45 micron) may be used to filter the medium and buffer solutions before using them.

The detailed conditions of the appearance of the nucleus and cell body which are present micrometers away from the surface of the waveguides and the illuminating evanescent field need to be analysed in future. The scattering behaviour of the waveguides, for example a criterion such as waveguide losses, need to be taken into account. We speculated that scattering, always present from waveguides and the huge amount of scattering centers with a relative high refractive index in comparison to the cytoplasm present in the nucleus and cell body might be responsible for the strong occurrences of them. However, there might be other reasons such as the architecture of the waveguides or scattering particles present on the waveguide surface due to fabrication process. Inhomogeneities from waveguides might be avoided by going into a polymer waveguide system. This would also enhance the ability to grow cells directly on the waveguides, as it is known that cells do not prefer to grow on plain glass surface.

The WEFS technology was demonstrated to have applications in water quality control. Bacteria was first UV sterilized at different doses and then allowed to culture on waveguide surfaces for 24 hours. Later, WEFS microscopy was performed and results quantitatively analyzed to confirm the hypothesis that bacteria sterilized with high doses of UV are unable to form colonies. From these data, a safety UV dose could be predicted to create water without biologically active bacteria. Thus WEFS microscopy can be employed for on-line monitoring of bacterial attachment to surfaces by simple scattering intensity measurement. The integrated scattered photons from a waveguide chip can be monitored and above a threshold level, removed from the environment and examined thoroughly with WEFS microscopy on the same chip. The technique described above can be utilized in other environments, where continuous monitoring is necessary such as hospitals or food and beverage industries as well.

Imaging osteoblasts without the application of any fluorescent stains can be highly advantageous. WEFS microscopy produced high contrast images of cells with a low cost set-up. Both focal contacts and granularity was displayed, however not distinguishable from each other. The granularity in cells is an important parameter as it is associated with cell deaths and apoptosis as well as it may act as a marker to detect diseases. The WEFS microscopy images depicting the granularity and the focal adhesions of immobilized cells deliver similar information as scattering flow cytometry on floating cells. Although fluorescence imaging is already employed alongside flow cytometry to gather knowledge about intracellular structures, WEFS microscopy may be able to contribute to situations where staining is not appropriate and deliver location information.

Oriented collagen for tissue engineering is a topic researched extensively. In this thesis, collagen was deposited on hydrophobic glass surfaces with Langmuir-Blodgett technology. Different orientation distributions of collagen on the sample surfaces were achieved by employing substrates with various geometrical shapes and sizes. It was also shown that these collagen films were stable up to at least three months under different solution and temperature conditions. However, collagen when using as a scaffold material, should be stable for a significantly longer period of time. The stability of the oriented collagen on glass substrate should be examined for a longer period of time

considering its application in medical implants. The question on how to sterilize the films has not been addressed yet.

It was intended to fabricate oriented collagen films on waveguides and then culture osteoblast cells on the surface of waveguides to image and analyse the behavior of these cells on oriented collagen. It is known from literature that cells usually sense and adapt anisotropies of their substrates, in this case the orientation of collagen when they are cultured. Unfortunately, there was not enough time to study and visualize the cells interacting to surfaces with different orientation distributions of collagen. However, it should be taken into account that there is always a possibility that collagen might scatter too much light while imaging with WEFS microscopy, therefore it might not be possible to view cells forming contacts and adhesions to the oriented collagen coated substrates.

The waveguides used in the work are the key element for microscopy. These waveguides, along with the coupling gratings on them, were fabricated at the University of Rüsselsheim, Germany using various processes: laser interference lithography, ion milling and glass sputtering, all of which are not available at the University of Western Ontario. Although the glass waveguides are reusable, they started to lose their workability after a few uses such as microscopic scratches enhancing noise and background. Also they had to be cleaned very carefully after each experiment otherwise leftover from cells of previous experiments would interfere. It was also found that the waveguide thickness decreased systematically with each cleaning step. This result was found by finding a decrease in available waveguide modes with increasing numbers of cleaning cycles. The decrease in modes happened in both polarization directions. Therefore, an inexpensive one time use waveguide would be advantageous. This leads to the mass fabricable polymer waveguides with hot embossed gratings packaged in a sterilized fashion.

6.2 Outlook

WEFS microscopy has proven to be a promising technology for biological cell imaging without any need to stain. Nevertheless, more engineering research needs to be performed to improve this microscopy system. In the present study, live cell imaging was performed

but not in a proper environmental condition. For the cells to be in a healthy environment during imaging, a temperature-controlled sample holder should be constructed. This chamber then can also act as a cuvette holding cells in medium during experiments. The waveguides are a major problem for commercialization of this technology as currently the fabrication of these waveguides is tedious and expensive. The fabrication of mass-producible polymer waveguides can solve this problem and research is already continuing in our lab for this purpose.

For the collagen films, additional investigations should be carried out to confirm the stability of the collagen films under heat treatment and different environments for a longer period of time. A thorough investigation about how to sterilize the LB collagen films is necessary. In a next step, a cleavable site can be introduced between the substrate and the collagen layer to allow peeling off of the collagen film after deposition. Large, thin, flexible collagen films can be produced in this way for applications such as wound dressing. The 3D orientation of collagen should also be researched in future by studying LB transfer onto real 3D implants.

The combination of oriented collagen with WEFS microscopy needs to be conducted. At present, only rectangular and square waveguides are available for use but in future one can produce different shaped polymer waveguides for this purpose.

Appendix A

Copyright permission for Chapter 3

Confirmation Number: 11151694

Order Date: 01/15/2014

Customer Information

Customer: Qamrun Nahar

Account Number: 3000739541

Organization: Qamrun Nahar

Payment Method: Invoice

Langmuir : the ACS journal of surfaces and colloids

Order Details

Order detail ID: 64329636

ISSN: 0743-7463

Publication Type: Journal

Publisher: AM CHEM SOC

Author/Editor: American Chemical Society

Permission Status: Granted

Permission type: Republish or display content

Type of use: Republish in a thesis/dissertation

Order License Id: 3310380673955

Order ref number: CAO2755

Requestor type: Author of requested content

Format: Print, Electronic

Portion: excerpt (up to 400 words)

Number of excerpts requested: 3

Title or numeric reference of the portion(s): Full article including images

Title of the article or chapter the portion is from: **Orientation Distribution of Highly Oriented Type I Collagen Deposited on Flat Samples With Different Geometries**

Editor of portion(s): N/A

Author of portion(s): Qamrun Nahar

Volume of serial or monograph: 29

Issue, if republishing an article from a serial: 22

Page range of portion: 6680-6686

Publication date of portion: 2013
Rights for: Main product
Duration of use: Life of current edition
Creation of copies for the disabled: No
With minor editing privileges: no
For distribution to: Worldwide
Permission Status: Granted
Billing Status:N/A

Note: This item was invoiced separately through our RightsLink service.

Total order items: 1

Order Total: \$0.00

Appendix B

Copyright permission for Chapter 4

Dear Qamrun Nahar,

We hereby grant permission for the requested use expected that due credit is given to the original source.

If material appears within our work with credit to another source, authorization from that source must be obtained.

Credit must include the following components:

- Books: Author(s)/ Editor(s) Name(s): Title of the Book. Page(s). Publication year. Copyright Wiley-VCH Verlag GmbH & Co. KGaA. Reproduced with permission.
- Journals: Author(s) Name(s): Title of the Article. Name of the Journal. Publication year. Volume. Page(s). Copyright Wiley-VCH Verlag GmbH & Co. KGaA. Reproduced with permission.
- Online Portal: Author(s): Title of the Online portal. Link or DOI. Publication year. Copyright Wiley-VCH Verlag GmbH & Co. KGaA. Reproduced with permission.

If you also wish to publish your thesis in electronic format, you may use the article according to the Copyright transfer agreement:

3. Final Published Version.

Wiley-VCH hereby licenses back to the Contributor the following rights with respect to the final published version of the Contribution:

- a. [...]
- b. Re-use in other publications. The right to re-use the final Contribution or parts thereof for any publication authored or edited by the Contributor (excluding journal articles) where such re-used material constitutes less

than half of the total material in such publication. In such case, any modifications should be accurately noted.

With kind regards

Bettina Loycke

Senior Rights Manager
Rights & Licenses
Wiley-VCH Verlag GmbH & Co. KGaA

Boschstraße 12
69469 Weinheim
Germany
www.wiley-vch.de

Curriculum Vitae

Name: **Qamrun Nahar**

Post-secondary Education and Degrees: The University of Western Ontario
London, Ontario, Canada
2011-2014 MEdSc

University of Dhaka
Dhaka, Bangladesh
1997-2003 B.Sc and M.Sc

Honours and Awards: Western Graduate Research Scholarship
(two-years)

Related Work Experience Research Assistant and Teaching Assistant
The University of Western Ontario
2011-2014

Publications:

Nahar, Q., Quach, D. M. L., Darvish, B., Goldberg, H. A., Grohe, B., & Mittler, S. (2013). Orientation distribution of highly oriented Type I Collagen deposited on flat samples with different geometries. *Langmuir*. 29(22), 6680-6686.

Nahar, Q., Fleissner, F., Shuster, J., Morawitz, M., Halfpap, C., Stefan, M., Langbein, U. & Mittler, S. (2013). Waveguide evanescent field scattering microscopy: bacterial biofilms and their sterilization response via UV irradiation. *Journal of Biophotonics*. DOI: 10.1002/jbio.201300135.